Department of Earth and Environmental Sciences
University of Milano-Bicocca

Optical proximal sensing for vegetation monitoring

PhD Dissertation

Candidate:
Tommaso Julitta

Tutor:
Dr. Roberto Colombo
Co-tutor:
Dr. Micol Rossini
Advisor:
Dr. Mirco Migliavacca
Coordinator
Prof. Marco Vighi

PhD school of Environmental Sciences. XXVII cycle

Acknowledgements

I guess it is only right to thank the people who contributed to my professional and personal growth during the last years spent at the Remote Sensing of Environmental Dynamics Laboratory.They are many. I am especially thankful to Drs. Micol Rossini for the support she always gave to me through her precious, not only scientific,suggestions. A special thanksalso to Dr. Roberto Colombo, to his curiosity and his contagious enthusiasm which supported all my activities. In general I have to thank all thelab. peopleI have worked with and who spent time with me,sharing experiences and discussions. I guess it is not easy to find a place like that, where research and friendship are so well mixed together. I'm referring to: Marco Celesti, Chiara Cilia, Sergio Cogliati, Biagio Di Mauro, Francesco Fava, Fabio Fussi, Roberto Garzonio and last but not least Cinzia Panigada.I need to thank my external SUPER-visor Dr.Mirco Migliavacca who has patiently and seriously revised all my studies.

I would like to thank people belonging to external research groups I had the chance to work with during the three years of my Ph.D. activity. ThusI am very grateful to the Climate Change Unit of the Environmental Protection Agency of Aosta Valley, in particular toEdoardoCremonese, Marta Galvagno, Umberto Morra di Cella, FabrizionDiotri and GianlucaFilippa for their support and for the fruitful exchange of ideas and knowledge. I want to thank Saudin Paolo and Luca Ghirardo from Ecometer S.nc., they gave to me the possibility of seeing some concrete applications of my analysis. Thanks to all the colleagues I met during the international ESA field campaigns, particularly to the Jülichgroup: Uwe Rascher, AnkeSchickling, Francisco Pinto and Andreas Burkart. Thanks to Luis Alonso as well for all the discussion we had at any hours. I am grateful to all the EUROSPEC COST ACTION members for the exchange of experiences shared with me and for the useful suggestions received. Thanks to the COST friends Javier Pacheco Labrador and Karolina Sakowskafor the time spent together. I am really thankful to the Field Spectroscopy Facility of the University of Edinburgh to have hosted me, in particular to Alasdair Mac Arthur for his supervision. I want to thank Elizabeth M. Middleton, Lawrence A. Corp, Milton Hom and Petya Campbell of theBiospheric Sciences Branch, NASA Goddard Space Flight Center for having me with them for sometimes and for the attention they gave me.

I finally want to thank all my friends and my family who supported me during this time. A special thanks to my nephew and to my niecebecause they were not here when I started and now they are.

Table of Contents

Abstract

Monitoring vegetation dynamics represents a fundamental practice to evaluate the response of the vegetation to environmental changes. It is well known that optical proximal sensing data allow the monitoring of the temporal and spatial variability of vegetation biochemical and biophysical properties under natural conditions. Vegetation optical properties can be also used to derive information about the phenological and the physiological status of the plants. Optical sensors commonly used in the field can be divided into broadband sensors (usually multispectral, e.g. RGB cameras) and narrowband sensors (both multispectral and hyperspectral devices, e.g. spectroradiometers). The potential applications of these two categories of sensors differ. While broadband sensors have been applied in the last years to track the phenological development of the vegetation, spectroradiometers have been shown to be suitable also for the characterization of plant physiological status. In fact, hyperspectral systems provide a more detailed optical characterization of the analysed targets, nevertheless the systems have to be accurately characterized in terms of spectral and radiometric performances in order to obtain repeatable and comparable measurements.

The main aim of this research is to use optical proximal sensing techniques for evaluating the role of multispectral and hyperspectral devices for monitoring vegetation parameters and processes (i.e. biovhemical7biophysical parameters and phenology and plant status processes). The specific objectives of the study are: i) characterization and reduction of the measurement uncertainty sources; ii) use of improved optical sensing techniques based on multispectral and hyperspectral data to monitor terrestrial ecosystems.

The first part of the research has been addressed to the determination of the sources of uncertainty of the optical measurement systems. Several of the most common optical devices available on the market have been characterized and compared. A particular attention has been paid to instrumental differences in the optical components which could affect the radiance measurements. Moreover, the performances of spectroradiometers have been evaluated both indoors and outdoors in order to evaluate the impact of sensor characteristics on the estimation of parameters commonly used in vegetation studies. The analysis has been initially focused on the effect of different cosine receptors on the estimation of biochemical and biophysical properties of the vegetation (i.e. leaf area index and chlorophyll content). In a second step the analysis referred to the impact of instrumental characteristics (mainly spectral resolution and signal to noise ratio) on the estimation of the absolute value of sun-induced chlorophyll fluorescence which is the most promising tool for inferring plant status from remote sensing. The results obtained suggest that instrument components affect the measurements and according to the required parameter estimations accuracy some instruments are more suitable rather than others.

The second part of the study has been focused on the use of proximal sensors to monitor the dynamics of terrestrial vegetation. For this purpose both broadband and narrowband sensors have been separately considered. The first analysis referred to the possibility of using broadband imaging systems to investigate the temporal and spatial phenological dynamics of an alpine ecosystem. The phenological analysis has been conducted using a 3-year time series of digital RGB images collected in a grassland site. This spatiotemporal analysis provided interesting insights into the role of plant species composition on phenology in complex ecosystems, such as the alpine grasslands. This casestudy indicates the potential of using RGB digital cameras as a tool for long term phenological monitoring, allowing the spatial characterization of the investigated ecosystem. The possibility of using hyperspectral narrowband sensors to detect vegetation physiological changes was also evaluated. In particular, this analysis focused on the use of sun-induced chlorophyll fluorescence for the early detection of vegetation stress. The study was conducted during a controlled experiment designed to modify the functional status of actual photosynthesis. The results indicate that fluorescence is immediately affected by physiological changes as a demonstration that such estimates can be used to track physiological traits better than traditional remote sensing techniques based on optical broadband vegetation indices.

Chapter 1

Introduction

1.1 Framework and rationale

The knowledge of temporal and spatial variability of vegetation canopy properties is recognised as a key element for understanding terrestrial biosphere processes and can assist in the parameterisation of various physical and ecological models which include the vegetation as a dynamic component (e.g. Reichstein et al., 2014; Richardson et al., 2013). Environmental sensor networks offer a powerful combination of distributed sensing capacity, real-time data acquisition and analysis, and integration with adjacent networks and remote sensing data streams (Rundel et al., 2009). Within environmental networks the vegetation monitoring through optical proximal sensing techniques gained importance in recent years. These techniques consist in measuring the optical properties (reflected or emitted electromagnetic radiation) of vegetation using non-contact devices positioned close to the plant or the canopy. Optical proximal sensing is considered as an important technique for characterising the optical properties of natural surfaces in situ, for supporting the vicarious calibration of airborne and satellite sensors, and for providing a means of scaling-up measurements from small areas to landscape scenes (Milton et al., 2009). In this context, field spectroscopy for the fluorescence measurement may represent a crucial topic to calibrate and validate algorithm for future satellite missions from Space Agency (e.g. European Space Agency, ESA), such as the FLuorescence EXplorer (FLEX) --currently an Earth Explorer 8 candidate.

In the last decade international efforts have been made to establish global network of continuous measurements of vegetation optical properties such as the Specnet (http://specnet.info, Gamon et al., 2014, 2006) and the PhenoCam (http://phenocam.sr.unh.edu, Richardson et al., 2007; Sonnentag et al., 2012) networks. While the latter aims to monitor the phenological cycle of the vegetation through changes in canopy greenness, Specnet goal is to additionally measure optical signals directly related to plant status.The PhenoCam network proved the reliability of devices such as RGB digital cameras for providing accurate phenological information. The RGB digital images can be used to characterize the phenological spatial variability within the monitored ecosystems. However, most of the studiespublished so far are only focused on the phenological temporal analysis. The spatial information of the images is usually ignored and lost when the analysis is performed averaging the pixel values on region of interest. The spatial information can be included in the analysis combining the temporal dynamics with the spatial analysis of the elements contained in the whole image. Such analysis can add valuable information in order to better understand at micro-scale the relationship between phenological cycle and environmental drivers.

On the contrary spectroradiometers commonly used in field spectroscopy are non-imaging

systems. In fact, the extremely high cost of hyperspectral imagining devices limits their use in the field surveys. Hyperspectral data collected by non-imaging spectroradiometers can provide moreinformative description of the vegetation optical properties compared to the data acquired with broadband multispectral systems (i.e. RGB cameras). In particular hyperspectral measurements can be used for monitoring at the same time phenological and physiological status of the plants. One of the limitationsof non-imaging spectroradiometers is the difficulty to make spectral measurements in the spatial domain to capture the spectral heterogeneity of the surfaces. This can be overcome spatially sampling the monitored scene making spatial transect samples manually or deployingthe instruments on unmanned aerial vehicle (UAV). At the same time an additional limitation of hyperspectral sensors is the high dependency of the measurement on instrumental characteristics. In fact, the different instruments and the acquisition strategies used need to be standardized in order to obtain high quality, reliable and comparable data across sites and time. Despite an international effort to promote opticalproximal sensing measurements there has been little consideration given to the comparability of measurement protocols and systems. For this reason, comparing data collected at different times and sites is currently problematic(Anderson et al., 2013; Ide and Oguma, 2010). This is one of the reasons why the COST Action EUROSPEC (Spectral Sampling Tools for Vegetation Biophysical parameters and flux measurements in Europe) and the more recent OPTIMISE (Innovative optical Tools for proximal sensing of eco-physiological processes) were approved by the European Cooperation in Science and Technology. The main goal of these Actions is to improve the reliability and efficiency of proximal optical sampling measurements within carbon flux monitoring networks by developing standardized protocols and methods. Further studies need to be done in order to quantify the impact of the instrumental characteristic (e.g. spectral resolution, signal to noise ratio) on the measurements. In fact, if instrumental differences are expected to influence less normalized vegetation index values related to the green biomass they can strongly affect the estimates of physical quantity (e.g. sun induced chlorophyll fluorescence).

1.2Objectives and thesis structure

The general objective of this research is exploiting optical proximal sensing to better describe vegetation phenological cycle and plant status using improved techniques based on multispectral and hyperspectral data. In particular,the first part of the study has been addressed to characterize measurement uncertainty sources in field spectroscopyuseful for defining the better configuration of these instruments for properlydetecting vegetation optical properties. In the second part, the performances of optical proximal sensing techniques in monitoring vegetation dynamics have been evaluated in two case studies: the phenological cycle of an alpine grassland(using RGB digital images) and the physiological changes of vegetation induced by herbicide treatment(using spectroradiometers).

The dissertation begins in chapter 2 with a brief review of the sensors currently used in optical proximal sensing vegetation monitoring. The proximal sensing techniques for characterizing vegetation properties are also reported in this chapter. In particular optical proximal sensing based approaches to estimate biochemical/biophysical parameters and to track plant phenological or physiological status of vegetation are introduced. A first part of the dissertation concerns the instrument characterization and evaluation of measurement uncertainties and includes Chapter 3, 4 and 5. The second part, chapter 6 and 7, is focused on the monitoring of terrestrial vegetation using proximal sensing sensors. Accordingly chapter 3 is referred to the characterization of several hyperspectral devices commonly used in field spectroscopy. Both laboratory and outdoor instruments characterizations are described in order to evaluate the measurement uncertainty sources. The calibration procedures applied to reduce instrumental artefacts in the measurements are presented and practical suggestions to reduce field measurement uncertaintiesare listed. Moreover Chapter 4 and Chapter 5 are focused on intercomparison experiments aimed at evaluating the effect of differences between devices on the measurements. Chapter 4 in particular has been addressed to define how non lambertian behaviour of reference standards used in the field (reference panels and cosine receptors) affect the measurements. The impact of the different reference standards angular response has been evaluated on reflectance, vegetation indices and biochemical/biophysical parameter estimation. Chapter 5 refers to the evaluation of different spectroradiometer characteristics effect on the estimation of sun-induced chlorophyll fluorescence. An intercomparison experiment was set under natural conditions and the effect of spectral resolution and of the signal to noise ratio of the devices used on the retrieval of the red and far-red fluorescence absolute values was evaluated.

The second part of the dissertation starts with Chapter 6 where a study showing the potential of automatic continuous digital camera images to monitor the seasonal development of a grassland ecosystem is reported. The analysis refers to a three year daily RGB image time series collected automatically and investigates both temporal and spatial relationships between phenology and snowmelt. Lastly in chapter 7 the potential of hyperspectral systems to monitor variations in the photosynthetic efficiency was evaluated.An herbicide known to reduce photosynthetic activity and tomodify energy dissipative pathways was applied and the physiological expected effects have been monitored using hyperspectral early stress indicators.

References

Anderson, K., Rossini, M., Pacheco-Labrador, J., Balzarolo, M., Mac Arthur, A., Fava, F., Julitta, T., Vescovo, L., 2013. Inter-comparison of hemispherical conical reflectance factors (HCRF) measured with four fibre-based spectrometers. Opt. Express 21, 605.

Balzarolo, M., Anderson, K., Nichol, C., Rossini, M., Vescovo, L., Arriga, N., Wohlfahrt, G., Calvet, J.-C., Carrara, A., Cerasoli, S., Cogliati, S., Daumard, F., Eklundh, L., Elbers, J.A., Evrendilek, F., Handcock, R.N., Kaduk, J., Klumpp, K., Longdoz, B., Matteucci, G., Meroni, M., Montagnani, L., Ourcival, J.-M., Sánchez-Cañete, E.P., Pontailler, J.-Y., Juszczak, R., Scholes, B., Martín, M.P., 2011. Ground-Based Optical Measurements at European Flux Sites: A Review of Methods, Instruments and Current Controversies. Sensors 11, 7954–7981.

Gamon, J.A., Coburn, C., Flanagan, L.B., Huemmrich, K.F., Kiddle, C., Sanchez-Azofeifa, G.A., Thayer, D.R., Vescovo, L., Gianelle, D., Sims, D.A., Rahman, A.F., Pastorello, G.Z., 2014. SpecNet revisited: bridging flux and remote sensing communities. Can. J. Remote Sens. 36, S376–S390.

Gamon, J.A., Peñuelas, J., Field, C.B., 1992. A narrow-waveband spectral index that tracks diurnal changes in photosynthetic efficiency. Remote Sens. Environ. 41, 35–44.

Gamon, J.A., Rahman, A.F., Dungan, J.L., Schildhauer, M., Huemmrich, K.F., 2006. Spectral Network (SpecNet)-What is it and why do we need it Remote Sens. Environ. 103, 227–235.

Hilker, T., Coops, N.C., Hall, F.G., Black, T.A., Wulder, M.A., Nesic, Z., Krishnan, P., 2008. Separating physiologically and directionally induced changes in PRI using BRDF models. Remote Sens. Environ. 112, 2777–2788.

Ide, R., Oguma, H., 2010. Use of digital cameras for phenological observations. Ecol. Inform. 5, 339–347.

Middleton, E.M., Cheng, Y.-B., Hilker, T., Black, T.A., Krishnan, P., Coops, N.C., Huemmrich, K.F., 2009. Linking foliage spectral responses to canopy-level ecosystem photosynthetic light-use efficiency at a Douglas-fir forest in Canada. Can. J. Remote Sens. 35, 166–188.

Migliavacca, M., Galvagno, M., Cremonese, E., Rossini, M., Meroni, M., Sonnentag, O., Cogliati, S., Manca, G., Diotri, F., Busetto, L., Cescatti, A., Colombo, R., Fava, F., Morra di Cella, U., Pari, E., Siniscalco, C., Richardson, A.D., 2011. Using digital repeat photography and eddy covariance data to model grassland phenology and photosynthetic CO2 uptake. Agric. For. Meteorol. 151, 1325–1337.

Milton, E.J., Schaepman, M.E., Anderson, K., Kneubühler, M., Fox, N., 2009. Progress in field spectroscopy. Remote Sens. Environ. 113, S92–S109.

Monteith, J.L., 1972. Solar radiation and productivity in tropical ecosystems. J. Appl. Ecol. 9, 747–766.

Porcar-Castell, A., Garcia-Plazaola, J.I., Nichol, C.J., Kolari, P., Olascoaga, B., Kuusinen, N., Fernández-Marín, B., Pulkkinen, M., Juurola, E., Nikinmaa, E., 2012. Physiology of the seasonal relationship between the photochemical reflectance index and photosynthetic light use efficiency. Oecologia 170, 313–23.

Reichstein, M., Bahn, M., Mahecha, M.D., Kattge, J., Baldocchi, D.D., 2014. Linking plant and ecosystem functional biogeography. Proc. Natl. Acad. Sci. 111, 13697–13702.

Richardson, A.D., Jenkins, J.P., Braswell, B.H., Hollinger, D.Y., Ollinger, S. V, Smith, M.-L., 2007. Use of digital webcam images to track spring green-up in a deciduous broadleaf forest. Oecologia 152, 323–34.

Richardson, A.D., Keenan, T.F., Migliavacca, M., Ryu, Y., Sonnentag, O., Toomey, M., 2013. Climate change, phenology, and phenological control of vegetation feedbacks to the climate system. Agric. For. Meteorol. 169, 156–173.

Rossini, M., Meroni, M., Migliavacca, M., Manca, G., Cogliati, S., Busetto, L., Picchi, V., Cescatti, A., Seufert, G., Colombo, R., 2010. High resolution field spectroscopy measurements for estimating gross ecosystem production in a rice field. Agric. For. Meteorol. 150, 1283–1296.

Rundel, P.W., Graham, E.A., Allen, M.F., Fisher, J.C., Harmon, T.C., 2009. Environmental sensor networks in ecological research. New Phytol. 182, 589–607.

Sonnentag, O., Hufkens, K., Teshera-Sterne, C., Young, A.M., Friedl, M., Braswell, B.H., Milliman, T., O'Keefe, J., Richardson, A.D., 2012. Digital repeat photography for phenological research in forest ecosystems. Agric. For. Meteorol. 152, 159–177.

Chapter 2

Theoretical background

In this chapter a description of the optical proximal sensing techniques used in the framework of vegetation monitoring and the possible applications of these measurements to retrieve structural or functional information of the monitored targets is presented. Optical proximal sensing measurements aim to collect information of the reflected radiation from a determined surface area. According to the instrument used, the gathered data can differ in terms of spectral range analysed (e.g. Visible range, 400-700 nm, Near Infrared 700-1400nm), number of spectral bands (Hyperspectral, Multispectral) and spectral resolution (narrow band or broad band). In addition spectral measurements can be expressed in term of absolute or relative units. Data in absolute units are expressed according to the international system of units (SI). On the contrary when relative measurements are performed, the traceability to SI units is not required, generally they are obtained by the ratio of two measurements. Absolute or relative measurements can be preferred according to the objective of the study. As example multispectral broadband sensors, usually operating in relative units, can be successfully used to track phenological changes in the canopy. On the other hand hyperspectral devices able to monitor narrow features of the reflected radiance of vegetation are preferred to detect physiological changes of plant status associated to faint variations of the reflected signal.

2.1 Radiometry, spectroradiometry and optical devices used in the field

Radiometry is the measurement of the energy of electromagnetic radiation fields and how this energy is transferred from a source, through a medium, to a detector (Zalewsky, 2007). Spectroscopy includes a very broad range of techniques (traditionally used in laboratory), which are all based on the investigation of interactions of light with materials, more specifically the interactions of photons of electromagnetic waves with the atoms or molecules of material. Spectroradiometry expresses the combination of spectroscopic techniques with radiometric measurements (Kardevan, 2007). Field spectroscopy involves the study of the interrelationships between the spectral characteristics of objects and their biophysical attributes in the field environment (Milton, 1987).

In field measurements illumination sources are uncontrolled, changing with time and having multiple components (directional beam of the sun, hemispherical diffuse irradiation, etc.). Therefore, the radiant fluxes of the spectral radiation components including the incoming and reflected radiations must be measured, in order to characterize the targets with spectral signatures being independent of timely variation of the irradiation and whether conditions. The ratio of the incoming and reflected fluxes (i.e. spectral reflectance) is considered then characteristic to the target only. This is true only in the case of perfect, isotropic, diffuse surfaces (Lambertian-surfaces). In the case of real materials, usually a strong angular dependence can be observed depending on the geometry of incoming and reflected radiation fluxes (Giardino and Brivio, 2003; Painter, 2004). An adequate description of this directional phenomenon is possible with the Bi-directional Reflectance Distribution Function (BRDF), (Hilker et al., 2007; Milton et al., 2009; Nicodemus, 1970; Schaepman-Strub et al., 2006), which appears in various forms depending on the radiation flux geometries used in the course of measurements (directional, conical, hemispherical referring both the illumination and viewing geometries). In order to inter-compare these field spectroradiometer data it is important to appreciate the differences in the measurement properties: precise nomenclature and device used characteristics, such as field-of-view and view and illumination geometries.(Martonchik et al., 2000). Before describing the application of optical proximal sensing techniques the next paragraph is dedicated to examine the configuration of the devices commonly used for field proximal sensing measurements.

2.2Optical instrument configuration

There are primarily two approaches that can be adopted for making optical measurements: i) the multiband approach and ii) hyperspectral approach. Multiband sensors measure a limited number of spectral bands, possibly from one or two to thirty or forty with band widths (full width at half the maximum response, FWHM) in the order of 10 nm or greater. Hyperspectral sensors normally measure hundreds of spectral bands, 600 or more, with band widths usually less than 10 nm up to sub-nanometer level. Each of these approaches has both scientific and practical advantages and disadvantages. Examples of multispectral and hyperspectral sensors installed in the field are reported in Figure 2.1.

Figure 2.1 Some examples of the use of sensors in the field. (a) Skye sensor at Hyytiälä forest site (FI-Hyy, Finland), (b) S-fluor box at Duke forest (Durham, NC, USA), (c) AMSPECsystem at the Majadas del Tiétar site (Spain), (d) Ocean Optics sensor at Zeilaushen (Germany), (e) RGB camera at Torgnon site (Italy), (f) Cropscan sensor at Monte Bondone grassland site (Italy)

2.2.1 Multispectral sampling

Multispectral sensors include imaging (e.g RGB cameras) or non-imaging sensors (e.g. and non-imaging radiometers). Radiometers commonly operated for field vegetation monitoring are typically based on a combination of photo-detectors made from gallium phosphide (GaP), gallium arsenide phosphide (GaAsP), or silicon, depending on wavelength and interference filters, which are used to determine the spectral selection (Eklundh et al., 2011; Robinson et al., 1979) (Figure 2.2a). On the contrary digital cameras are based on CCD (charge-coupled device) or CMOS (Complementary Metal Oxyde Semiconductor) detectors that are linear photoconductive devices (Lebourgeois et al., 2008), having different spectral bands response according to the detector used, generally wider than the radiometersand spectrometers (Figure 2.2b).

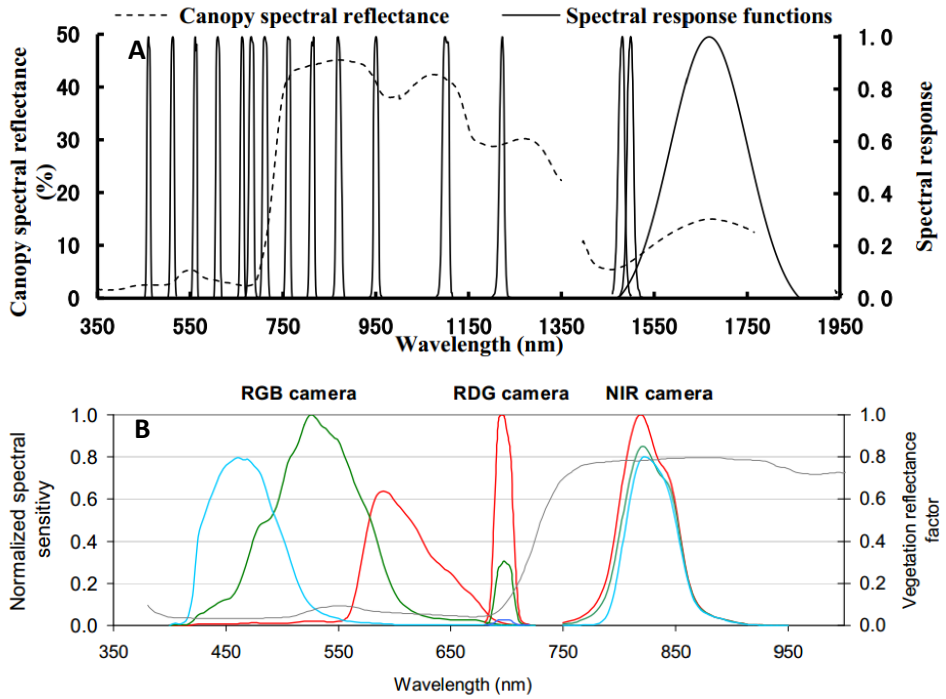

Figure 2.2 a)The canopy spectral reflectance of winter wheat (dashed line) and the spectral response function of multiband radiometer Cropscan(Yao et al., 2013). b) Normalized spectral sensitivity of the original (RGB) and modified (Red edge green, RGD and Near infrared, NIR) channels of a CANON EOS 400D cameras. The colours of the lines correspond to the camera channels. The grey line is a standard reflectance profile of a green vegetation canopy (Lebourgeois et al., 2008)

In the vegetation monitoring context multispectral sensors are used to provide data on vegetation growing status and phenology or to define empirical relationship with biochemical or biophysical parameters of the vegetation (e.g. leaf area index and chlorophyll content). Multispectral sensors are characterized by relatively low cost, easy maintenance, and low power consumption, and are hence useful tool for long-term unmanned field measurements.The multi-band radiometer sensors typically measure at 10-50 nm bandwidth in visible, near infrared (NIR), and shortwave infrared (SWIR) wavelength bands. The most common bands are Red (~650 nm) and NIR (~850 nm) due to the contrasting vegetation response in Red and NIR wavelengths (Balzarolo et al., 2011). Digital camera for phenological cycle analysis have bands centered in Red and NIR (Petach et al., 2014; Sakamoto et al., 2011) even if the more common analyses make use of the green channel, expressed as green chromatic coordinate, to track phenological development of vegetation (Migliavacca et al., 2011; Richardson et al., 2007; Sonnentag et al., 2012).

2.2.2 Hyperspectral devices

Hyperspectral data are acquired with spectroradiometers systems. Spectroradiometers are devices designed to measure the radiation in a given wavelength interval, typically with high spectral sampling intervals (~1 to 3 nm) and with narrow band widths (<10 nm).Example of the spectral response of a spectroradiometer is reported in Figure 2.3. The incoming radiation

isusually dispersed by optical elements (i.e gratings) at different wavelengths. Generally, a spectrometer is made by three different categories of component:

- Optical components such as lenses, mirrors, gratings and aperture slit which allow the dispersion of the radiation at different wavelength.

- Detectors (example for the visible and near infrared region is the Charge-Coupled Device, CCD) which are photosensitive elements able to accumulate electric charge proportional to the incident radiation.

- Processor designed to convert electrons into appropriate digital signal.

The specific design can vary according to technical differences in spectrometer models. Each of the optical components, the detector performances and the processor can produce differences which can affect the reliability and the repeatability of the measurements. The description of the instrument performances referred to standard references is called characterization (see chapter 3 for more detailed description of the characterization process).

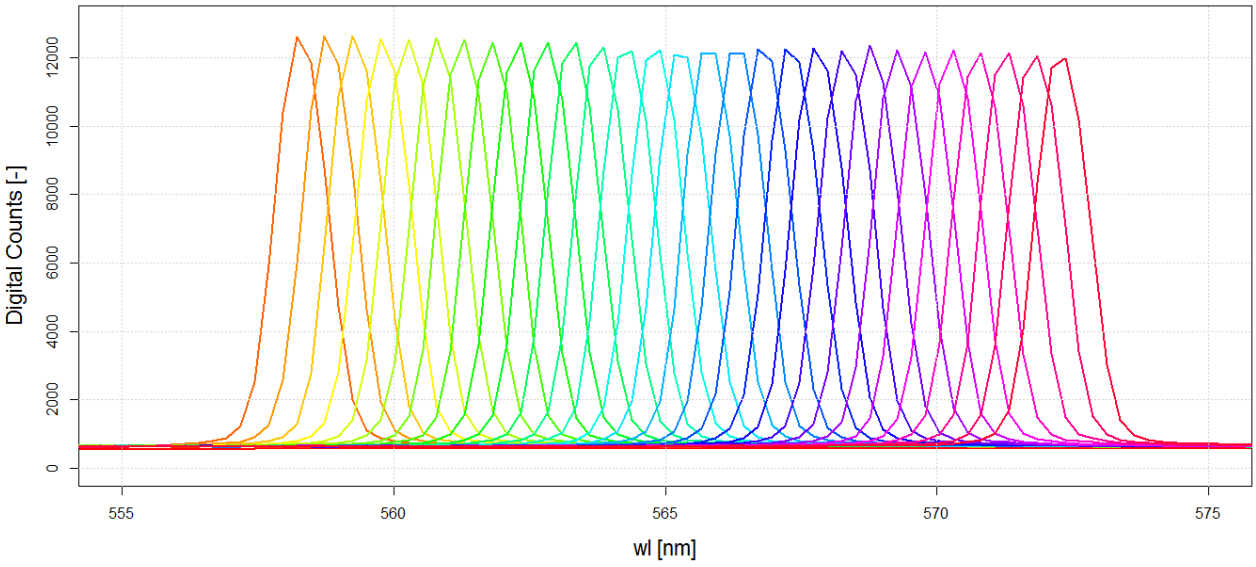

Figure 2.3 Spectral response functions scan of the Ocean Optics (USA) HR4000spectroradiometer (FWHM = 0.1 nm, Spectral sampling 0.02 nm). Measurements are performed using a double monochromator(OL 750-M-D, OPTE-E-MA Engineering GmbH)scanning at 0.5 nm. The measurements reported refer to the spectral range 560 nm – 580 nm, with an interval equal to 0.5 nm.

Spectroradiometers differ from multispectral instruments in their cost (approximately €3000 for multispectral sensors to upwards of €60,000 for a full wavelength (400 nm to 2,500 nm) hyperspectral system). Similarly, they vary from their multispectral counterparts in being more susceptible to damage (many have complex electronic components and internal moving parts), and have thus been generally considered less suitable for year-round unattended deployment in the field (with a few notable exceptions, e.g. Hilker et al.,(2011), Nakaji et al., (2007),Sims et al., (2006) and Meroni et al., (2011)). Their optical configuration relies on either

fibre-optic cable bundle or a complex optical path comprising of mirrors, lens and beam. As a result, some of such systems are also considerably larger and heavier than their multispectral counterparts, which in some cases present a challenge to their deployment in the field. Primarily there are two field spectroscopy measurement approaches: single beam (SB), and dual beam (DB) mode (Milton et al., 2009). In SB mode a measurement is first taken of a reference standard, most commonly a Spectralon reference panel, followed as quickly as possible by a measurement of the target surface. The target measurements per wavelength interval are subsequently divided by the reference measurement per wavelength interval to calculate Relative Reflectance factors. To attempt to make these measurements simultaneously, and minimise changes in irradiance between them, DB mode may be adopted. DB mode normally requires two spectrometers and takes longer to set up in the field so its use for periodic field sampling is limited. However can be reliably made and high quality data acquired if contemporary field-derived spectrometer inter-calibration functions are determined (Anderson et al., 2006).

2.3Potential of optical proximal sensing methods to monitor vegetation properties

A wealth of previous research has pointed to the capability of field optical measurements for providing high quality, detailed information on key vegetation parameters that could potentially be used to derive information about leaf and canopy biochemistry, vegetation stress and seasonal dynamics (Ustin et al., 2009). Optical proximal sensing techniques can offer different information if deployed at different scales. At a fine spatial scale the optical properties of individual reflecting elements such as leaves can be investigated; at a coarser spatial scale the properties of spatial assemblages of elements of the vegetation canopies can be investigated, whilst at the coarsest scale, these instruments could potentially be used to provide data for the vicarious calibration of satellite sensors that are measuring vegetation dynamics at global scales, and potentially to validate measurements made from airborne or satellite sensors(Milton et al., 2009; Morisette et al., 2002; Schaepman et al., 2009). At field level, proximal sensed measurementscan provide valuable information for monitoring phenological and physiological traits of the vegetation(Gitelson and Merzlyak, 1996; Pettorelli et al., 2005; Tucker and Sellers, 1986).

Broad band and narrowband sensors have been largely used for field level sampling of the optical properties of the vegetation and to indirectly derive biochemical and biophysical properties of the monitored vegetation (Biging and Larrieu, 2003; Haboudane et al., 2002; Sims and Gamon, 2002). Moreover, optical proximal sensed data are commonly used to calibrate and validate airborne or satellite products (Morisette et al., 2002) and to constrain process-based models of Earth' surface and atmosphere (Milton et al., 2009)both at local and global scale.

In the next paragraphs the application of optical proximal sensing technique to retrieve information of the vegetation is described.

2.2.1 Plant biochemical and biophysical parameter estimates

2.2.1.1 Leaf Area Index

Leaf Area Index (LAI) was firstly defined by Watson (1947) as the total one-sided area of leaf tissue per unit ground surface area (i.e. m^2/m^2). According to this definition, LAI is a dimensionless quantity characterizing the canopy of an ecosystem. Leaf area index drives both the within- and the below-canopy microclimate, determines and controls canopy water interception, radiation extinction, water and carbon gas exchange and is, therefore, a key component of biogeochemical cycles in ecosystems (Bréda, 2003). LAI can be measured by either direct or indirect methods. Direct methods are the most accurate, but they have the disadvantage of being extremely time-consuming and as a consequence making large-scale implementation only marginally feasible (Jonckheere et al., 2004). Indirect methods use generally information of other variable to infer leaf area of the analysed canopy. Generally they are faster and useful for sampling wider areas. These techniques became more and more important and largely diffused in recent years. The most common indirect methods used for LAI estimation are briefly described below. LAI can be infer through its allometric relationship with other forest variables(Le Dantec et al., 2000)describing plant dimension (i.e. tree height, diameter-at-breast-height). In the last two decades indirect non-contact methods have been implemented and applied. These methods are based on the Beer–Lambert law to take into account the fact that the total amount of radiation intercepted by a canopy layer depends on incident irradiance, canopy structure and optical properties (Jonckheere et al., 2004). The most widely used sensors belonging to this category of measurements are ceptometers (i.e. LAI-2000) and digital cameras equipped with hemispherical optics(Mailly et al., 2013). Such techniques are affected by errors that can occur at any stage of data acquisition or analysis. Richardson et al., (2011)evaluated that the uncertainty associated with indirect LAI measurements (both with digital hemispheric cameras and ceptometers) can be about 10-20%.

Alternative methods to extract LAI values from optical remote and proximal sensing data have been successfully tested. Two main types of approaches have been developed to estimateLAI using optical spectral properties of the vegetation: i) inversions of canopy radiative transfermodels (Fang, 2003; Meroni et al., 2004; Schlerf and Atzberger, 2006); and ii) empirical linear and non-linear relationshipsbetween LAI andspectral vegetation indices(Biging and Larrieu, 2003; Colombo et al., 2003; Darvishzadeh et al., 2009, 2008; Haboudane, 2004). The two approaches are quite complementary but the vegetationindices have seen a more widespread use due to their ease ofcomputation compared to the extreme difficulty to obtain optimal parameters for radiativetransfer model inversions (Viña et al., 2011). Most of the spectral vegetation indices used for LAI estimatesare mathematical combinations of different spectral

bands mostly in the visible and near infrared regions of the electromagnetic spectrum. Spectral vegetation indices constitute a simple and convenient approach to extract information from remotely sensed data, due to their ease of use, which facilitates the processing and analysis of large amounts of data. In fact linear and non-linear (Figure 2.4) relationships between optical spectral vegetation indices and LAI have been found for different vegetation types and climatic conditions. However these empirical relationships depend on a number of external factors as vegetation species, site and sampling conditions, sensor characteristics, and generally are unsuitable for application to large areas or in different phenological season.

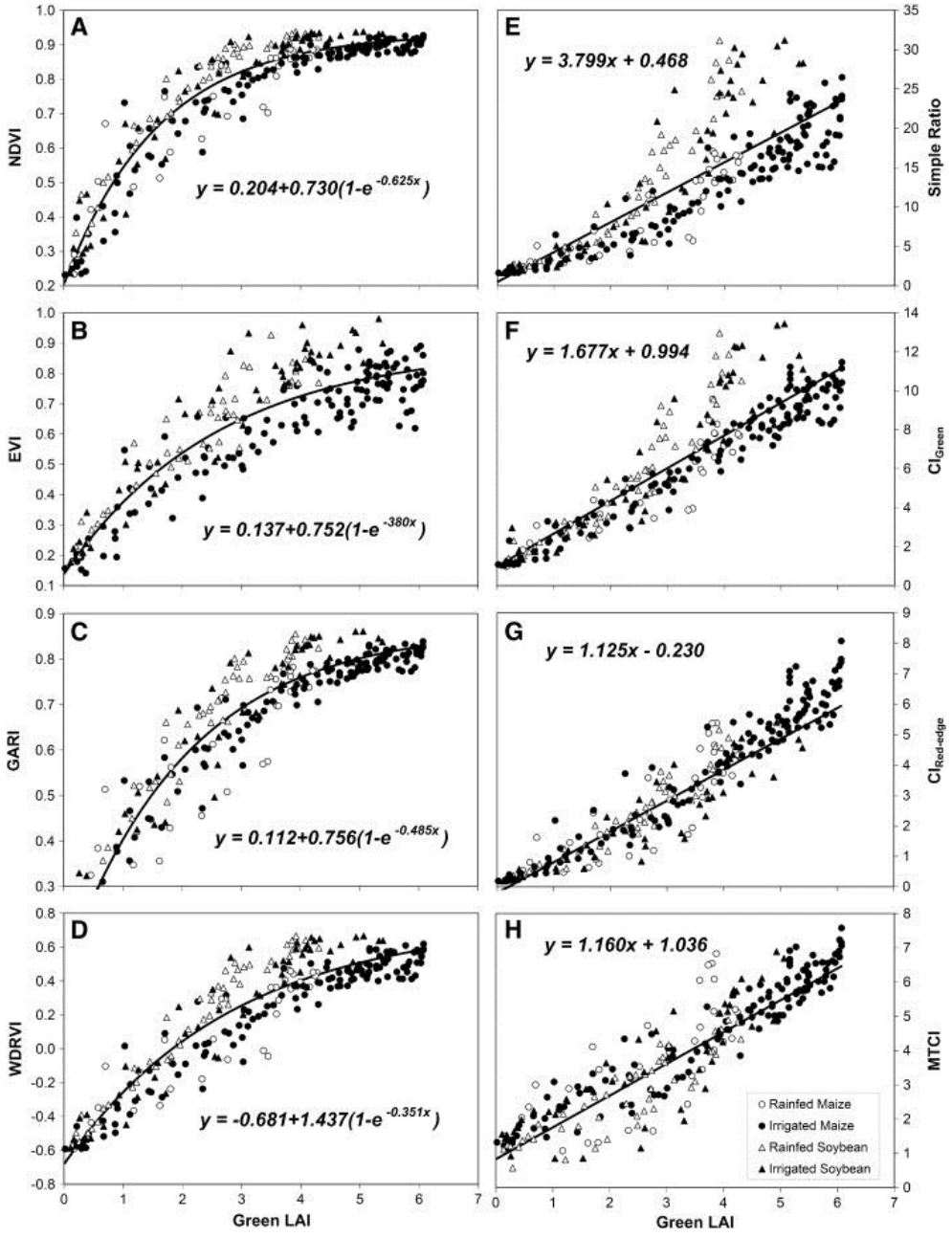

Figure 2.4 Relationshipsbetween spectral vegetation indices such as (A) NDVI, (B) EVI, (C) GARI, (D) WDRVI (E) Simple Ratio, (F) CI_{Green}, (G) $CI_{Red-edge}$, and (H) MTCI and Green LAI, for maize and soybean in irrigated and rainfedfieldsduring the growingseasons of 2001–2004. Lines correspond to best fit functions.Reference:Viña et al., (2011).

2.2.1.2 Chlorophyll content estimation

There are various techniques to measure destructively chlorophyll content, including spectrophotometry and high performance liquid chromatography (HPLC). Spectrophotometry is the classical method of determining the quantity of chlorophyll. It involves the collection of a fairly large, mechanical rupturing of the collected cells, and extraction of the chlorophyll from the disrupted cells into the organic solvent. The extract is then analysed by either a spectrophotometric method exploiting the known optical properties of chlorophyll, or by HPLC. All these techniques are expensive and time consuming. Therefore in the last decades alternative solutions of leaf pigment content determination with in-situ non-destructive optical methods have been developed (Gitelson et al., 2003; Haboudane, 2004). In fact, research activities have focused on understanding the relationships between vegetation optical properties and photosynthetic pigments concentrations within green leaves tissues, namely: chlorophyll-a, chlorophyll-b (Haboudane et al., 2002). These pigments have specific absorption features and they typically affect leaf reflectance in the visible region.The spectral regions that are identified as the most suitable to chlorophyll effects are those around 680 nm, corresponding to absorption peak of chlorophyll-a, and 550 nm matching with the minimum chlorophyll absorption in the visible domain. These characteristics have promoted the development of various approaches, based on optical data through model inversion (Zarco-Tejada et al., 2004, 2001) or the use of empirical and semi-empirical methods, to estimate the chlorophyll content at canopy scales as depicted in Figure 2.5 (Card et al., 1988; Darvishzadeh et al., 2008; Dash and Curran, 2004; Gitelson et al., 2003, 1996; Thiemann and Kaufmann, 2000).

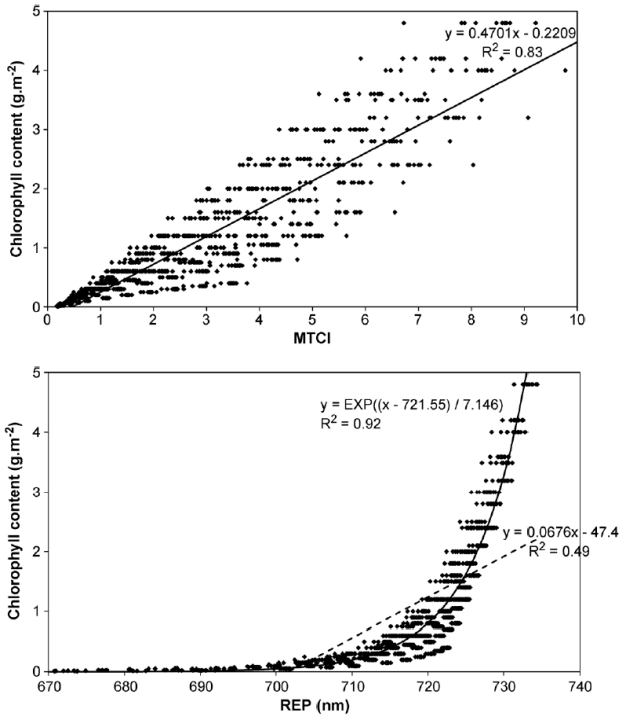

Figure 2.5Left panel: Relationship between MTCI and chlorophyll content; right panel relationship between REP and chlorophyll content (based on PROSAIL model simulations withvarying input parameters). Reference: Clevers and Kooistra, (2012).

As for LAI calculation the difficulty in parameterize radiative transfer model facilitates the diffusion of empirical based approach for chlorophyll content estimation. Investigations have been carried out evaluating the relationship between chlorophyll contentand reflectance based vegetation indices (as individual narrow bands, band reflectance ratios and combinations). Several indices have been proposed in literature (e.g. MERIS Terrestrial Chlorophyll Index (MTCI), Red Edge Position (REP), Soil-Adjusted Vegetation Index (OSAVI), Red-edge Chlorophyll index, CI). This indices have been developed to minimize dependency of vegetation canopy reflectance owing to extraneous factors (influences of below canopy bare soil, canopy structure, amount of biomass, overlap absorption spectra of different pigments etc.) and maximizing the sensitivity to chlorophyll content (Chappelle et al., 1992; Penuelas et al., 1995). Each index can show a different relationship with the Chl content, and especially for high Chl content the saturation effect can appear. Therefore indices with linear relationship are therefore preferred (e.g. MTCI, CI).

2.2.2 *Plant phenology*

Phenology is defined as "the study of the timing of recurrent biological events, the causes of their timing with regard to biotic and abiotic forces, and the interrelation among phases of the same or different species" (Lieth, 1976). Phenological studies have been performed in agriculture to document events such as plant emergence, fruiting and harvest. More recently phenology has been recognized as an important integrative method for assessing the impact of climate variability and climate change on ecosystems(Menzel, 2002; Peñuelas et al., 2009; Richardson et al., 2013). Recent global warming has had significant effects on the seasonality of ecosystems. Phenological events such as green-up, flowering and senescence offer the possibility to get information about ecosystem responses to climate and can be used in climatological and ecological models(Cleland et al., 2007; Jolly et al., 2005; Vitasse et al., 2011). Shifts in phenology can significantly affect the global carbon and water cycle. Consequently, the knowledge and understanding of these phenological processes is needed for the parameterization of models used in climate predictions(Arora and Boer, 2005; Wolkovich et al., 2012).

Traditional methods used to monitor plant phenology mainly consist of field observations and remote sensing satellite data(e.g. Busetto et al., 2010; Linderholm, 2006). However, both strategies present some limits in terms of spatial and temporal resolution. Direct phenological surveys can hardly provide continuous and quantitative information on plant phenology and do not allow the covering of wide areas (Schwartz et al., 2002). Moreover, those observations do not often refer to the phenology of a whole community but to single species, and they might be affected by observer subjectivity. While satellite products can provide invaluable synoptic phenological information, they do not allow a detailed evaluation of the variability in species responses (Ide and Oguma, 2013). Furthermore, according to the monitored site the use of

medium to coarse resolution satellite data is often challenging due to variable complex topography and habitat fragmentation (e.g. in mountainous areas).

Several studies have demonstrated the capability of optical proximal sensors provide accurate phenological information. The sensors are usually fixed above a vegetated target (e.g. forests, croplands, grasslands and peatlands) and the data are continuously acquired during the season. The optical informationacquired by the instruments are usually expressed in terms of vegetation indices (e.g. Normalized difference Vegetation Index, NDVI) for radiometers or spectroradiometers or in terms of chromatics coordinates per region of interest (e.g. green chromatic coordinates, gcc) for digital camera.The indices are used as indicators of canopy development and the time series of the indices extracted can be then analysed to identify the timing of key phenological events.To minimise the effects of changing illumination conditions in the season generally normalized indices are considered. The indices time series data noise is usually reduced applying filtering strategies (Sakamoto et al., 2005; Sonnentag et al., 2012) and fitted with different functions (e.g. cubic spline or logistic function). Phenological dates are then associated to specific metrics calculated on the fitted function. As an example the beginning of the season can be defined as the date when the index curve reaches the half of the growth (Bradley et al., 2007). More recently the Bayesian multiple change point analysis has been applied in phenological studies to estimate reliably phenological events in the growing season, especially when handling low quality digital camera data(Henneken et al., 2013). Example of metrics extraction based on the last Bayesian method is reported in Figure 2.6.

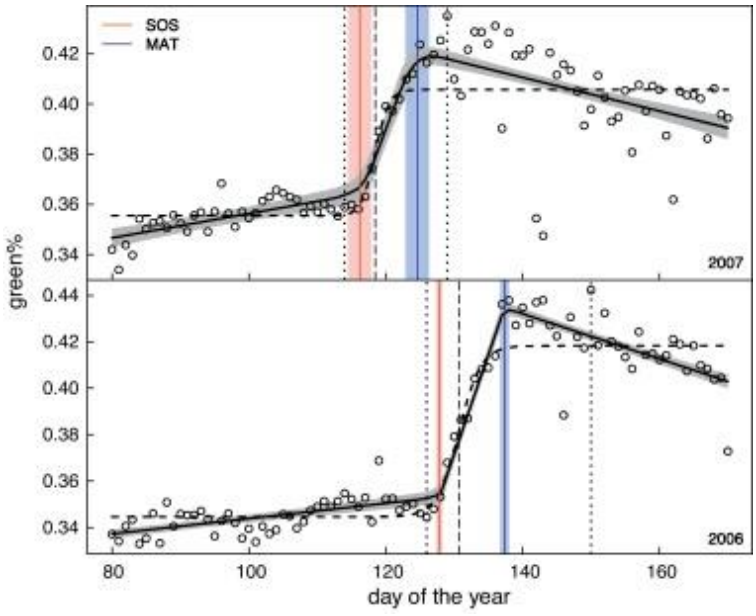

Figure 2.6Bayesian change point models of green% of aspen in spring 2006 and 2007. The heavy continuous curve is the expectation value, the shaded band the ±1σ uncertainty of this estimate. Dashed vertical line shows spring value based on the sigmoidal logistic fit, dashed line, dotted lines show the beginning of the season and maturity dates. Reference: Henneken et al., (2013.)

Digital cameras have been demonstrated to be excellent tools for observing the greenness and leaf status of vegetation stands(Ahrends et al., 2008; Richardson et al., 2007). Data from these cameras are useful for investigating effects of weather events(Ide and Oguma, 2013), and can,

depending on how they are mounted, be used for observing different parts of the forest stand(Alberton et al., 2014; Mizunuma et al., 2013). However, there is a lack of common standards for phenology cameras. Absolute calibration of the recorded data is rarely done, and signal and spectral drifts are problems that are difficult to quantify (Hufkens, 2012; Ide, 2010).Cameras and radiometric sensors should be viewed as complementary tools for monitoring the phenology of vegetation stands(Eklundh et al., 2011).

2.2.3 *Plant physiology via fluorescence and optical indices*

Plant physiology is defined as the study of plant functions, referred to growth dynamics, metabolism and reproductive processes (Taiz and Zeiger, 2010). Photosynthesis is the physiological process by which plants synthesize complex molecules as carbohydrates and produce oxygen (O_2), starting from simple molecules as carbon dioxide (CO_2) and water and using light as source of energy. The light-dependent reactions are the first stage of photosynthesis and involve photosynthetic pigments, chlorophylls and carotenoids to capture and store energy from sunlight. During this process, light energy is converted into chemical energy, in the form of molecules of ATP and NADPH and water is oxidized with production of O_2. In higher plants, light-dependent reactions (which use the so called Photosynthetically Active Radiation, PAR, approximately between 400 and 700 nm.) take place on the internal membranes (thylakoid) inside the photosynthetic organelles, the chloroplasts, where specialized molecular complexes (photosystems) catalyse the light-dependent reactions through a series of redox reactions, called on the whole, electron transport chain. On a daily as well as seasonal basis most plants receive more sunlight than they can actually use for photosynthesis. Under these circumstances, regulation of light harvesting is necessary to balance the absorption and utilization of light energy, thereby minimizing the potential for photo-oxidative damage (Muller, 2001). In fact over-reduction and over-oxidation of the electron transport carriers prevents the smooth running of photosynthesis, necessitating of mechanism that regulate cellular redox potential (Flexas et al., 2012). Typically two dissipative pathways have been described to dissipate the exceeding energy: Non-Photochemical Quenching (NPQ) and Chlorophyll fluorescence.

Although the exact mechanisms of NPQ are not completely understood,NPQ is generally divided into at least three different components according to their relaxation kinetics in darkness following a period of illumination, as well as their response to different inhibitors (Horton and Hague, 1988). The major and most rapid component is the pH- or energy dependent component, qE. A second component, qT, relaxes within minutes and is more important in algae, but rather negligible in most plants during exposure to excess light. The third component of NPQ shows the slowest relaxation and is the least defined. It is related to photo-inhibition of photosynthesis and is therefore called qI. Absorption of sunlight that exceeds a plant's capacity

for CO_2 fixation results in a build-up of the thylakoid ΔpH that is generated by photosynthetic electron transport. The decrease in pH within the thylakoid lumen is an immediate signal of excessive light that triggers the feedback regulation of light harvesting by qE. A decrease in lumen pH induces qE through protonation of Photosystem II proteins and activation of xanthophyll synthesis via a xanthophyll cycle. The latter involves the conversion of the violaxanthin carotenoid, a xanthophyll with two epoxide groups, first to antheraxanthin and then to zeaxanthin (no epoxide group). Laboratory studies have identified an absorbance feature at 505 nm (Bilger et al., 1989) and a reflectance feature at 531 nm (Gamon et al., 1990) associated with the conversion of violaxanthin to zeaxanthin.

Beside the NPQ the second pathway of energy dissipation is operated by the chlorophyll pigments as fluorescence, the emission of light at a longer wavelength than ones for excitation. Fluorescence is emitted by Chlorophyll *a* of both Photosystem (PS) I and II, protein-pigment complexes involved in the first stages of photosynthesis. It's a radiative deactivation process (Photochemical quenching, qP) and competes with NPQ for the dissipation of exceeding light energy. The fluorescence emission spectrum exhibits two peaks in the red and near infrared regions, with maxima around 690 nm and 740 nm (Buschmann, 2007; Lichtenthaler et al., 1986). The first peak has been attributed primarily to Chls associated with PS II, whereas the second has been attributed to antenna Chls of both PSs II and I (Agati et al., 2000; Bose, 1982; Pfündel, 1998). In particular the intensity of Chlorophyll fluorescence is mainly affected by the redox state of the electron carrier QA, a plastoquinone that undergoes a one-electron photo-reduction in the PSII (Franck et al., 2002).

The physiological processes previously described occur on a short-term by altering or rearranging the pigments within the leaves without determining any detectable changes in reflectance regions (Red and Near Infrared regions) traditionally used for the calculation of vegetation indices related to green biomass (such as the NDVI). New generation ofremote/proximal techniques offers the possibility to monitor these dissipation pathways of vegetation (Meroni et al., 2008). In fact photochemical reflectance index (PRI) and the emission of chlorophyll fluorescence have been used for a number of years to assess photosynthetic efficiency at the leaf level (Gamon et al., 1992; Porcar-Castell et al., 2012). Recent technological advances now make it possible to estimate PRI and the emission of sun induced fluorescence (SIF) at canopy level (Drolet et al., 2014; Frankenberg et al., 2012; Meroni et al., 2010; Panigada et al., 2014; Rossini et al., 2014, 2012, 2010). Both PRI and SIF can be monitored by using multispectral narrow band radiometers or spectroradiometers.

PRI is based on the reflectance change due to the conversion of violaxanthin to zeaxanthin occurring during the xanthophyll cycle at 531 nm(Figure 2.7), and it is shown to be inversely related to NPQ (Filella et al., 2009; Penuelas et al., 1997). It is typically calculated as $[R_{531}-R_{570}]/[R_{531}+R_{570}]$, where R indicates reflectance and numbers indicate wavelength nanometers at the center of the bands. The 531 reflectance bands is affected by chlorophyll

and carotenoids absorption while R_{570} only refer to chlorophyll. Consequently, it can serve as an index of relative chlorophyll/carotenoid ratio (Stylinski et al., 2002). Together, these responses to de-epoxidation state of the xanthophyll cycle and to chlorophyll/carotenoid ratios ensure that PRI scales with photosynthetic efficiency across a wide range of conditions, species and functional types (Garbulsky et al., 2011).

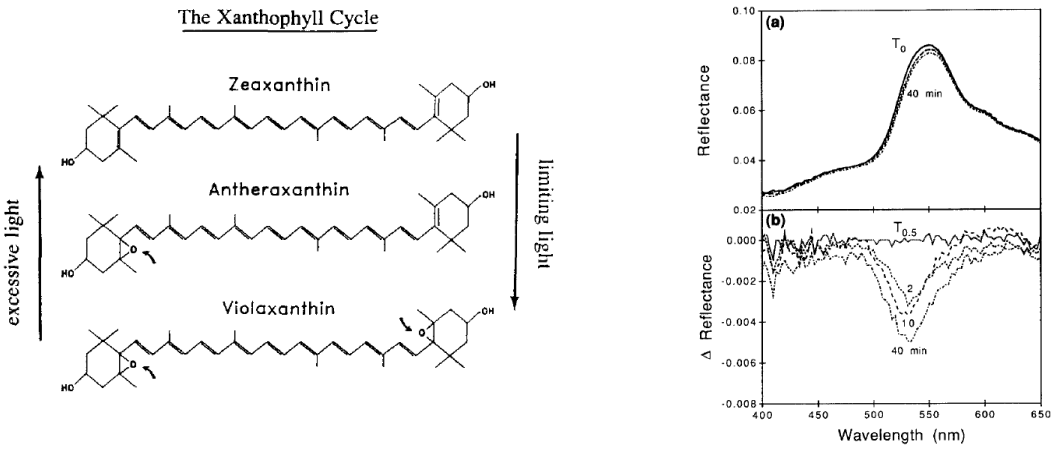

Figure 2.7. Left panel: The xanthophyll cycle. Excessive absorbed PAR causes the deepoxidation of violaxanthin to zeaxanthin via antheraxanthin, and this process is reversed under limiting PAR. The difference spectrum associated with these pigment conversions results in a detectable "signal" near 531 nm in the reflectance spectra of intact leaves and canopies. Right panel: A) Reflectance spectra from a control sunflower canopy upon sudden removal of shade at midday. B) Delta reflectance (reflectance at time n minus reflectance at time zero) following shade removal. Reference: Gamon et al., (1992).

On the contrary SIF adds a weak signal to reflected solar radiation (1–5% of the reflected radiation in the near). Zarco-Tejada et al. (2000) first recognized the effect of fluorescence on reflectance and demonstrated that it is possible to detect the SIF signal using hyperspectral reflectance measurements. The SIF signal can be detected passively exploiting regions of the atmospheric spectrum where the incident irradiance is strongly reduced due to absorption in the Earth's atmosphere or in the solar atmosphere. In the visible and near-infrared, the solar spectrum at ground level exhibits three main "*Fraunhofer*" features which have been exploited for SIF estimation: Ha due to hydrogen (H) absorption in the solar atmosphere (centered at 656.4 nm) and two telluric oxygen (O_2) absorption bands in the Earth atmosphere, O_2-B (687.0 nm) and O_2-A (760.4 nm). The O_2 absorption bands were used more extensively than the H feature because, when observed with typical resolutions from a tenth of a nanometer to a few nanometers they appear wider and deeper. Moreover, they are spectrally closer to the peaks of the fluorescence emission spectrum positioned at about 690 and 740 nm thus making the contribution of fluorescence to the overall upwelling signal more significant. Example of solar irradiance, refected radiance and target reflectance are depicted in Figure 2.8. The Figure refers to the O_2-A absorption band that is exploited to decouple the fluorescence signal from the reflected radiance. The peak in the reflectance (black line) is due to the fluorescence emission when the target radiance is normalized by the solar irradiance.

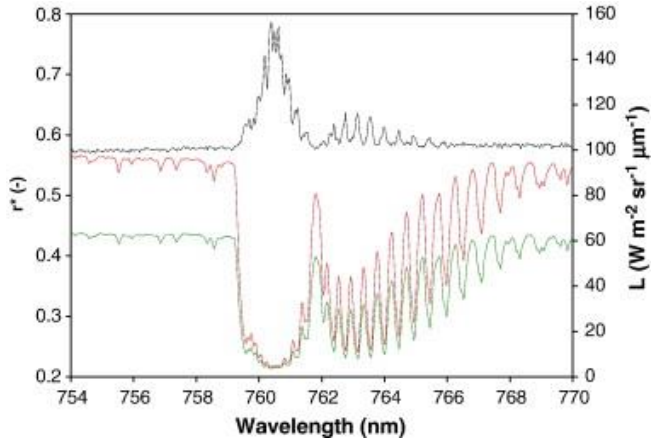

Figure 2.8Apparent reflectance (black curve) at the O_2-A band calculatedfrom incident and upwelling radiances (red and green curves, respectively) over a white clovercanopy. Measurements collected by a spectroradiometer characterized by a FWHM of 0.13 nm. Reference: Meroni et al.,(2009).

An exhaustive review of the methods applied in the SIF estimates is reported in (Meroni et al., 2009). Overall methods used to quantify SIF are divided into two major categories: radiance-based and reflectance-based approaches. The former makes use of radiance measurements (in physical units or instrument counts) and exploits the Fraunhofer line to decouple SIF from the reflected flux. The latter operates with spectral reflectance and does not necessarily require correspondence to a Fraunhofer line. While the radiance-based approach is able to estimate SIF, either in physical or auxiliary units, the reflectance-based approach provides spectral indices which are related to the effect of SIF on reflectance. Radiance-based approaches allow fluorescence estimation in physical units (i.e., radiance units) if the data are radiometrically calibrated. They exploit the narrow absorption feature of a Fraunhofer line and thus make use of high spectral resolution data. Some methods proposed in the literature require 2–3 spectral channels near the investigated absorption line (i.e. FLD, Fraunhofer Line Depth; 3FLD, 3 bands FLD; cFLD, corrected FLD) while some other require a set of contiguous channels covering the whole spectral range of interest, a characteristic of hyperspectral data (iFLD, improved FLD; eFLD, extended FLD; SFM, Spectral Fitting Method).

References

Agati, G., Cerovic, Z.G., Moya, I., 2000. The Effect of Decreasing Temperature up to Chilling Values on the in vivo F685/F735 Chlorophyll Fluorescence Ratio in Phaseolus vulgaris and Pisum sativum: The Role of the Photosystem I Contribution to the 735 nm Fluorescence Band¶. Photochem. Photobiol. 72, 75.

Ahrends, H.E., Bräugger, R., Stöckli, R., Schenk, J., Michna, P., Jeanneret, F., Wanner, H., Eugster, W., 2008. Quantitative phenological observations of a mixed beech forest in northern Switzerland with digital photography. J. Geophys. Res. Biogeosciences 113, G04004.

Alberton, B., Almeida, J., Helm, R., da S. Torres, R., Menzel, A., Morellato, L.P.C., 2014. Using phenological cameras to track the green up in a cerrado savanna and its on-the-ground validation. Ecol. Inform. 19, 62–70.

Anderson, K., Milton, E.J., Rollin, E.M., 2006. Calibration of dual-beam spectroradiometric data. Int. J. Remote Sens. 27, 975–986.

Arora, V.K., Boer, G.J., 2005. A parameterization of leaf phenology for the terrestrial ecosystem component of climate models. Glob. Chang. Biol. 11, 39–59.

Balzarolo, M., Anderson, K., Nichol, C., Rossini, M., Vescovo, L., Arriga, N., Wohlfahrt, G., Calvet, J.-C., Carrara, A., Cerasoli, S., Cogliati, S., Daumard, F., Eklundh, L., Elbers, J.A., Evrendilek, F., Handcock, R.N., Kaduk, J., Klumpp, K., Longdoz, B., Matteucci, G., Meroni, M., Montagnani, L., Ourcival, J.-M., Sánchez-Cañete, E.P., Pontailler, J.-Y., Juszczak, R., Scholes, B., Martín, M.P., 2011. Ground-Based Optical Measurements at European Flux Sites: A Review of Methods, Instruments and Current Controversies. Sensors 11, 7954–7981.

Biging, G.S., Larrieu, M.R., 2003. Estimation of forest leaf area index using vegetation indices derived from hyperion hyperspectral data. IEEE Trans. Geosci. Remote Sens. 41, 1355–1362.

Bilger, W., Björkman, O., Thayer, S.S., 1989. Light-induced spectral absorbance changes in relation to photosynthesis and the epoxidation state of xanthophyll cycle components in cotton leaves. Plant Physiol. 91, 542–551.

Bose, S., 1982. CHLOROPHYLL FLUORESCENCE IN GREEN PLANTS AND ENERGY TRANSFER PATHWAYS IN PHOTOSYNTHESIS. Photochem. Photobiol. 36, 725–731.

Bradley, B.A., Jacob, R.W., Hermance, J.F., Mustard, J.F., 2007. A curve fitting procedure to derive inter-annual phenologies from time series of noisy satellite NDVI data. Remote Sens. Environ. 106, 137–145.

Bréda, N.J.J., 2003. Ground-based measurements of leaf area index: a review of methods, instruments and current controversies. J. Exp. Bot. 54, 2403–17.

Buschmann, C., 2007. Variability and application of the chlorophyll fluorescence emission ratio red/far-red of leaves. Photosynth. Res. 92, 261–71.

Busetto, L., Colombo, R., Migliavacca, M., Cremonese, E., Meroni, M., Galvagno, M., Rossini, M., Siniscalco, C., Morradi Cella, U., PARI, E., 2010. Remote sensing of larch phenological cycle and analysis of relationships with climate in the Alpine region. Glob. Chang. Biol.

Card, D.H., Peterson, D.L., Matson, P.A., Aber, J.D., 1988. Prediction of leaf chemistry by the use of visible and near infrared reflectance spectroscopy. Remote Sens. Environ. 26, 123–147.

Chappelle, E.W., Kim, M.S., McMurtrey, J.E., 1992. Ratio analysis of reflectance spectra (RARS): An algorithm for the remote estimation of the concentrations of chlorophyll A, chlorophyll B, and carotenoids in soybean leaves. Remote Sens. Environ. 39, 239–247.

Cleland, E.E., Chuine, I., Menzel, A., Mooney, H.A., Schwartz, M.D., 2007. Shifting plant phenology in response to global change. Trends Ecol. Evol. 22, 357–65.

Clevers, J.G.P.W., Kooistra, L., 2012. Using hyperspectral remote sensing data for retrieving canopy chlorophyll and nitrogen content. IEEE J. Sel. Top. Appl. Earth Obs. Remote Sens. 5, 574–583.

Colombo, R., D. Bellingeri, D. Fasolini, C. M. Marino, 2003. Retrieval of leaf area index in different vegetation types using highresolution satellite data. Remote Sens. Environ.86, 120 – 131.

Darvishzadeh, R., Atzberger, C., Skidmore, A.K., Abkar, A.A., 2009. Leaf Area Index derivation from hyperspectral vegetation indicesand the red edge position. Int. J. Remote Sens. 30, 6199–6218.

Darvishzadeh, R., Skidmore, A., Schlerf, M., Atzberger, C., Corsi, F., Cho, M., 2008. LAI and chlorophyll estimation for a heterogeneous grassland using hyperspectral measurements. ISPRS J. Photogramm. Remote Sens. 63, 409–426.

Dash, J., Curran, P.J., 2004. The MERIS terrestrial chlorophyll index. Int. J. Remote Sens. 25, 5403–5413.

Drolet, G., Wade, T., Nichol, C.J., MacLellan, C., Levula, J., Porcar-Castell, A., Nikinmaa, E., Vesala, T., 2014. A temperature-controlled spectrometer system for continuous and unattended measurements of canopy spectral radiance and reflectance. Int. J. Remote Sens. 35, 1769–1785.

Eklundh, L., Jin, H., Schubert, P., Guzinski, R., Heliasz, M., 2011. An optical sensor network for vegetation phenology monitoring and satellite data calibration. Sensors (Basel). 11, 7678–709.

Fang , H., 2003. Retrieving leaf area index using a genetic algorithm with a canopy radiative transfer model. Remote Sens. Environ.85, 257 – 270.

Filella, I., Porcar-Castell, A., Munné-Bosch, S., Bäck, J., Garbulsky, M.F., Peñuelas, J., 2009. PRI assessment of long-term changes in carotenoids/chlorophyll ratio and short-term changes in de-epoxidation state of the xanthophyll cycle. Int. J. Remote Sens. 30, 4443–4455.

Franck, F., Juneau, P., Popovic, R., 2002. Resolution of the Photosystem I and Photosystem II contributions to chlorophyll fluorescence of intact leaves at room temperature. Biochim. Biophys. Acta - Bioenerg. 1556, 239–246.

Frankenberg, C., O'Dell, C., Guanter, L., McDuffie, J., 2012. Remote sensing of near-infrared chlorophyll fluorescence from space in scattering atmospheres: implications for its retrieval and interferences with atmospheric CO_2 retrievals. Atmos. Meas. Tech. 5, 2081–2094.

Gamon, J.A., Field, C.B., Bilger, W., Björkman, O., Fredeen, A.L., Peñuelas, J., 1990. Remote sensing of the xanthophyll cycle and chlorophyll fluorescence in sunflower leaves and canopies. Oecologia 85, 1–7.

Gamon, J.A., Peñuelas, J., Field, C.B., 1992. A narrow-waveband spectral index that tracks diurnal changes in photosynthetic efficiency. Remote Sens. Environ. 41, 35–44.

Garbulsky, M.F., Peñuelas, J., Gamon, J., Inoue, Y., Filella, I., 2011. The photochemical reflectance index (PRI) and the remote sensing of leaf, canopy and ecosystem radiation use efficienciesA review and meta-analysis. Remote Sens. Environ. 115, 281–297.

Giardino, C., Brivio, P.A., 2003. The application of a dedicated device to acquire bidirectional reflectance factors over natural surfaces. Int. J. Remote Sens. 24, 2989–2995.

Gitelson, A.A., Gritz, Y., Merzlyak, M.N., 2003. Relationships between leaf chlorophyll content and spectral reflectance and algorithms for non-destructive chlorophyll assessment in higher plant leaves. J. Plant Physiol. 160, 271–82.

Gitelson, A.A., Kaufman, Y.J., Merzlyak, M.N., 1996. Use of a green channel in remote sensing of global vegetation from EOS-MODIS. Remote Sens. Environ. 58, 289–298.

Gitelson, A.A., Merzlyak, M.N., 1996. Signature Analysis of Leaf Reflectance Spectra: Algorithm Development for Remote Sensing of Chlorophyll. J. Plant Physiol. 148, 494–500.

Haboudane, D., 2004. Hyperspectral vegetation indices and novel algorithms for predicting green LAI of crop canopies: Modeling and validation in the context of precision agriculture. Remote Sens. Environ. 90, 337–352.

Haboudane, D., Miller, J.R., Tremblay, N., Zarco-Tejada, P.J., Dextraze, L., 2002. Integrated narrow-band vegetation indices for prediction of crop chlorophyll content for application to precision agriculture. Remote Sens. Environ. 81, 416–426.

Henneken, R., Dose, V., Schleip, C., Menzel, A., 2013. Detecting plant seasonality from webcams using Bayesian multiple change point analysis. Agric. For. Meteorol. 168, 177–185.

Hilker, T., Coops, N.C., Nesic, Z., Wulder, M.A., Black, A.T., 2007. Instrumentation and approach for unattended year round tower based measurements of spectral reflectance. Comput. Electron. Agric. 56, 72–84.

Hilker, T., Gitelson, A., Coops, N.C., Hall, F.G., Black, T.A., 2011. Tracking plant physiological properties from multi-angular tower-based remote sensing. Oecologia 165, 865–876.

Horton, P., Hague, A., 1988. Studies on the induction of chlorophyll fluorescence in isolated barley protoplasts. IV. Resolution of non-photochemical quenching. Biochim. Biophys. Acta - 932:107-115.

Hufkens, K., Friedl, M., Sonnentag, O., Braswell, B.H., Milliman, T., Richardson, A.D., 2012. Linking near-surface and satellite remote sensing measurements of deciduous broadleaf forest phenology. Remote Sens. Environ. 117, 307–321.

Ide, R., Oguma, H., 2010. Use of digital cameras for phenological observations. Ecol. Inform. 5, 339–347.

Ide, R., Oguma, H., 2013. A cost-effective monitoring method using digital time-lapse cameras for detecting temporal and spatial variations of snowmelt and vegetation phenology in alpine ecosystems. Ecol. Inform. 16, 25–34.

J., Flexas et al. (eds.) (2012). Terrestrial Photosynthesis in a Changing Environment. [Online]. Cambridge: Cambridge University Press. Available from: Cambridge Books Online

Jolly, W.M., Nemani, R., Running, S.W., 2005. A generalized, bioclimatic index to predict foliar phenology in response to climate. Glob. Chang. Biol. 11, 619–632.

Jonckheere, I., Fleck, S., Nackaerts, K., Muys, B., Coppin, P., Weiss, M., Baret, F., 2004. Review of methods for in situ leaf area index determination. Agric. For. Meteorol. 121, 19–35.

Kardevan, P., 2007. Reflectance spectroradiometry - a new tool for environmental mapping. Carpathian J. Earth Environ. Sci. 2, 29–38.

Le Dantec, V., Dufrêne, E., Saugier, B., 2000. Interannual and spatial variation in maximum leaf area index of temperate deciduous stands. For. Ecol. Manage. 134, 71–81.

Lebourgeois, V., Bégué, A., Labbé, S., Mallavan, B., Prévot, L., Roux, B., 2008. Can Commercial Digital Cameras Be Used as Multispectral Sensors A Crop Monitoring Test. Sensors 8, 7300–7322.

Lichtenthaler, H.K., Buschmann, C., Rinderle, U., Schmuck, G., 1986. Application of chlorophyll fluorescence in ecophysiology. Radiat. Environ. Biophys. 25, 297–308.

Lieth, H.H., 1976. Contributions to phenology seasonality research. Int. J. Biometeorol. 20, 197–199.

Linderholm, H.W., 2006. Growing season changes in the last century. Agric. For. Meteorol. 137, 1–14.

Mailly, D., Turbis, S., Chazdon, R.L., 2013. solarcalc 7.0: An enhanced version of a program for the analysis of hemispherical canopy photographs. Comput. Electron. Agric. 97, 15–20.

Martonchik, J. V., Bruegge, C.J., Strahler, A.H., 2000. A review of reflectance nomenclature used in remote sensing. Remote Sens. Rev.

Menzel, A., 2002. Phenology: Its importance to the global change community: An editorial comment. Clim. Change.54: 379–385.

Meroni, M., Barducci, A., Cogliati, S., Castagnoli, F., Rossini, M., Busetto, L., Migliavacca, M., Cremonese, E., Galvagno, M., Colombo, R., di Cella, U.M., 2011. The hyperspectral

irradiometer, a new instrument for long-term and unattended field spectroscopy measurements. Rev. Sci. Instrum. 82, 043106.

Meroni, M., Busetto, L., Guanter, L., Cogliati, S., Crosta, G.F., Migliavacca, M., Panigada, C., Rossini, M., Colombo, R., 2010. Characterization of fine resolution field spectrometers using solar Fraunhofer lines and atmospheric absorption features. Appl. Opt. 49, 2858–71.

Meroni, M., Colombo, R., Panigada, C., 2004. Inversion of a radiative transfer model with hyperspectral observations for LAI mapping in poplar plantations. Remote Sens. Environ. 92, 195–206.

Meroni, M., Rossini, M., Guanter, L., Alonso, L., Rascher, U., Colombo, R., Moreno, J., 2009. Remote sensing of solar-induced chlorophyll fluorescence: Review of methods and applications. Remote Sens. Environ. 113, 2037–2051.

Meroni, M., Rossini, M., Picchi, V., Panigada, C., Cogliati, S., Nali, C., Colombo, R., 2008. Assessing Steady-state Fluorescence and PRI from Hyperspectral Proximal Sensing as Early Indicators of Plant Stress: The Case of Ozone Exposure. Sensors 8, 1740–1754.

Migliavacca, M., Galvagno, M., Cremonese, E., Rossini, M., Meroni, M., Sonnentag, O., Cogliati, S., Manca, G., Diotri, F., Busetto, L., Cescatti, A., Colombo, R., Fava, F., Morra di Cella, U., Pari, E., Siniscalco, C., Richardson, A.D., 2011. Using digital repeat photography and eddy covariance data to model grassland phenology and photosynthetic CO2 uptake. Agric. For. Meteorol. 151, 1325–1337.

Milton, E.J., 1987. Review Article Principles of field spectroscopy. Int. J. Remote Sens. 8, 1807–1827.

Milton, E.J., Schaepman, M.E., Anderson, K., Kneubühler, M., Fox, N., 2009. Progress in field spectroscopy. Remote Sens. Environ. 113, S92–S109.

Mizunuma, T., Wilkinson, M., L. Eaton, E., Mencuccini, M., I. L. Morison, J., Grace, J., 2013. The relationship between carbon dioxide uptake and canopy colour from two camera systems in a deciduous forest in southern England. Funct. Ecol. 27, 196–207.

Morisette, J.T., Privette, J.L., Justice, C.O., 2002. A framework for the validation of MODIS Land products. Remote Sens. Environ. 83, 77–96.

Moulin, S., 1999. Impacts of model parameter uncertainties on crop reflectance estimates: A regional case study on wheat. Int. J. Remote Sens. 1,213-218.

Muller, P., 2001. Non-Photochemical Quenching. A Response to Excess Light Energy. PLANT Physiol. 125, 1558–1566.

Nakaji, T., Ide, R., Oguma, H., Saigusa, N., Fujinuma, Y., 2007. Utility of spectral vegetation index for estimation of gross CO2 flux under varied sky conditions. Remote Sens. Environ. 109, 274–284.

Nicodemus, F.E., 1970. Reflectance nomenclature and directional reflectance and emissivity. Appl. Opt. 9, 1474–5.

Painter, T.H., 2004. Measurements of the hemispherical-directional reflectance of snow at fine spectral and angular resolution. J. Geophys. Res. 109, D18115.

Panigada, C., Rossini, M., Meroni, M., Cilia, C., Busetto, L., Amaducci, S., Boschetti, M., Cogliati, S., Picchi, V., Pinto, F., Marchesi, A., Colombo, R., 2014. Fluorescence, PRI and canopy temperature for water stress detection in cereal crops. Int. J. Appl. Earth Obs. Geoinf. 30, 167–178.

Penuelas, J., Filella, I., Gamon, J.A., 1995. Assessment of photosynthetic radiation-use efficiency with spectral reflectance. New Phytol. 131, 291–296.

Penuelas, J., Llusia, J., Pinol, J., Filella, I., 1997. Photochemical reflectance index and leaf photosynthetic radiation-use-efficiency assessment in Mediterranean trees. Int. J. Remote Sens. 18, 2863–2868.

Peñuelas, J., Rutishauser, T., Filella, I., 2009. Ecology. Phenology feedbacks on climate change. Science 324, 887–888.

Petach, A.R., Toomey, M., Aubrecht, D.M., Richardson, A.D., 2014. Monitoring vegetation phenology using an infrared-enabled security camera. Agric. For. Meteorol. 195-196, 143–151.

Pettorelli, N., Vik, J.O., Mysterud, A., Gaillard, J.-M., Tucker, C.J., Stenseth, N.C., 2005. Using the satellite-derived NDVI to assess ecological responses to environmental change. Trends Ecol. Evol. 20, 503–10.

Pfündel, E., 1998. Estimating the contribution of Photosystem I to total leaf chlorophyll fluorescence. Photosynth. Res. 56, 185–195.

Porcar-Castell, A., Garcia-Plazaola, J.I., Nichol, C.J., Kolari, P., Olascoaga, B., Kuusinen, N., Fernández-Marín, B., Pulkkinen, M., Juurola, E., Nikinmaa, E., 2012. Physiology of the seasonal relationship between the photochemical reflectance index and photosynthetic light use efficiency. Oecologia 170, 313–23.

Richardson, A.D., Dail, D.B., Hollinger, D.Y., 2011. Leaf area index uncertainty estimates for model–data fusion applications. Agric. For. Meteorol. 151, 1287–1292.

Richardson, A.D., Jenkins, J.P., Braswell, B.H., Hollinger, D.Y., Ollinger, S. V, Smith, M.-L., 2007. Use of digital webcam images to track spring green-up in a deciduous broadleaf forest. Oecologia 152, 323–34.

Richardson, A.D., Keenan, T.F., Migliavacca, M., Ryu, Y., Sonnentag, O., Toomey, M., 2013. Climate change, phenology, and phenological control of vegetation feedbacks to the climate system. Agric. For. Meteorol. 169, 156–173.

Robinson, B.F., Bauer, M.E., DeWitt, D.P., Silva, L.F., Vanderbilt, V.C., 1979. <title>Multiband Radiometer For Field Research</title>, in: Field, H.P., Zalewski, E.F., Zweibaum, F.M. (Eds.), 23rd Annual Technical Symposium. International Society for Optics and Photonics, pp. 8–15.

Rossini, M., Cogliati, S., Meroni, M., Migliavacca, M., Galvagno, M., Busetto, L., Cremonese, E., Julitta, T., Siniscalco, C., Morra di Cella, U., Colombo, R., 2012. Remote sensing-based estimation of gross primary production in a subalpine grassland. Biogeosciences 9, 2565–2584.

Rossini, M., Migliavacca, M., Galvagno, M., Meroni, M., Cogliati, S., Cremonese, E., Fava, F., Gitelson, A., Julitta, T., Morra di Cella, U., Siniscalco, C., Colombo, R., 2014. Remote estimation of grassland gross primary production during extreme meteorological seasons. Int. J. Appl. Earth Obs. Geoinf. 29, 1–10.

Sakamoto, T., Shibayama, M., Kimura, A., Takada, E., 2011. Assessment of digital camera-derived vegetation indices in quantitative monitoring of seasonal rice growth. ISPRS J. Photogramm. Remote Sens. 66, 872–882.

Sakamoto, T., Yokozawa, M., Toritani, H., Shibayama, M., Ishitsuka, N., Ohno, H., 2005. A crop phenology detection method using time-series MODIS data. Remote Sens. Environ. 96, 366–374.

Schaepman, M.E., Ustin, S.L., Plaza, A.J., Painter, T.H., Verrelst, J., Liang, S., 2009. Earth system science related imaging spectroscopy—An assessment. Remote Sens. Environ. 113, S123–S137.

Schaepman-Strub, G., Schaepman, M.E., Painter, T.H., Dangel, S., Martonchik, J. V., 2006. Reflectance quantities in optical remote sensing-definitions and case studies. Remote Sens. Environ. 103, 27–42.

Schlerf, M., Atzberger, C., 2006. Inversion of a forest reflectance model to estimate structural canopy variables from hyperspectral remote sensing data. Remote Sens. Environ. 100, 281–294.

Sims, D., Luo, H., Hastings, S., Oechel, W., Rahman, A., Gamon, J., 2006. Parallel adjustments in vegetation greenness and ecosystem CO2 exchange in response to drought in a Southern California chaparral ecosystem. Remote Sens. Environ. 103, 289–303.

Sims, D.A., Gamon, J.A., 2002. Relationships between leaf pigment content and spectral reflectance across a wide range of species, leaf structures and developmental stages. Remote Sens. Environ. 81, 337–354.

Sonnentag, O., Hufkens, K., Teshera-Sterne, C., Young, A.M., Friedl, M., Braswell, B.H., Milliman, T., O'Keefe, J., Richardson, A.D., 2012. Digital repeat photography for phenological research in forest ecosystems. Agric. For. Meteorol. 152, 159–177.

Stylinski, C.D., Gamon, J.A., Oechel, W.C., 2002. Seasonal patterns of reflectance indices, carotenoid pigments and photosynthesis of evergreen chaparral species. Oecologia 131, 366–374.

Taiz, L., Zeiger, E., 2010. Plant Physiology.y, Sinauer Associates, Inc., Publishers, Sunderland, Massachusetts, 700 pp

Thiemann, S., Kaufmann, H., 2000. Determination of Chlorophyll Content and Trophic State of Lakes Using Field Spectrometer and IRS-1C Satellite Data in the Mecklenburg Lake District, Germany. Remote Sens. Environ. 73, 227–235.

Tucker, C.J., Sellers, P.J., 1986. Satellite remote sensing of primary production. Int. J. Remote Sens. 7, 1395–1416.

Ustin, S.L., Gitelson, A.A., Jacquemoud, S., Schaepman, M., Asner, G.P., Gamon, J.A., Zarco-Tejada, P., 2009. Retrieval of foliar information about plant pigment systems from high resolution spectroscopy. Remote Sens. Environ. 113, S67–S77.

Viña, A., Gitelson, A.A., Nguy-Robertson, A.L., Peng, Y., 2011. Comparison of different vegetation indices for the remote assessment of green leaf area index of crops. Remote Sens. Environ. 115, 3468–3478.

Vitasse, Y., François, C., Delpierre, N., Dufrêne, E., Kremer, A., Chuine, I., Delzon, S., 2011. Assessing the effects of climate change on the phenology of European temperate trees. Agric. For. Meteorol. 151, 969–980.

Watson, D.J., 1947. Comparative physiological studies on the growth of field crops I. Variation in Net Assimilation Rate and leaf area between species and varieties, and within and between years. Ann. Bot. 11, 41–76.

Wolkovich, E.M., Cook, B.I., Allen, J.M., Crimmins, T.M., Betancourt, J.L., Travers, S.E., Pau, S., Regetz, J., Davies, T.J., Kraft, N.J.B., Ault, T.R., Bolmgren, K., Mazer, S.J., McCabe, G.J., McGill, B.J., Parmesan, C., Salamin, N., Schwartz, M.D., Cleland, E.E., 2012. Warming experiments underpredict plant phenological responses to climate change. Nature 485, 494–7.

Yao, X., Yao, X., Jia, W., Tian, Y., Ni, J., Cao, W., Zhu, Y., 2013. Comparison and intercalibration of vegetation indices from different sensors for monitoring above-ground plant nitrogen uptake in winter wheat. Sensors (Basel). 13, 3109–30.

Zarco-Tejada, P., 2000. Chlorophyll Fluorescence Effects on Vegetation Apparent Reflectance I. Leaf-Level Measurements and Model Simulation. Remote Sens. Environ. 74, 582–595.

Zarco-Tejada, P.J., Miller, J.R., Harron, J., Hu, B., Noland, T.L., Goel, N., Mohammed, G.H., Sampson, P., 2004. Needle chlorophyll content estimation through model inversion using hyperspectral data from boreal conifer forest canopies. Remote Sens. Environ. 89, 189–199.

Zarco-Tejada, P.J., Miller, J.R., Noland, T.L., Mohammed, G.H., Sampson, P.H., 2001. Scaling-up and model inversion methods with narrowband optical indices for chlorophyll content estimation in closed forest canopies with hyperspectral data. IEEE Trans. Geosci. Remote Sens. 39, 1491–1507.

Part 1 - Instrument characterization and evaluation of measurement uncertainties

Chapter 3

Optical systems measuring vegetation: source of uncertainties and protocol standard definition

This study was conducted in the context of COST Action, ES0903 (EUROSPEC). The growing interest on optical proximal sensing measurements is highlighted by recently developed global networks such as Phenocamand Specnet. However,the different instruments and the acquisition strategies used within these communities need to be standardized in order to obtain high quality, reliable and comparable data across sites. This chapter and the objective of this part are devoted to the characterization of uncertainty sources of the measurements and to the definition of field of protocol standards. In particular, the characterization procedures here presented refer to hyperspectral instruments commonly used in field spectroscopy. Hyperspectral data acquired by spectroradiometers can readily be transformed into bands equivalent to those of multispectral sensor bands. Hyperspectral data offer considerable advantages over multispectral data, albeit with additional complexity of acquisition and analysis. For these reasons hyperspectral sensors are described more in details in the following paragraph. The main instrumental uncertainty sources (i.e. detector nonlinearity response, signal to noise ratio, radiometric and spectral calibration etc.) have been considered and characterized mainly in laboratory conditions for a large set of spectroradiometers. The laboratory instrument characterization is a complex but fundamental practice to determine and reduce eventual biases of the measurement due to instrumental artefact. In addition the importance of a proper system's setup (i.e. specific angular view), the selection of the proper site and the definition of a common data processing strategy is underlined. Finally, a common protocol standard covering the instrumental characterization, the system set-up and the data acquisition and processing chain is presented.

3.1 Introduction

Remote sensing provides a means of acquiring spatially explicit data that can be used to integrate measurements commonly punctually taken such as carbon fluxes at the ecosystem level (i.e. Eddy covariance technique). Global networks of continuous measurements of vegetation optical properties such as Specnet (http://specnet.info, Gamon et al., 2014, 2006) and Phenocam (http://phenocam.sr.unh.edu, Richardson et al., 2007; Sonnentag et al., 2012)have been promoted in the last decade. These networks aimed at better characterize the role of terrestrial ecosystems in the global carbon cycle process using proximal sensed data. However, to realize reliable proximal sensing networks, standardized and inter-comparable optical measurements across study sites are needed. Here, one of the specific objectives is to determine a guideline of the optical measurement sampling strategies which should be used to minimize the measurements uncertainty of the collected data.In fact, current measurements are performed with instruments that have variable design (e.g. imaging vs non-imaging system, broadband vs hyperspectral; single beam vs dual beam), performance (e.g. different degrees of non-linearity in response, different signal-to-noise, different cosine receptors material and design), measurement geometry (e.g. hemispherical vs conical and their combinations, different fields-of-view (FOV)), installation geometry (e.g. nadir or off-nadir; height of sensor), and that are run under variable calibration schemes (e.g. regularly calibrated by manufacturer, calibrated *in situ*, not regularly calibrated). Hence there is a need to understand the instruments and methods being used and develop standardized procedures for optical sampling within the carbon flux research community. Generally VIs related to greenness track evident changes in the optical properties of the vegetation strictly related to the phenological cycle, such as spring leaf emergence and autumn senescence. These VIs can be measured using multi-band broadband sensors. Thus given their lower costs and easier field installation and maintenance compared to hyperspectral systems, they are considered as suitable tools for long-term phenological analysis. However when more dynamic processes related to variations in plant photosynthetic efficiency have to be monitored, hyperspectral or narrowband multispectral systems are needed. Variations in plant physiology can be detected using faint optical signals such as PRI and sun-induced chlorophyll fluorescence. Thus their accurate retrieval need a proper characterization and calibration of the systems used to estimate them.

The definition of protocol standards is a fundamental practice for all kinds of networks.Hufkens (2012) and Ide (2010) have underlined the need of standardized technical protocol to reduce measurements errors due to technical limitations of the devices (such as temperature disturbance and channel color drift in the time) in networks which make use of digital camera. Nonetheless this chapter want to focus on the characterization of the possible source of uncertainties related only to hyperspectral measurements. Hyperspectral measurements provide in fact the possibility to exploit a wider range of indices which can be used for vegetation monitoring purposes (both related to phenology and physiology analysis). The chapter is hence

dedicated to define the source of uncertainties in filed spectroscopy measurements and the definition of necessary guidelines which should be taken into account to reduce artificial errors in the measurements both due to acquisition methodology and technical instrumental aspects.

3.2 Field spectroscopy: sources of measurement uncertainties

Field spectroscopy aims to measure the reflected or emitted radiance or the reflectance factor of natural surfaces under natural illumination conditions. According to Nicodemus et al. (1977) the reflectance factor is defined as "the ratio of the radiant flux actually reflected by a sample surface to that which would be reflected into the same reflected-beam geometry by an ideal (lossless) perfectly diffuse (Lambertian) standard surface irradiated in exactly the same way as the sample". However natural surfaces measured with field spectrometers do not have a lambertian behaviour in irradiating the incoming solar radiation. The anisotropy of the reflected radiation field over natural surfaces may be described by the bidirectional reflectance distribution function (BRDF) equations representing how the reflectance of a surface varies with the solar-view geometry (Giardino and Brivio, 2003). In the case of vegetation monitoring reflection, absorption and transmission of sunlight depend on canopy structure, foliar chemistry and distribution and solar zenith angle (Balzarolo et al., 2011). The measurements acquired by field spectrometers can be generally described, according to the optics used, as hemispherical–conical reflectance factors (HCRF) or bi-hemispherical reflectance (BHR)(Milton et al., 2009) according to the terminology proposed by Schaepman-Strub et al., (2006). Therefore real measurements of irradiance and radiance over finite solid angles can only ever provide an average estimate of the true BRDF (Milton et al., 2009). Several studies have been published to analyze the anisotropy of different natural surfaces (Dumont et al., 2010; Giardino and Brivio, 2003; Kriebel, 1978; Painter, 2004; Painter et al., 2003) but the complex BRDF measurements rarely can be evaluated directly in the field to compensate the effect in the measurement (Balzarolo et al., 2011; Hilker et al., 2010). Anisotropy of the natural surfaces and instrumental characteristics cause uncertainties of the measurements which make difficult reliable and repeatable comparison of the measured values. While instrumental laboratory calibrations are suitable techniques in order to obtain reliable spectroscopy measurements the spectroscopy applied in the field is necessarily biased by external factors, first of all bidirectional effects. Therefore to get repeatable measurements of a natural target (such as vegetation ecosystems) standard protocols are often the best solution to reduce the uncertainties of the measurements (i.e. indication on the geometrical acquisition view, on the preferable solar zenith angles to consider in the acquisition, etc.). An effort to produce reliable and repeatable measurements has been done in the last years from the scientific community both in characterizing the instrument performances and in defining common protocol of setup, acquisition and data processing of field spectrometer measurements.

3.3 Measurement uncertainties characterization

The following paragraphs are dedicated to the characterization procedures of instrumental uncertainty sources of portable spectrometers such as:

- Temperature dependency;
- Dark current variability;

- Signal to noise ratio;
- Non linearity detector response;
- Wavelength validation and calibration;
- Radiometric calibration;
- Field of view response;
- Reference standard performance;

Figures reported in this chapter refer to laboratory measurements acquired at the Natural Environment Research Council (NERC) Field Spectroscopy Facility (FSF), University of Edinburgh. The models and characteristics of the used are reported in Table 3.1.

Type	Company	Spectral range(nm)	Sampling interval(nm)	FWHM(nm)
HR4000	Ocean Optics	350-1050	0.25	1
HR4000	Ocean Optics	700-800	0.02	0.1
QE65000	Ocean Optics	348-1148	0.81	2
QE65000	Ocean Optics	725-800	0.06	0.3
QE65000	Ocean Optics	656-743	0.06	0.3
STS	Ocean Optics	337 -824	0.45	2.5
Unispec	Unispec	301-1121	3.38	10
USB2000	Ocean Optics	339-1022	0.38	2
USB2000+	Ocean Optics	339-1024	0.38	1

Table 3.1. Instruments used during the STSM for the laboratory characterization. The characteristics declared by the manufacture here reported are: the company, the sampling interval, the spectral range and the spectral resolution expressed ad Full Width at Half Maximum (FWHM).

3.3.1 Temperature dependency

Temperature can affect differently the components of the spectroradiometer, such as gratings and detectors. Effects of the temperature dependency can produce an offset of the dark current, which is modulated by temperature (Kantzas et al., 2009). Temperature variations can also affect the spectral response of the device, detectable as a change in the full width at half maximum and channel positions of the spectrometer. While in laboratory condition temperature can be maintain stable, in field condition the temperature effect is one of the major sources of uncertainty in the measurements (Schaepman and Dangel, 2000). The effect is especially evident during the warming up phase of the instrument that can last differently according to the devices. The temperature characterization can be done by varying temperature of the spectrometers and evaluating its response in the spectrum. The best practice to avoid

unpredictable effect of the temperature on the measurements consists in operating the instrument in thermo-regulated stable condition. Nevertheless field conditions have often limitations in the power supply of cooling systems. In these cases measurements of the temperature changes during the acquisition process can be used to model in a proper way the effect, once the temperature effect has been previously characterized in laboratory.

3.3.2 Dark current

The dark current (DC) is the measurement acquired when no input signal reaches the entrance of the spectrometer. In this study it has been measured by closing the aperture of the spectrometer using shutters or dark channels of optical switcher. The dark current is due both to radiometric and electronic effects and it is proportional to the integration time of the measurement (Figure 3.1)

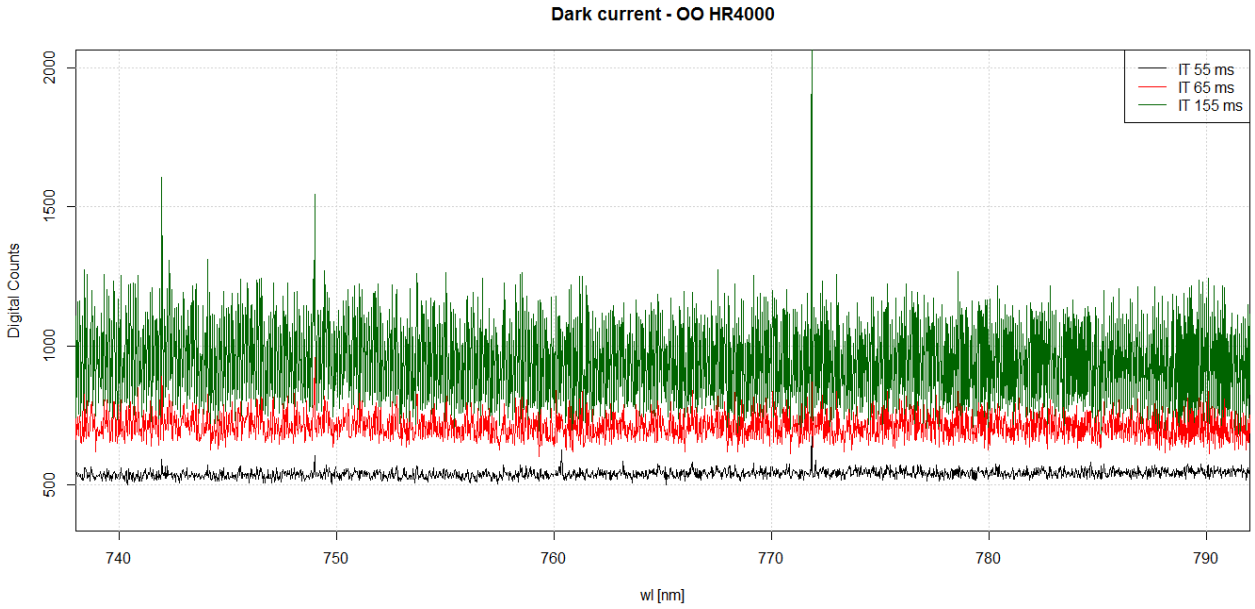

Figure 3.1. Dark current spectra of an HR4000 spectrometer (Ocean Optics) collected at different integration times. Spectral dependency can be noticed observing the shape of the dark spectrum.

Figure 3.1 reports dark current signal in digital counts collected with the HR4000 spectroradiometer at different integration time. It can be noticed the direct dependency of the signal on the integration time. In fact the signal increases for higher integration time. Moreover, spectral patterns can be noticed in the dark spectrum as the deflection recorded at around 745 nm, the high spikes at 773 nm or the bump at 790. Generally, the DC spectral dependency can vary accordingly to the spectrometer model and has to be taken into account to compensate the effect in the final measurement simply by subtracting the dark spectra to the measurement collected. It can occur that spectrometers have optically black pixels at the edges of the CCD detector (i.e. most of the models produced by Ocean Optics, Inc.). According to the suggestion of the manufacturer the values of these pixels can be used as an average value to be

subtracted instead of the dark spectrum. Nevertheless in this case the spectral dependency of the dark signal is not considered or compensated and errors can be introduced in the measurement.

3.3.3 Signal to noise ratio

The measurement acquired using a spectrometer is given by the sum of the signal and the instrumental noise. The noise of a measurement is mainly produced by the electronic components and the processing of the signal acquired by the detector. Higher is the signal compared to the instrumental noise and higher is the information carried by the measurement. Therefore instruments with high signal to noise ratio (SNR) can provide a more informative signal. SNR has been characterized in the laboratory according to the methodology proposed by Schaepman and Dangel (2000) using the following equation:

$$\mathrm{SNR} = \frac{\mathrm{S}}{\mathrm{N}} = \frac{\mathrm{R}_{DN},\mathrm{total} - \mathrm{R}_{DN},\mathrm{dark}}{[\sigma^2(\mathrm{R}_{DN},\mathrm{total}) + \sigma^2(\mathrm{R}_{DN},\mathrm{darkl})]^{1/2}} \qquad [3.1]$$

where $R_{DN,total}$ is the total measured signal and $R_{DN,dark}$ the dark current, DN means digital number, and σ^2 is the standard deviation. The total signal refers to the average of repeated measurements of a stable reference lamp. Usually the manufacturer reports a SNR value as an average of the spectral SNR obtained optimizing the signal in the higher part of the dynamic range of the instrument, where the SNR is maximized. Obviously the SNR decreases when the signal is optimized to lower values, therefore measurements acquired with a low optimization are expected to be more affected by the noise.The comparison of different instruments in terms of SNR is reported in Figure 3.2.

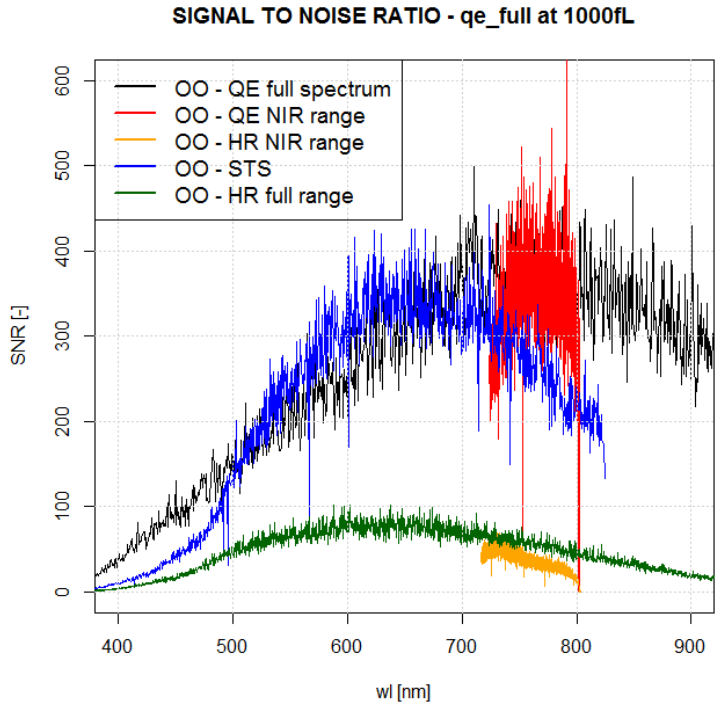

Figure 3.2.Spectral signal to noise ratio of five portable spectrometers from Ocean Optics. All the measurements have been collected optimizing the signal at the 80% of the dynamic range.

In Figure 3.2 the SNR of five spectrometers is compared. It can be generally noticed that the two HR4000 have the lower SNR (green and orange lines in Figure). On the contrary, STS and QEs spectrometers show higher values. The SNR wavelength dependency can be extremely high. In fact in the edge of the spectral range covered by an instrument the SNR can decrease also up to 300 times compare the central and general more sensitive part of the detector. This is especially true for instruments covering the full range (visible and near infrared region), in Figure depicted in blue, black and green lines.

3.3.4 Non linearity

The relationship between the amount of light received by the detector and the photocurrent it produces is generally desirable to be linear. However, the detector response can be affected by factors related to both the electronics and/or the detector elements themselves (Baranows, 2008). Normally, this implies a nonlinear response of the detector to the light intensity. Generally, the nonlinear response is higher in the high part of the dynamic range where the anti-blooming structures start draining part of the charge before saturation (Pacheco-Labrador et al., 2014) and in the lower part where the signal is mostly affected by the instrumental noise. To reduce the effect of the nonlinearity response in the measurements two possible approaches can be used: i) to optimize the signal in the expected linear part of the detector, ii) to characterize the instrument non linearity correcting the signal in the post-processing phase. In both cases the characterization of the instrument performance is important both to define the dynamic range

to be used and to define a correction factor for the measurements. Several methods have been proposed to determine the nonlinear response of a device (Kostkowski, 1997; Zalewski, 1994). A straightforward method to determine the nonlinearity response of a detector is to collect measurements at different level of illumination (typically using a stable reference lamp) keeping fix the integration time (the reverse is also possible, keeping fixed the light source and measuring at different integration times). After the dark current subtraction the response of each channel can be computed normalizing each spectrum (in Digital Number) by the luminance level used (usually expressed as footlambert, fL) and then by the highest normalized value of each spectrum.

$$\text{Response} = \frac{\frac{R_{DN,\text{total}} - R_{DN,\text{dark}}}{fL}}{\max\left(\frac{R_{DN,\text{total}} - R_{DN,\text{dark}}}{fL}\right)} \quad [3.2]$$

whereR_{DN} is the measured signal either the dark current or the total signal, DN means digital number, fL represents the light source intensity (Footlambert).

The response has been calculated over a randomly selected subset of pixels of the detector, assuming homogeneity of the response along the detector array. A fitted polynomial (generally 7th order) is then applied to derive the correction factor used for correcting the measurement.

The nonlinearity effect of the STS spectrometer is reported in Figure 3.3AHoffman radiance standard was used for the characterization of the non-linearity. Keeping constant the integration time ten consecutive measurements with different luminance levels were taken, from 1000 up to 100 fL with a 100 fL step.

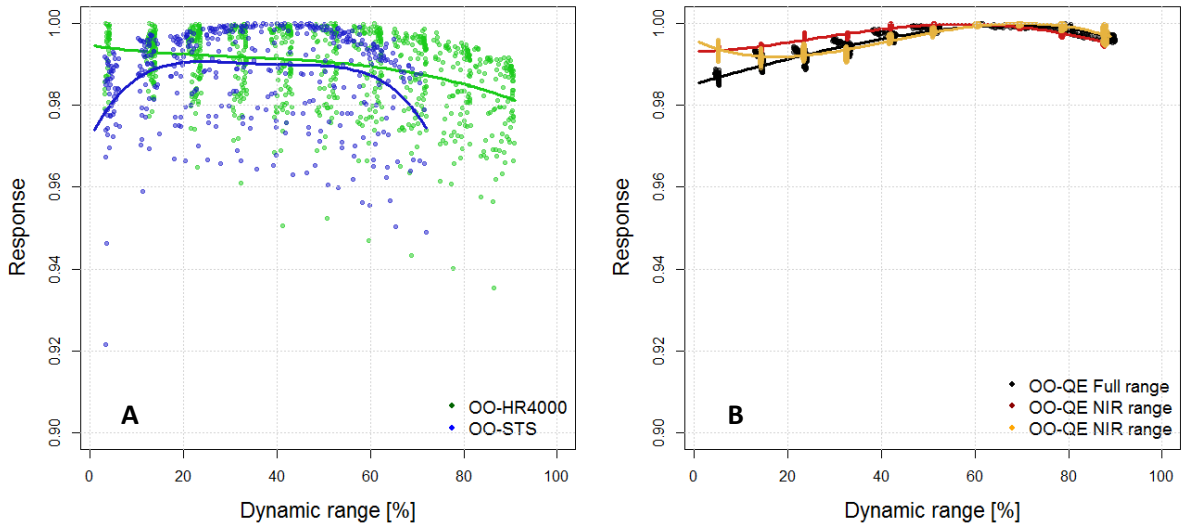

Figure 3.3. Example of the non linear response of the five spectroradiometers. A) OO- HR4000 and OO- STS; B) OO-QE65000 covering different spectral range.

Figure 3.3 reports the non-linear response of five spectroradiometers.Left panel refers to noisier spectroradiometers (OO-STS and OO-HR4000) while the right panel depicts the non-linear responses of three OO-QE65000 covering different spectral range. The response has been calculated following the formula 3.2, considering the central portion of the spectral range (100

pixels)because less noisy than the edges.Finally, a 7th order polynomial has been fitted to the clouds of obtained points. It can be noticedthat the noisier detectorsprovided more spread values and the polynomial fitting seems to be influenced by low spread values. On the contrary, the spectrometer responses reported in the right panel are less scatteredand a more reliable fitting can be obtained. Therefore this correction method can be applied when the stability of the device used is strong enough otherwise an additional method dependent uncertainty can be introduced. Overall, thedynamic range portion more affected by nonlinearity effect is located at low and high values (lower than 20% or higher than 70-80%). Moreover, in thecases examined the nonlinearity effect is affecting the measurements with an error lower than 3%. The nonlinear effect is detector dependent and even if the related error can be low in absolute values, the impact on optical measurements can differ according to the objective of the measurements taken (Pacheco-Labrador and Martin 2014).

3.3.5 Wavelength validation and calibration

The spectral resolution of a spectrometer is defined according to the full width at half maximum (FWHM) of the response function of the system analysed (Schaepman and Dangel, 2000). On the contrary, the peak of the response function represents the center wavelength. Finally the spectral sampling refers to the distance (in wavelength units) between two adjacent points sampled in the spectrum. Each instrument has been characterized defining these three terms. To characterize the wavelengths position and the spectral resolution wavelength standards are needed. In laboratory a commonly used technique to spectrally calibrate the spectroradiometers consists in using lamp with known atomic emission lines (i.e. Pencil Style Calibration Lamps, Forter Tech). According to the spectral range covered by the spectrometers different atomic emission lines, such as Mercury, Krypton or Argon, can be used. In Figure 3.4 the wavelength response of five spectrometers (same used for Figure 3.3.) is reported. The emission lines produced by Krypton gas lamp in the 765-775 nm spectral range are detected in a different way by the five spectrometers. In fact only the spectrometers with a spectral resolution lower than 1 nm (HR4000 NIR, and QE65000 NIR) are able to clearly separate the two emission peaks centered a 768.3 and 769.6 respectively. On the contrary, the others spectrometer with higher spectral resolution just detect a singular peak. The use of lamp with fixed and known atomic emission lines allowed the determination of the spectral shift of the instrument analysed. In fact in Figure 3.4 a shift in the peak of the can be quantified and therefore corrected to calibrate the system.

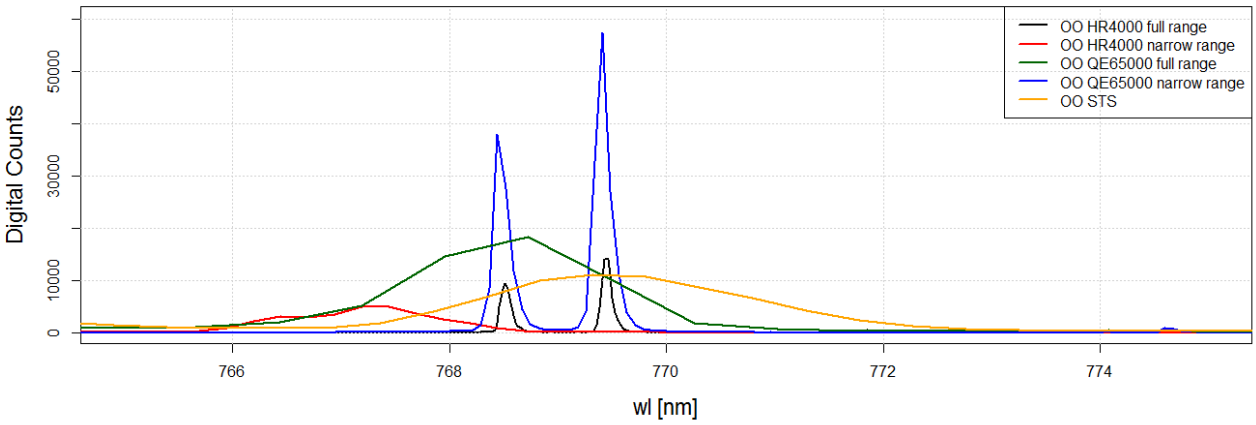

Figure 3.4 Krypton emision lines measured looking at the wavelength calibration lamp. The colors refer to different spectrometers used. Spectrometer with higher spectral resolution detect the two emission peaks. The lower resoluted spectrometers detect a unique peak around 769 nm. The spectral shift is also visble considering the center wavlenght corresponidng to the peak of each response.

Each atomic emission line has been characterized to model a response function usually approximated to a Gaussian. The fitted Gaussian function will give the spectral resolution in terms of FWMH and spectral shift for all the singular points of the spectrum where the atomic light is measured. The information derived by the variability of the spectral shift across the spectrum can be used to model the spectral shift and to correct it. Different approaches have been suggested to model the spectral shift across the spectrum (Xiong et al., 2014) each varying the model explaining this variation (usually polynomial functions). The accuracy of the calibration and the quality of the fitting strongly depend on the goodness of the characterization process such as the number of the sampled emission lines.

Beside laboratory spectral characterization and calibration several approaches have been proposed to determine instrumental spectral shift and FWHM from data measured in the field (Gao et al., 2004; Green et al., 2003; Guanter et al., 2006; Meroni et al., 2010). All these methods are based on the comparison between measured and modeled solar radiance spectra. In Figure 3.5 an example of the spectral characteristics of the instrument is reported. In this study the spectral shift and the FWHM determination have been estimated by comparing specific atmospheric absorption features present in the compared spectra using the SpecCal software (Busetto et al., 2011).

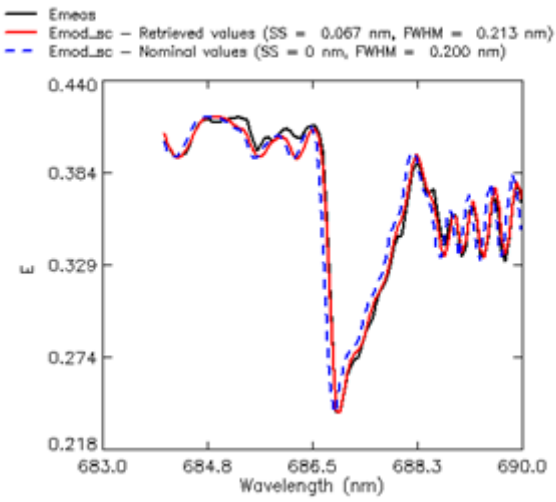

Figure 3.5. Example of spectral characterization made using SpecCal software. Plots showing the results of the Spectral Calibration process at the O2-B absorption window for an HR4000 field spectrometer. In the graph the comparison between the measured spectra, the MODTRAN4 spectra resampled to nominal SS and FWHM (blue dashed lines), and the MODTRAN4 spectra resampled to SSCal and FWHMCal.

The accuracy of the spectral characterization using these techniques is directly related to the number of the absorption features existing within the spectral range measured by the spectrometer used. Nevertheless the in situ calibration offers the great advantage of using the collected measurements to characterize the system without moving it to laboratory facilities.

3.3.5 Radiometric calibration

The radiometric calibration consists in the determination of the spectral coefficients needed to convert the digital counts recorded by the spectrometer in physical units (radiance $W*m^{-2}*sr^{-1}*nm^{-1}$). To determine the coefficient values a reference standard is needed. In laboratory the absolute radiance standards consist of stable and calibrated lamp source (i.e. tungsten halogen lamp, deuterium lamps or argon lamps). The radiance emitted by the source has been accurately determined and continuously checked in the time to assess the stability of the source. To get reliable measurements of the radiance standard avoiding directional and positional effects due to measurement setup the lamp source was coupled by integrating spheres which reduce directional effects. Repeated measurements of the light source recorded by the device have been used to determine the coefficients of calibration according to the following formula (Schaepman and Dangel, 2000).

$$g(\lambda) = \frac{L(\lambda)}{R_{DN}(\lambda),\text{total} - R_{DN}(\lambda),\text{dark}} \quad [3.3]$$

g represents the wavelength dependent calibration gains, L is the calibrated at sensor radiance; R_{DN} is the measured signal either the dark current or the total signal normalized for the integration time used in the measurement.

Examples of calibration coefficients referred to four different spectroradiometers obtained using the Hoffman Engineering LS-65-8Dsource are reported in Figure 3.6. As depicted the coefficients

are different according to the different instrument used. In general the spectral shape and the intensity values depend on the sensitivity of the detector used. As noticeable from the Figure the spectral coefficient are smoothed, this is important in order to avoid including in the radiometric calibration process the instrumental noise.

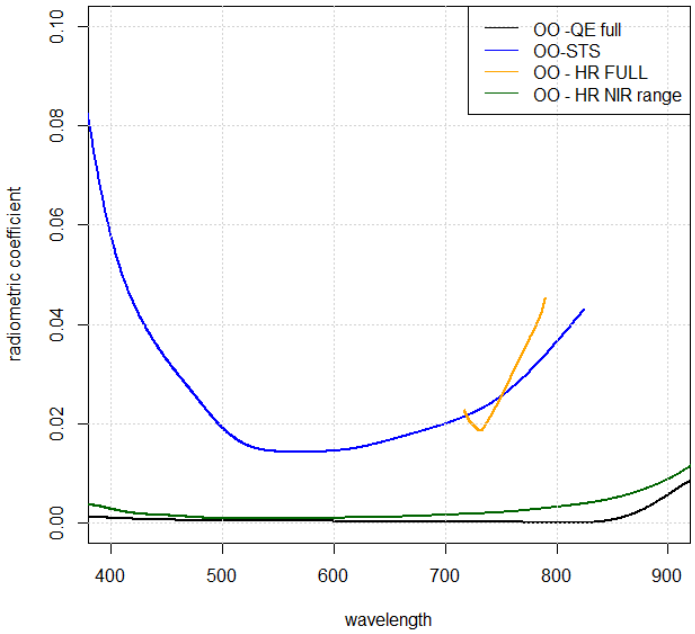

Figure 3.6. Radiometric coefficients of different spectrometers are depicted in different colors. The different spectral range is varying according to the spectral range of the device

When field spectrometers are installed in the field the accuracy of laboratory calibration can deteriorate in the time. Therefore, accurate periodically characterization/calibration of spectrometric systems in the time is needed in order to continuously deliver high quality spectral data. Periodic laboratory radiometric calibration is time consuming and the spectrometers need to be displaced from the monitoring site. Thus methodologies for in situ calibration have been developed in order to reach these purposes (Cogliati et. al 2014, submitted to RSE). In situ radiometric cross-calibration measurements are recorded collecting simultaneously and at the same place the solar radiance using the spectrometer that need to be calibrated and a reference calibrated spectrometer. It is important that during the operation reference standards (both panel and cosine receptor) are horizontally placed and checked with the level with a precision better than 0.5°. The coefficient factors calculated comparing reference radiance values with digital counts recorded by the spectrometer that need to be calibrated employing the following equation:

$$L_s(\lambda) = \frac{\mathrm{R}_{DN}(\lambda),\mathrm{total} - \mathrm{R}_{DN}(\lambda),\mathrm{dark}}{IT}\, g(\lambda) \qquad [3.4]$$

Where R_{DN} is the measured signal either the dark current or the total signal in digital numbers, *IT* is the integration time used for each measurements, and $g(\lambda)$ is the spectral gains factor.

This approach allows to periodically check the radiometric calibration coefficients of an instrument without bringing the spectrometers to calibration facilities. Example of calibration gains calculated in the field and cross comparison check is reported in Figure 3.7. In the left panel of the Figure the spectral radiometric coefficient of the HR4000 NIR spectrometer are reported. The deepest atmospheric absorption features (i.e. O_2-A band, centered at 760 nm) have to be removed in the calibration operation in order to avoid influences on the calibration gains due to atmospheric changes occurring during the calibration process. Consequently, a gap-filling of the missing values has to be performed. In the case reported in Figure a spline function was used (green line). The plot of the average incoming radiance detected with the HR4000 NIR and ASD FieldSpec PRO (reference in the comparison) is reported in the right panel. The agreement between the two measurements attests the goodness of the calibration process. The spectrum collected with the HR4000 (red in Figure) appears to be more noise affected. This is due to both to the lower SNR and to the higher spectral resolution which allow detecting narrow absorption feature in the solar irradiance.

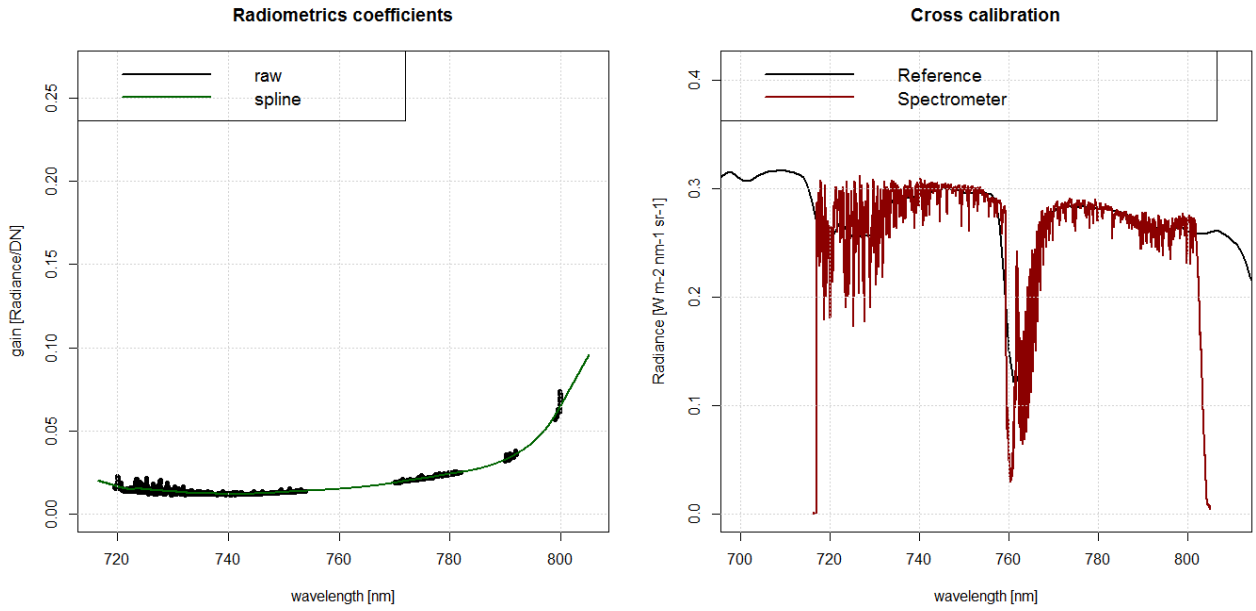

Figure 3.7.Left panel. Radiometric coefficients are reported as the ratio (black dots) between the at sensor radiance measurements collected at the same time with a reference calibrated spectrometers (ASD Fieldspec Pro) and a HR4000. The green line represents the spline function used to fill the gap create in filtering the ratio due to variability of the atmospheric absorption features. In the right panel the calibration check between the two instruments used is reported.

3.3.6 Field of view

The field of view (FOV) of the fore optic of the spectroradiometer defines the area from which the radiance is recorded. The FOV is normally defined as a solid angle through which light incident on the fore optic enters into the spectroradiometer (Mac Arthur et al., 2007). The FOV is determined by the combination of fore optic lens, the distance of the spectroradiometer fore

optic from the target surface and the view angle of the measurement. The FOV response is generally considered as Gaussian and the spectrometer manufacturer company only specifies a nominal solid angular value as the FOV of the fore optics (Mac Arthur et al., 2012). Nevertheless, optical components of the devices can cause in-filling due to regions outside the main area which can significantly change the expected FOV shape. A characterization of the FOV response is therefore useful to determine the area of the target surface that the instrument is effectively measuring at a specific distance (Zhao et al., 2015). To characterize the FOV response, specific laboratory instruments need to be used. In particular the FOV responses depicted in Figure 3.8 have been characterized following the approach described in Mac Arthur et al., (2012). The Figure depicts the sensitivity of the detector at a specified wavelength in the space.

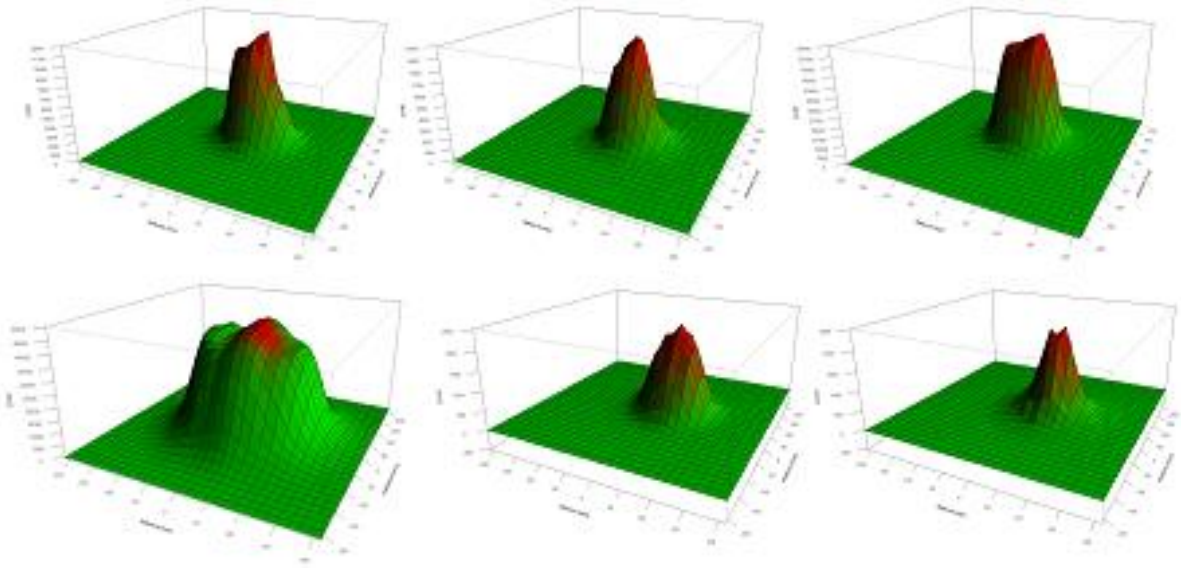

Figure 3.8. Field of View responses of different spectrometers associated to different singlecore fiber optics. The nominal declared FOV is 25°. Nevertheless the assumed Gaussian shape of the response is not always properly described. D panel reports the Unispec system FOV response which has been found to be equal to 40°.

The nominal solid angle of the spectrometers characterized and reported in the previous Figure is declared to be 25° by the manufacturer. However the characterization results showed that the effective FOV, which cannot be always assumed to be gaussian, in some cases can be even the double of the expected. The FOV characterization can be extremely significant in explaining the measurement value, when the instrument is pointing to heterogeneous targets where the signal reaching the spectrometer fore optic refers to mixed area.

3.3.7 Reference standards

The solar incoming irradiance (E_{tot}) measurement in field spectroscopy is commonly made using reference standards. The main characteristic of the reference standards is the highly lambertian behaviour which allows to measure E_{tot} with a certain degree of uncertainty at different solar

zenith angles (SZA) (Milton et al., 2009). Examples of reference standard materials are magnesium carbonate, chalk, magnesium oxide,barium sulphate and polytetrafluoroethylene (PTFE) (Guzman et al., 1991; Springsteen, 1999). Measurements of E_{tot} are commonly taken using a reference panel or a cosine corrected receptors (Balzarolo et al., 2011; Milton et al., 2009). In the first case the measurements are acquired collecting the upwelling radiance reflected by panels with high and constant reflectivity across the spectrum (e.g. Spectralon white panels, Labsphere, Inc.). In the second case the reference measurement is acquired by pointing the spectrometer (or its fore optic) looking upward and measuring the transmitted radiance of the. To obtain a reliable measurement of the reference both panels and cosine diffusers need to be characterized in order to determine the transmittance or the reflectance factor and to compensate these effects in the measurements. In particular, the field reference (both reflectance and transmittance) has been characterized in laboratory to evaluate the wavelength angular response of the reference used in the field. The angular response of the panels or of the cosine receptors can be determined mounting the reference standard on an optical table allowing to control its angular position with respect to a fixed light source (Carmagnola et al., 2013). This measurement setup allowed to evaluate the angular response deviation from an ideal cosine response and to quantify the impact of this deviation on the measured fluxes (Figure 3.9). Particular attention to the effect of the different angular response of the reference standards is reported in chapter 4.

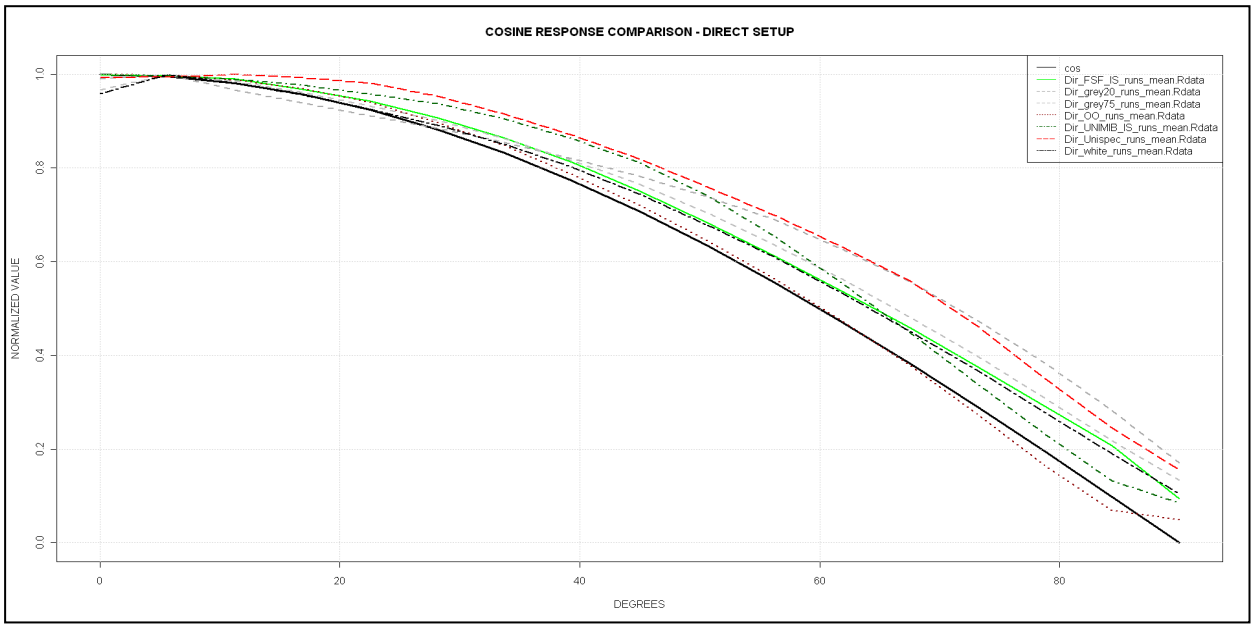

Figure 3.9. Angular response of 8 cosine receptors commonly used in the field. The response has been measured using a goniometer fixed to an optical table and varying the light source position in respect to the cosine receptor.

Therefore,the evaluation of the angular dependency of the references determines the reliability of the measurement at different angles (in the field SZA). However to compensate the measurement for the angular dependency the exact diffuse and the direct radiation components at the time of the measurement need to be known and taken into account to

apply the correction. Nevertheless, the angular dependency can be considered in defining acquisition protocols for reducing such effects in the acquired measurements.

3.4 Summary and recommendation

Uncertainties of the spectral measurements of a natural surface cannot be completely removed by the characterization and the calibration process. Nevertheless common protocols of measurement and post-processing chain can be adopted to reduce the uncertainty sources. In fact it has been shown that when the same protocol of measurements and post-processing corrections is followed instrument with different specific characteristics produce extremely comparable results (Anderson et al., 2013).

In the following paragraphs guidance for measurement collection and post-processing correction arose from the previously described experiment are summarised.

3.4.1 Optical sensors installation

1. The ground spectral measurement target should provide good representativeness of the vegetation type under study. Hence, the sensor viewing target should avoid areas influenced by external disturbance. The physical support should be strong enough to bear the payload of the instrument limiting oscillations.
2. The sensor should be firmly mounted; however, considering that it should be easily dismounted for re-calibration and cleaning maintenance. Reference standard (both panel and cosine receptors) should be mounted horizontally, with accuracy better than ±3°.
3. The downward looking sensor should be mounted as to avoid seeing direct sky light, sun glint or any other light sources or shining surfaces, like metal or water surfaces. It should be set in a rainproof housing with open bottom, and a matt black inside color. The FOV response should be known in order to precisely measure the target area of interest.
4. Nadir view of the sensor is generally preferable to reduce the BRDF effect in the measurements. In this case, the installation of the sensor towards south is suggested. In case the sensors has to be installed off-nadir the measurements is biased by the anisotropy of the canopy. Off-nadir installation towards south would mean looking at the dark spot but at the same time shadows due to operator or mast are limited. On the contrary, sensor installation towards north would measure the target hot spot but the shadowing effect could be included in the FOV.
5. Field spectrometers with cooling systems are preferable to not temperature controlled device. In case no power supply can be provided at the site a trace back of the operating temperature of the instrument is needed to correct the measurements according to previous laboratory temperature effect characterization. Generally, these instruments are operated in laboratory condition and the suggested temperature, unless specific cases, can be

considered between 20 °C and 25 °C.

3.4.2 Spectral data collection

1. In case a single beam system is used the suggested cycle of measurements consists in:

    - Optimization of the signal. The signal has to be optimized in order to find the best compromise taking into account the nonlinearity of the detector used and to maximize the SNR. This information can be obtained after a laboratory characterization of the spectrometers.
    - Number of spectra average can be decided according to the SNR of the spectrometer and the limitations due to the cycle acquisition time
    - Dark current measurement. The dark spectrum can be measured completely closing the entrance of the spectrometer.
    - First reference measurement using reference panels or cosine receptors.
    - Target measurement.
    - Second reference measurement.

    In case a dual beam system is used the reference and target measurement are simultaneously collected. Nevertheless, the first three steps have to be followed.

2. Data sampling interval should not be over 10 seconds, in order to sample at the same light condition for all the channels of a site. The average time should not exceed 30 minutes. The data should be saved as a sample at the middle time point of the average period. For example, the value for 12:00 hour should be the average measurements from 11:45 to 12:15 if using 30 min. averaging time. Note, however, that such long averages may introduce unknown large errors in days with rapidly changing cloud cover, and are not suitable for studying daily spectral patterns.

3.4.3 Signal data processing

A general procedure for data processing to obtain radiance value and reflectance factor is given here for both single and dual beam systems.

1. Correction for temperature variability. The temperature dependency of the measurement need to be known from laboratory test in order to correct the signal. A trace back of the temperature measurements has to be collected.
2. Correction for dark current. The dark current signal collected with the same integration time has to be subtracted from the spectrum.

3. Nonlinearity correction. The nonlinearity laboratory characterization has to be applied to reduce the measurement uncertainty. Is generally suggested to avoid optimizing the signal in the higher part of the spectrum (80%)
4. Wavelength correction. Wavelength corrections gains need to be applied to compensate the spectral shift of the detector.
5. Radiometric calibration. In order to obtain measurement expressed in physical unit the previous calculated radiometric coefficients have to be applied.
6. Calculation of the reference value at the measurement time. This step refers to single beam device. To overcome the problem related to different time acquisition of reference and target the reference value has to be referred at the target acquisition times using a linear interpolation between the two references.
7. Reflectance factor computation is finally calculated as followed

$$R = \frac{\pi \cdot L_{Down\_radiance}}{E_{Up\_irradiance}} \quad [3.5]$$

Where $L_{Down\_radiance}$ is reflected radiance (unit: $w \cdot m^{-2} \cdot nm^{-1} \cdot sr^{-1}$), and $E_{Up\_irradiance}$ is the incoming irradiance (unit: $w \cdot m^{-2} \cdot nm^{-1}$). Notice, if the radiometric calibration factor has the π factor already included π should not be included in the equation again.

3.4.4 Data averaging

Averaging is often necessary in data processing to reduce random measurement noise. Because of the BRDF effect, the averaging process on reflectance and indices should be made cautiously, preferably not including data outside the 11:30 to 12:30 period, if one wants to extract solar noon data to study the annual patterns. Too long averaging periods will introduce systematic error from BRDF effects, sun position variations, and varied cloud cover.

3.5 Conclusions

Currently, within the proximal sensing community there is no agreement on one particular instrument to be used for field measurements. Indeed it is quite difficult to have an agreement on the protocol because it can vary depending on the aim of the study and on the instrument used. However, several instruments (hyperspectral and multispectral) have been proposed to measure optical properties of the vegetation. Getting reliable and repeatable high quality data is therefore strictly related to the definition of standard protocol used. The measurement uncertainties can be reduced by laboratory characterization of the instruments and by following the same acquisition strategy in the field. The calibration processes should be done yearly and checked periodically during the acquisition season. Beside a deep knowledge of the instrumental characteristics of the device used the target characterization is important to define the more suitable acquisition scheme. In fact, the more representative spot have to be selected

as target of the measurement considering at the same time the angular view of the instrument (i.e. nadir view is preferable). If physical constraints exist at the site the selection of the angular view should be carefully evaluated in order to reduce uncertainties due to hotspot, darkspot or shadowing in the instrument field of view. In addition to reduce even more the directional effects data averaging should be made just considering midday data. Finally, a rigorous data processing chain of the acquired measurements has to be implemented in order to get high quality data considering all the calibration coefficients previously defined (nonlinearity factors, spectral shift correction, radiometric coefficients etc.) and to filter the data time series removing data collected under unfavorable condition (e.g. variable illumination conditions, extreme value of solar zenith angle).

Acknowledgement

This work was funded by COST Action, ES0903 (EUROSPEC). The main researchers involved in the project are listed below:

Mac Arthur, A., Porcar Castell, A., Rossini, M., Vescovo, L, Anderson, K., Balzarolo, M., Cerasoli, S. Eklundh, L., Hueni, A. Jin, H., Pacheco-Labrador, J., I., Martin, P., Nichol, C., Sakowska, K.,Tomelleri, E.

References

Alton, P.B., 2013. From site-level to global simulation: Reconciling carbon, water and energy fluxes over different spatial scales using a process-based ecophysiological land-surface model. Agric. For. Meteorol. 176, 111–124.

Anderson, K., Rossini, M., Pacheco-Labrador, J., Balzarolo, M., Mac Arthur, A., Fava, F., Julitta, T., Vescovo, L., 2013. Inter-comparison of hemispherical conical reflectance factors (HCRF) measured with four fibre-based spectrometers. Opt. Express 21, 605–17.

Baldocchi, D., 2008. TURNER REVIEW No. 15. "Breathing" of the terrestrial biosphere: lessons learned from a global network of carbon dioxide flux measurement systems. Aust. J. Bot. 56, 1.

Balzarolo, M., Anderson, K., Nichol, C., Rossini, M., Vescovo, L., Arriga, N., Wohlfahrt, G., Calvet, J.-C., Carrara, A., Cerasoli, S., Cogliati, S., Daumard, F., Eklundh, L., Elbers, J.A., Evrendilek, F., Handcock, R.N., Kaduk, J., Klumpp, K., Longdoz, B., Matteucci, G., Meroni, M., Montagnani, L., Ourcival, J.-M., Sánchez-Cañete, E.P., Pontailler, J.-Y., Juszczak, R., Scholes, B., Martín, M.P., 2011. Ground-Based Optical Measurements at European Flux Sites: A Review of Methods, Instruments and Current Controversies. Sensors 11, 7954–7981.

Baranows, R., 2008. Spectrograph Design Fundamentals. Imaging Sci. Journal, 56, 121–121.

Beer, C., Reichstein, M., Tomelleri, E., Ciais, P., Jung, M., Carvalhais, N., Rödenbeck, C., Arain, M.A., Baldocchi, D., Bonan, G.B., Bondeau, A., Cescatti, A., Lasslop, G., Lindroth, A., Lomas, M., Luyssaert, S., Margolis, H., Oleson, K.W., Roupsard, O., Veenendaal, E., Viovy, N., Williams, C., Woodward, F.I., Papale, D., 2010. Terrestrial gross carbon dioxide uptake: global distribution and covariation with climate. Science 329, 834–8.

Biging, G.S., Larrieu, M.R., 2003. Estimation of forest leaf area index using vegetation indices derived from hyperion hyperspectral data. IEEE Trans. Geosci. Remote Sens. 41, 1355–1362.

Busetto, L., Meroni, M., Crosta, G.F., Guanter, L., Colombo, R., 2011. SpecCal: Novel software for in-field spectral characterization of high-resolution spectrometers. Comput. Geosci. 37, 1685–1691.

Carmagnola, C.M., Domine, F., Dumont, M., Wright, P., Strellis, B., Bergin, M., Dibb, J., Picard, G., Libois, Q., Arnaud, L., Morin, S., 2013. Snow spectral albedo at Summit, Greenland: measurements and numerical simulations based on physical and chemical properties of the snowpack. Cryosph. 7, 1139–1160.

Drolet, G., Wade, T., Nichol, C.J., MacLellan, C., Levula, J., Porcar-Castell, A., Nikinmaa, E., Vesala, T., 2014. A temperature-controlled spectrometer system for continuous and unattended measurements of canopy spectral radiance and reflectance. Int. J. Remote Sens. 35, 1769–1785.

Dumont, M., Brissaud, O., Picard, G., Schmitt, B., Gallet, J.-C., Arnaud, Y., 2010. High-accuracy measurements of snow Bidirectional Reflectance Distribution Function at visible and NIR wavelengths – comparison with modelling results. Atmos. Chem. Phys. 10, 2507–2520.

Frankenberg, C., O'Dell, C., Guanter, L., McDuffie, J., 2012. Remote sensing of near-infrared chlorophyll fluorescence from space in scattering atmospheres: implications for its retrieval and interferences with atmospheric CO_2 retrievals. Atmos. Meas. Tech. 5, 2081–2094.

Gamon, J.A., Coburn, C., Flanagan, L.B., Huemmrich, K.F., Kiddle, C., Sanchez-Azofeifa, G.A., Thayer, D.R., Vescovo, L., Gianelle, D., Sims, D.A., Rahman, A.F., Pastorello, G.Z., 2014. SpecNet revisited: bridging flux and remote sensing communities. Can. J. Remote Sens. 36, S376–S390.

Gamon, J.A., Peñuelas, J., Field, C.B., 1992. A narrow-waveband spectral index that tracks diurnal changes in photosynthetic efficiency. Remote Sens. Environ. 41, 35–44.

Gamon, J.A., Rahman, A.F., Dungan, J.L., Schildhauer, M., Huemmrich, K.F., 2006. Spectral Network (SpecNet)-What is it and why do we need it? Remote Sens. Environ. 103, 227–235.

Gao, B.-C., Montes, M.J., Davis, C.O., 2004. Refinement of wavelength calibrations of hyperspectral imaging data using a spectrum-matching technique. Remote Sens. Environ. 90, 424–433.

Giardino, C., Brivio, P.A., 2003. The application of a dedicated device to acquire bidirectional reflectance factors over natural surfaces. Int. J. Remote Sens. 24, 2989–2995.

Gitelson, A.A., Merzlyak, M.N., 1996. Signature Analysis of Leaf Reflectance Spectra: Algorithm Development for Remote Sensing of Chlorophyll. J. Plant Physiol. 148, 494–500.

Green, R.O., Pavri, B.E., Chrien, T.G., 2003. On-orbit radiometric and spectral calibration characteristics of eo-1 hyperion derived with an underflight of aviris and in situ measurements at salar de arizaro, argentina. IEEE Trans. Geosci. Remote Sens. 41, 1194–1203.

Guanter, L., Richter, R., Moreno, J., 2006. Spectral calibration of hyperspectral imagery using atmospheric absorption features. Appl. Opt. 45, 2360.

Guzman, C.T., Palmer, J.M., Slater, P.N., Bruegge, C.J., Miller, E.A., 1991. Requirements of a solar diffuser and measurements of some candidate materials, in: Guenther, B.W. (Ed.), Orlando '91, Orlando, FL. International Society for Optics and Photonics, pp. 120–131.

Haboudane, D., Miller, J.R., Tremblay, N., Zarco-Tejada, P.J., Dextraze, L., 2002. Integrated narrow-band vegetation indices for prediction of crop chlorophyll content for application to precision agriculture. Remote Sens. Environ. 81, 416–426.

Hilker, T., Coops, N.C., Hall, F.G., Black, T.A., Wulder, M.A., Nesic, Z., Krishnan, P., 2008. Separating physiologically and directionally induced changes in PRI using BRDF models. Remote Sens. Environ. 112, 2777–2788.

Hilker, T., Nesic, Z., Coops, N.C., Lessard, D., 2010. A NEW, AUTOMATED, MULTIANGULAR RADIOMETER INSTRUMENT FOR TOWER-BASED OBSERVATIONS OF CANOPY REFLECTANCE (AMSPEC II). Instrum. Sci. Technol. 38, 319–340.

Hufkens, K., Friedl, M., Sonnentag, O., Braswell, B.H., Milliman, T., Richardson, A.D., 2012. Linking near-surface and satellite remote sensing measurements of deciduous broadleaf forest phenology. Remote Sens. Environ. 117, 307–321.

Ide, R., Oguma, H., 2010. Use of digital cameras for phenological observations. Ecol. Inform. 5, 339–347.

Joos, F., Prentice, I.C., Sitch, S., Meyer, R., Hooss, G., Plattner, G.-K., Gerber, S., Hasselmann, K., 2001. Global warming feedbacks on terrestrial carbon uptake under the Intergovernmental Panel on Climate Change (IPCC) Emission Scenarios. Global Biogeochem. Cycles 15, 891–907.

Jung, M., Reichstein, M., Margolis, H.A., Cescatti, A., Richardson, A.D., Arain, M.A., Arneth, A., Bernhofer, C., Bonal, D., Chen, J., Gianelle, D., Gobron, N., Kiely, G., Kutsch, W., Lasslop, G., Law, B.E., Lindroth, A., Merbold, L., Montagnani, L., Moors, E.J., Papale, D., Sottocornola, M., Vaccari, F., Williams, C., 2011. Global patterns of land-atmosphere fluxes of carbon dioxide, latent heat, and sensible heat derived from eddy covariance, satellite, and meteorological observations. J. Geophys. Res. 116, G00J07.

Kantzas, E.P., McGonigle, A.J.S., Bryant, R.G., 2009. Comparison of Low Cost Miniature Spectrometers for Volcanic SO(2) Emission Measurements. Sensors (Basel). 9, 3256–68.

Keenan, T.F., Baker, I., Barr, A., Ciais, P., Davis, K., Dietze, M., Dragoni, D., Gough, C.M., Grant, R., Hollinger, D., Hufkens, K., Poulter, B., McCaughey, H., Raczka, B., Ryu, Y., Schaefer, K., Tian, H., Verbeeck, H., Zhao, M., Richardson, A.D., 2012. Terrestrial biosphere model performance for inter-annual variability of land-atmosphere CO2 exchange. Glob. Chang. Biol. 18, 1971–1987.

Kostkowski, H.J., 1997. Reliable spectroradiometry. Reliab. spectroradiometry, Publ. La Plata, MD Spectroradiometry Consult. 1997.

Kriebel, K.T., 1978. Measured spectral bidirectional reflection properties of four vegetated surfaces. Appl. Opt. 17, 253–9.

Mac Arthur, A., MacLellan, C.J., Malthus, T., 2012. The Fields of View and Directional Response Functions of Two Field Spectroradiometers. IEEE Trans. Geosci. Remote Sens. 50, 3892–3907.

Mac Arthur, A.A., MacLellan, C., Malthus, T.J., 2007. The implications of non-uniformity in fields-of-view of commonly used field spectroradiometers, in: 2007 IEEE International Geoscience and Remote Sensing Symposium. IEEE, pp. 2890–2893.

Meroni, M., Busetto, L., Guanter, L., Cogliati, S., Crosta, G.F., Migliavacca, M., Panigada, C., Rossini, M., Colombo, R., 2010. Characterization of fine resolution field spectrometers using solar Fraunhofer lines and atmospheric absorption features. Appl. Opt. 49, 2858–71.

Migliavacca, M., Galvagno, M., Cremonese, E., Rossini, M., Meroni, M., Sonnentag, O., Cogliati, S., Manca, G., Diotri, F., Busetto, L., Cescatti, A., Colombo, R., Fava, F., Morra di Cella, U., Pari, E., Siniscalco, C., Richardson, A.D., 2011. Using digital repeat photography and eddy covariance data to model grassland phenology and photosynthetic CO2 uptake. Agric. For. Meteorol. 151, 1325–1337.

Milton, E.J., Schaepman, M.E., Anderson, K., Kneubühler, M., Fox, N., 2009. Progress in field spectroscopy. Remote Sens. Environ. 113, S92–S109.

Morisette, J.T., Privette, J.L., Justice, C.O., 2002. A framework for the validation of MODIS Land products. Remote Sens. Environ. 83, 77–96.

Pacheco-Labrador, J., Ferrero, A., Martín, M.P., 2014. Characterizing integration time and gray-level-related nonlinearities in a NMOS sensor. Appl. Opt. 53, 7778.

Pacheco-Labrador, J., Martin, M.P., 2014. Nonlinear Response in a Field Portable Spectroradiometer: Characterization and Effects on Output Reflectance. IEEE Trans. Geosci. Remote Sens. 52, 920–928.

Painter, T.H., 2004. Measurements of the hemispherical-directional reflectance of snow at fine spectral and angular resolution. J. Geophys. Res. 109, D18115.

Painter, T.H., Paden, B., Dozier, J., 2003. Automated spectro-goniometer: A spherical robot for the field measurement of the directional reflectance of snow. Rev. Sci. Instrum. 74, 5179.

Panigada, C., Rossini, M., Meroni, M., Cilia, C., Busetto, L., Amaducci, S., Boschetti, M., Cogliati, S., Picchi, V., Pinto, F., Marchesi, A., Colombo, R., 2014. Fluorescence, PRI and canopy temperature for water stress detection in cereal crops. Int. J. Appl. Earth Obs. Geoinf. 30, 167–178.

Pettorelli, N., Vik, J.O., Mysterud, A., Gaillard, J.-M., Tucker, C.J., Stenseth, N.C., 2005. Using the satellite-derived NDVI to assess ecological responses to environmental change. Trends Ecol. Evol. 20, 503–10.

Porcar-Castell, A., Garcia-Plazaola, J.I., Nichol, C.J., Kolari, P., Olascoaga, B., Kuusinen, N., Fernández-Marín, B., Pulkkinen, M., Juurola, E., Nikinmaa, E., 2012. Physiology of the seasonal relationship between the photochemical reflectance index and photosynthetic light use efficiency. Oecologia 170, 313–23.

Potter, C.S., Randerson, J.T., Field, C.B., Matson, P.A., Vitousek, P.M., Mooney, H.A., Klooster, S.A., 1993. Terrestrial ecosystem production: A process model based on global satellite and surface data. Global Biogeochem. Cycles 7, 811–841.

Richardson, A.D., Jenkins, J.P., Braswell, B.H., Hollinger, D.Y., Ollinger, S. V, Smith, M.-L., 2007. Use of digital webcam images to track spring green-up in a deciduous broadleaf forest. Oecologia 152, 323–34.

Rossini, M., Cogliati, S., Meroni, M., Migliavacca, M., Galvagno, M., Busetto, L., Cremonese, E., Julitta, T., Siniscalco, C., Morra di Cella, U., Colombo, R., 2012. Remote sensing-based estimation of gross primary production in a subalpine grassland. Biogeosciences 9, 2565–2584.

Rossini, M., Migliavacca, M., Galvagno, M., Meroni, M., Cogliati, S., Cremonese, E., Fava, F., Gitelson, A., Julitta, T., Morra di Cella, U., Siniscalco, C., Colombo, R., 2014. Remote estimation of grassland gross primary production during extreme meteorological seasons. Int. J. Appl. Earth Obs. Geoinf. 29, 1–10.

Schaepman, M.E., Dangel, S., 2000. Solid Laboratory Calibration of a Nonimaging Spectroradiometer. Appl. Opt. 39, 3754.

Schaepman-Strub, G., Schaepman, M.E., Painter, T.H., Dangel, S., Martonchik, J. V., 2006. Reflectance quantities in optical remote sensing-definitions and case studies. Remote Sens. Environ. 103, 27–42.

Sims, D.A., Gamon, J.A., 2002. Relationships between leaf pigment content and spectral reflectance across a wide range of species, leaf structures and developmental stages. Remote Sens. Environ. 81, 337–354.

Sonnentag, O., Hufkens, K., Teshera-Sterne, C., Young, A.M., Friedl, M., Braswell, B.H., Milliman, T., O'Keefe, J., Richardson, A.D., 2012. Digital repeat photography for phenological research in forest ecosystems. Agric. For. Meteorol. 152, 159–177.

Springsteen, A., 1999. Standards for the measurement of diffuse reflectance – an overview of available materials and measurement laboratories. Anal. Chim. Acta 380, 379–390.

Tucker, C.J., Sellers, P.J., 1986. Satellite remote sensing of primary production. Int. J. Remote Sens. 7, 1395–1416.

Xiong, G., Zhang, J., Yang, G., Yang, J., Li, H., Hu, Z., Zhao, Y., Wei, M., Yi, T., 2014. Different approaches to precise wavelength calibration of a flat-field grating spectrometer for laser-produced plasmas. Phys. Scr. 89, 065005.

Zalewski, E.F., 1994. Radiometry and Photometry, in: Handbook of Optics, Vol. 2: Devices, Measurements, and Properties. p. 1568.

Zhao, F., Li, Y., Dai, X., Verhoef, W., Guo, Y., Shang, H., Gu, X., Huang, Y., Yu, T., Huang, J., 2015. Simulated impact of sensor field of view and distance on field measurements of bidirectional reflectance factors for row crops. Remote Sens. Environ. 156, 129–142.

Zhao, M., Heinsch, F.A., Nemani, R.R., Running, S.W., 2005. Improvements of the MODIS terrestrial gross and net primary production global data set. Remote Sens. Environ. 95, 164–176.

Chapter 4

Impact of reference standard differences on biophysical and biochemical parameter estimation

The study presented in this chapter has been conducted during a Short Term Scientific Mission at the NERC Field Spectroscopy Facility, University of Edinburgh and funded by the EUROSPEC COST Action.

In field spectroscopy the solar irradiance (E_{tot}) measurement is commonly collected using field reference standards (RS) (i.e white panels and cosine receptors) made by materials with highly lambertian behaviour. Reflected radiance of the surfaces is normalized by E_{tot} to compute the Hemispherical Directional Reflectance Factor (HDRF) then used for Vegetation Indices (VI) calculation. Differences in the standard reference types, designs and materials could artificially affect the measured E_{tot} and indirectly the reflectance factor. The objective of the study presented in this chapter is to determine how five different reference standards (one spectralon panel and four cosine receptors)commonly used in the field can affect the E_{tot} measurements and consequently HDRF, VIs and finally the estimation of biochemical and biophysical parameters based on empirical relationships with VIs. The angular response of the different reference standards has been characterized in laboratory. Different HDRF were modeled using Prospect 5 coupled with 4SAIL, according to different canopy types, solar zenith angles and biochemical/biophysical parameter values.Errors due to the measured angular response have been subsequently applied to the modelled reflectances and datasets of modelled HDRF for each reference standard have been produced. VIs and biochemical/biophysical parameter values have been calculated on all the modelled datasets (true-ref and mod-ref) and compared in order to quantify the angular response effect on reflectance regions, on the VIs calculation and on the biochemical/biophysical parameter estimation. The obtained results show that depending on the RS considered the effect can be high on the HDRF (exceeding 20%) for Zenith Angle (ZA) greater than 60°, while it can be reduced using normalized VIs. The effect on the biochemical/biophysical parameter estimation is generally low and it follows the behaviours of the indices used for the model parameterization, the worst cases (obtained with commercially available cosine receptors) show an error of approximately 20%.

4.1 Introduction and objectives

Leaf area index (LAI), which quantifies the amount of foliage area per unit ground surface area and Chlorophyll*a* and *b* contents (Chl) are important parameters controlling many biological and physical processes associated with vegetation on the Earth's surface, such as photosynthesis, respiration, transpiration, carbon and nutrient cycle (Filella et al., 1995; Moran et al., 2000; Zhu et al., 2013). Chlorophyll content determination is commonly made in laboratory, with organic solvents and determined by spectrophotometric measurements(Lichtenthaler et al., 1986). Several techniques have been proposed for in situ measurements of LAI, both destructive and not destructive(Jonckheere et al., 2004). All these techniques are expensive and time consuming. Therefore in the last decades alternative solutions of LAI estimation and leaf pigment content determination with non-destructive optical methods have been developed (Gitelson et al., 2003; Haboudane, 2004). These methods, based on optical properties of the vegetation, are non-destructive and less expensive. Specific spectral region of canopy reflectance are related to chlorophyll absorption (i.e. red region) or to the canopy scattering (i.e. near infrared, NIR). The use of Vegetation Indices (VIs) based on reflectance values in these specific regions have been used to establish empirical relation (mostly linear or logarithmic) with LAI or Chl content (Card et al., 1988; Gitelson and Merzlyak, 1997; Haboudane et al., 2002; Hyer and Goetz, 2004; Li et al., 2014; Sims and Gamon, 2002). As describe in previous chapters reflectance measurement is obtained by field spectroscopy techniques measuring the reflected radiance (I_r) of the target and the solar irradiance (E_{tot}). The reflectance factor is then computed as the ratio of the two. E_{tot} measurements are generally made performing reference standard scans before and after that from the target(Milton et al., 2009). Reference standards (panels or cosine receptors) are made by material with highly lambertian behaviour and once their reflectance or transmittance properties are characterized the measurements are usually approximated to E_{tot}. Efforts have been made in characterizing the anisotropy of different reference standards both panels and cosine receptors (Bruegge et al., 1991; Lubin and Vogelmann, 2011; Meywerk and Ramanathan, 1999) in order to determine possible corrections factor to apply to the measurements collected in the field. Nevertheless to our knowledge no works have been proposed to quantify the impact of the reference standard angular response on vegetation optical properties measurements. Therefore the objectives of the study proposed here are the determination of the angular response effect of the reference standards on the vegetation reflectance, on the vegetation indices calculation and finally on the biochemical or biophysical parameter estimation. In order to achieve these aims the angular response of five commonly used reference standards has been characterized in laboratory condition. Prospect 5 coupled with 4SAIL (Jacquemoud et al., 2009) was used toproduced a modelled dataset considering different canopy types, Chl contents, LAI values and Solar Zenith Angle (SZA). The measured angular response has been then used to introduce expressly an error in the simulated dataset. The errors due to the introduction of the real angular response factors have been

quantified and evaluated comparing reflectance and VIs obtained with and without considering the RS angular response. Finally the angular response effect of the five reference standards has been evaluated on the Chl and LAI estimation.

4.2 Materials and methods

4.2.1 Laboratory characterization: experimental set up

The experiment was conducted at the NERC Field spectroscopy laboratory, University of Edinburgh. Fourcosine receptors (CR) and one white panelcommonly used in the field for outdoor E_{tot} measurements have been initially spectrally characterized. In particular, the reference standards (RS) used are: Spectralon panel (99% reflectivity, Labsphere, Inc.), Cosine Corrector 3 from Ocean Optics (hereafter called CC3), Cosine corrector from Unispec, (hereafter UNI435), and two prototypes consisting in one Integrating spheres (IS) designed at the NERC Field Spectroscopy Facility (FSF) (hereafter FSF IS) and one at the University of Milano Bicocca (hereafter Unimib IS). Typologies and materials of the receptors are reported in Table 4.1.

Name	Type	Material
Ocean Optics	CC3	**Opaline glass**
Unispec	UNI435	**PTFE**
Unimib IS	Prototype Integrating Sphere	**Polycarbonate**
FSF IS	Prototype Integrating Sphere	**---**
White panel	SRT-99-180	**Spectralon**

Table 4.1 Name, type/model and material of reference standards used are reported in the table.

The angular response of the RSs was characterized in laboratory in order to evaluate their differences and to quantify the impact of this deviation on the measured radiance. For this purpose, the RSs were fixed on an optical Table where a rotating arm allowed to control the angular position of a halogen lamp powered by a stabilised power supply (Figure 4.1). Intensity measurements (reflected light for white panel and transmitted light for CRs) for zenith angles varying from 90to 0 (with a step of 5.625°) were collected using an Ocean Optics USB2000+ spectrometer coupled with an optical fibre (2 meters, 400 μm, VIS/NIR). Per each step 9 measurements were acquired and at the beginning and at the end of the run the dark current was measured. Then, the RSs were rotated around their symmetry axis to change the azimuth angle (from 0° to 270°with a 90° step) and the measurements at the different zenith angles were acquired following the same acquisition scheme in order to measure the four principal axes.

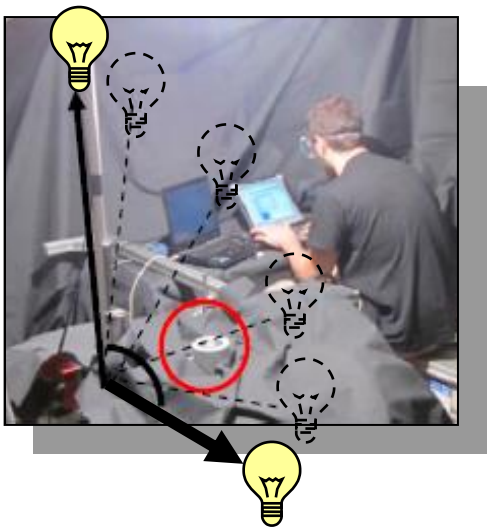

Figure 4.1 Set up used for the laboratory characterization. In the horizontal plane the cosine receptor is fixed (in the picture the FSF IS, rounded in red). The rotating arm allows a movement from the vertical position up to the horizontal one. The arm stops each 5.625 degree. The receptor response at 17 zenith angles has been characterized per each sensor.

Relative intensities normalized by light intensity measured at Zenith Angle(ZA) of 0° were calculated. The angular response has been calculated following Carmagnola et al. (2013) using the equation 4.1:

$$AR(\lambda, \Theta, \varphi) = \frac{I(\lambda,\Theta,\varphi)}{I(\lambda,0,\varphi)} \quad [-] \qquad [4.1]$$

whereAR is the angular response, I is the measured radiance, λ is the wavelength, Θ and φ are the zenith and azimuth angle respectively. The angular cosine response has been finally calculated as the average of the four values measured at different azimuth angle for each zenith angle.

To minimize the effect of the diffuse light conditions all the measurements have been conducted in a dark room with black wall reflecting less than 10%. In order to determine the proportion of direct and diffuse light at the different ZA the measurements of the direct to diffuse ratio were acquired following the approach proposed in Milton (2009). An opaque black small parasol has been used to shade the panel or CRs from the direct lamp beam for each zenith angle. At each step two measurements of irradiance are made: sensor shaded and not shaded. The ratio of the shaded and not shaded measurements provides an estimate of the proportion of irradiance diffusing from the walls, compared to that fromthe lamp and walls combined.

$$DGR(\lambda, \Theta, \varphi) = \frac{Is(\lambda,\Theta,\varphi)}{I(\lambda,\Theta,\varphi)} \quad [-] \qquad [4.2]$$

where DGR is the diffuse to global ratio, Is is the measured radiance shading the reference standard, I is the measured radiance without shading the reference standard, λ is the wavelength, Θ and φ are the zenith and azimuth angles.

4.2.2 Simulated vegetation spectra

In order to quantify a possible effect of the angular response of the different RSs considered on vegetation spectra a simulated data set has been produced.
Reflectance spectra were modeled using Prospect 5 coupled with 4SAIL (Jacquemoud et al., 2009) varying the canopy type, the Solar Zenith Angle (SZA), the chlorophyll content and the LAI values (Figure 4.2). In particular, the simulations have been calculated for:

- 6 Canopy types (C): Planophile, Erectophile, Plagiophile, Extremophile, Spherical and Uniform.
- 17 Zenith Angles (ZA) (the same measured in laboratory): from 90° up to 0°, step of 5.625°
- 7 levels of Leaf Area Index (LAI): from 0.5m^2/m^2 to 6.5m^2/m^2– step of 1m^2/m^2
- 10 levels of Chlorophyll content: from 10µg /cm^2 to 100µg /cm^2– step of 10 µg /cm^2

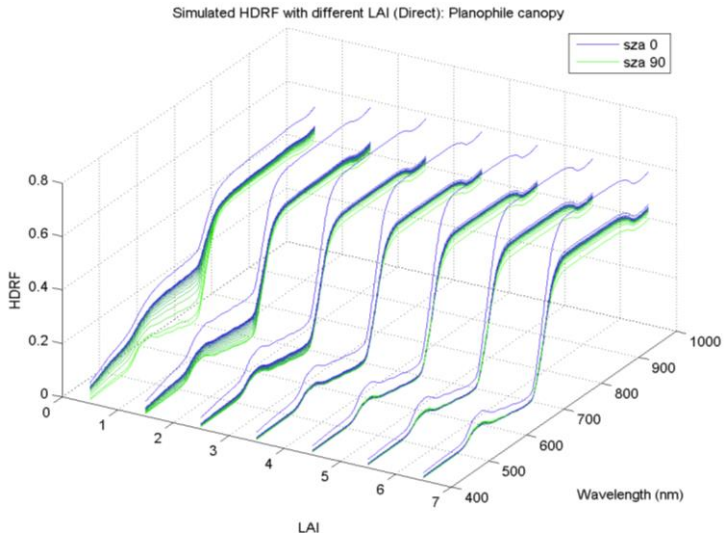

Figure 4.2 Examples of the simulated dataset. The graph represents the variation of reflectance considering the Planophile canopy. The x axis corresponds to 7 different LAI; y axis represents the wavelength; z axis is the reflectance value (HDRF). The colours refer to the 17 SZA angles considered in the simulation.

Spectra have been generated under different illumination conditions, similar to those produced in the laboratory mixing the pure Bidirectional Reflectance Distribution Factor (BRDF, direct light) and Hemispherical Directional Reflectance Factor (HDRF, diffuse light). Different illumination conditions have been defined according to the measured angular DGRs.
Assuming that only the direct beamintroduces a significant deviationfrom the ideal cosine response to the global irradiance as reported in Meywerk and Ramanathan (1999), the reflectances simulated with the model (hereafter true-ref) were used to simulate new reflectances (hereafter mod-ref) considering the effect of the measured RS angular response. The mod-ref has been calculated following the formulation reported below:

$$\rho b(\lambda,\theta,C,bio,RS) = \frac{\rho(\lambda,\theta,C,bio)\times\left[(1-DGR_0)\times I_0\times\cos(\theta)+I_0\times DGR_0\right]}{I(\lambda,\theta,RS)} \quad [-] \quad [4.3]$$

Wherepb is the modelled reflectance, λ is the wavelength, Θ is the Solar Zenith Angle (SZA), C corresponds to canopy type,bio is biophysical/biochemical parameter level (LAI, Chl), RS is the Reference Standard, DGR_0 is the diffuse to global ratio measured at Nadir (equation 4.2) and I is the incoming radiance measured at Nadir (I_0) or at different SZA (Θ.

4.2.3 Vegetation Indices and empirical estimation ofbiochemical and biophysical parameters

True-ref and mod-ref have been used to calculate four VIs commonly considered in field measurements for parameterize empirical model to derive LAI and Chl content of the vegetation targets. The Indices considered in this study are: Normalized Difference Vegetation Index (NDVI and in a different formulation $NDVI_{rededge}$), Soil Adjusted Vegetation Index (SAVI), MERIS Terrestrial Vegetation Index (MTCI). The Index formulations and the relative references are reported in Table 4.2.

Index	Formulation	Bandwidth (nm)	Reference
NDVI	$\frac{\boldsymbol{\rho}865 - \boldsymbol{\rho}655}{\boldsymbol{\rho}865 + \boldsymbol{\rho}655}$	10	Rouse et al. (1973)
SAVI	$\frac{\boldsymbol{\rho}800 - \boldsymbol{\rho}680}{\boldsymbol{\rho}800 + \boldsymbol{\rho}680} * (1 + L)$	10	Huete (1988)
MTCI	$\frac{\boldsymbol{\rho}753.75 - \boldsymbol{\rho}708.75}{\boldsymbol{\rho}708.75 - \boldsymbol{\rho}681}$	10	Dash and Curran(2004)
$NDVI_{(red\ edge)}$	$\frac{\boldsymbol{\rho}750 - \boldsymbol{\rho}680}{\boldsymbol{\rho}750 + \boldsymbol{\rho}680}$	10	Gitelson and Merzlyak (1994)

Table 4.2 Vegetation Indices considered in the analysis. The reflectance value reported in the formulation refers to the central wavelength of the considered bandwidth. In case of SAVI the default value of L = 0.5 is considered.

The original LAI values and Chl content used to parameterize the PROSAIL model are fixed for different Zenith angle and canopy types. The indices calculated on the modelled reflectance can therefore be used in order to model the index variation according to a known biochemical/biophysical parameter, both in the true-ref and in mod-ref. According to the index used and the vegetation parameter which has to be retrieved, linear or logarithmic models can be applied. In particular, linear models have been applied to relate MTCI and $NDVI_{rededge}$to Chl content, while logarithmic models have been applied to all the other index-variable combinations.

4.2.4 Evaluation of the impact of reference standard angular response

To quantify the effect of the five RS angular responses on the reflectance measurements, different variables have been considered: i) two different regions of the spectrum relevant for vegetation analysis: red region (600-700 nm) and Near Infrared (NIR) region (750 – 900 nm); ii) the 4 VIs previously defined; iii) LAI values and Chl content estimation based on index-variable empirical models.

The deviation of values derive from the mod-ref have been expressed as angular percentage error (normalised difference between mod-ref and true-ref derived values):

$$pe(\Theta) = \frac{\mathrm{xb}(\Theta) - \mathrm{x}(\Theta)}{\mathrm{x}(\Theta)} \times 100 \qquad [4.3]$$

where*pe* is the percentage error, xb is the mod-ref derived variable (e.g. spectral region) and x is the true-ref derived variable.

4.3 Results and discussion

4.3.1 RS angular responses

The angular responses of the five RSs, calculated following equation 4.1, are reported in Figure 4.3. It can be noted that different RSs are characterized by specific spectral dependencies.

The white panel, the FSF IS and the Unimib ISshow a stable response across the spectrum (Fig 4.3A, 4.3B and 4.3C). On the contraryfor CC3 and UNI435 cosine receptors a strong wavelength dependency can be noticed (Figure 4.3D and 4.3E).

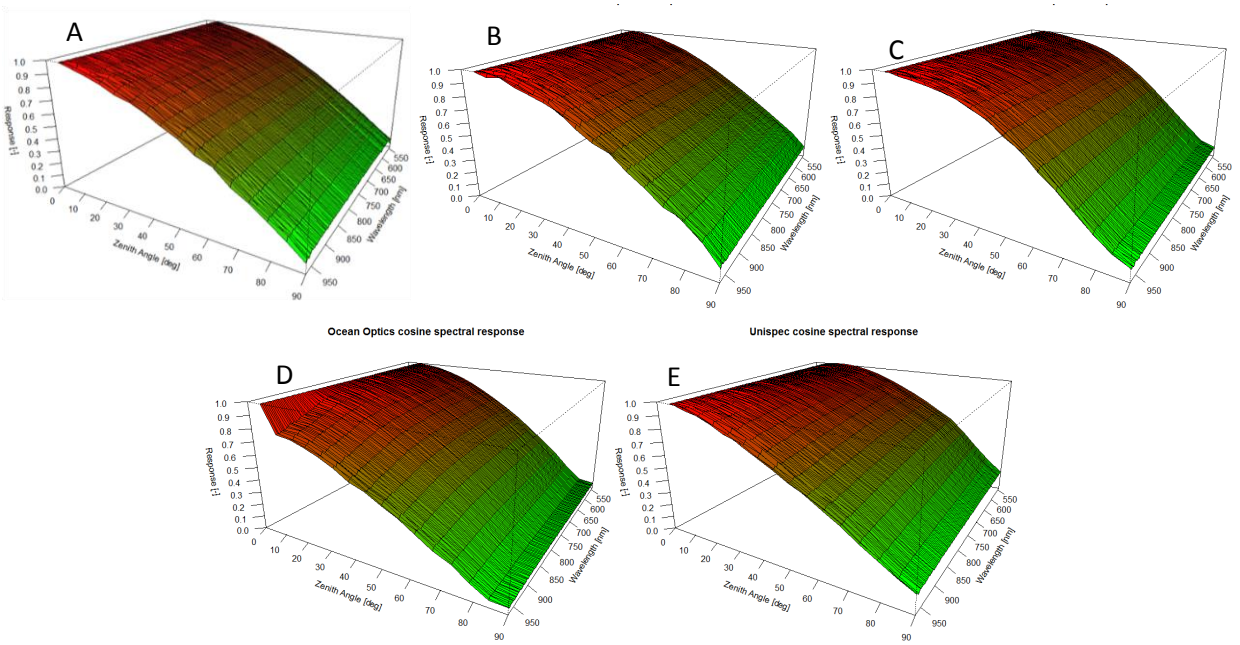

Figure 4.3 A) spectral angular response of the white panel. In the x axis the SZA (degree) is reported; in the y axis the wavelength (from 950nm to 500 nm), in the z axis the angular response. The colours refer to the angular response intensity. B) Spectral response of the FSF IS. C) Spectral response of the Unimib IS. D) Spectral response of the Ocean Optics CC3. E) Spectral response of the Unispec UNI435.

In particular, the CC3 (Fig 4D) shows a strong decrease in correspondence of high SZA in the NIR region (approximately after 900 nm). The shape of the UNI435 response changes with wavelength: while for wavelengthslower than 500 nm the response is akin to a cosine function, for higher wavelengths (800 nm) the response is close to linear. In general, the differences between the angular responses of RSs do not exceed 10% in the visible range. The highest differences can be noticed for Unimib IS in the range of ZA between 25° and 45° and for UNI435 where the differences increase with the ZA. Higher differences (20%) can be detected in the NIR region at ZA lower than 45° for CC3 cosine receptor. On the contrary differences around 15% can be detected in the UNI435 for ZA in the range 25°-65°.

4.3.2 Angular response effect on vegetation spectra and VIs

The magnitude of the angular response effect has been expressed in terms of *pe* (equation 4.3). In particular the analysis has been conducted on all the possible combinations of the modelled reflectances (1020 spectra varying the 10 Chl content levels and 714 varying the 7 LAI values) recalculated taking into account the angular response of the five RSs (equation 4.1). The first variable considered in the *pe* calculations has been the mean reflectance in the red and in the near infrared region. In Figure4.4 the five RSs *pe* variation as a function of ZA is reported for the worst case obtained: Erectophilecanopy, LAI equal to 0.5 and Chl content equal to100 µg /cm^2. It can be noticed that the absolute value of *pe* is increasing with the ZA.

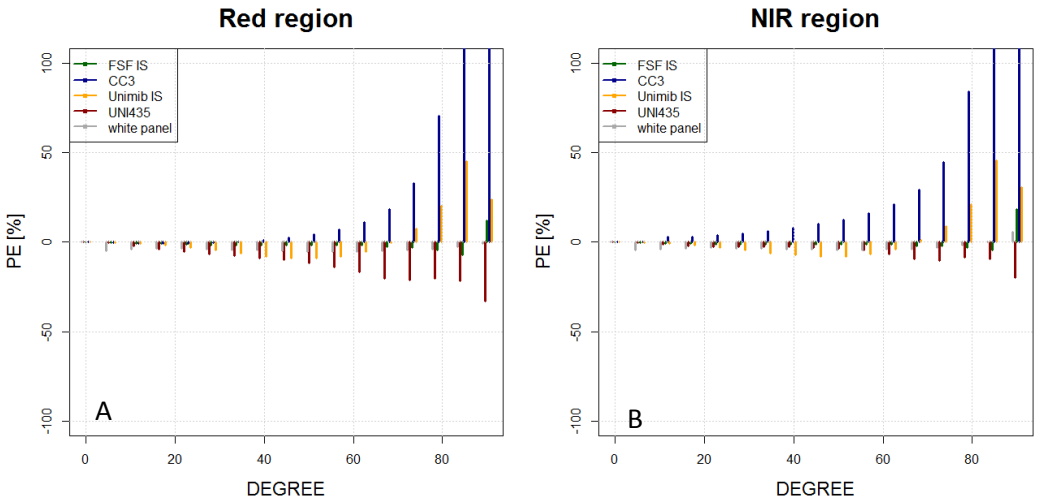

Figure 4.4 A) Percentage error variation on the reflectance in the red region (600-700 nm). The colours represent the RS considered. The variation increases with ZA, reaching the 20% at ZA greater than 60°. B) Percentage of variation in NIR reflectance region. The graphs represent the worst case (with maximum error detected) and correspond to an erectophile canopy with a LAI equal to 0.5 m^2 m^{-2} and Chl content equal to100 µg /cm^2.

The signal recorded at ZA greater than 80° was generally very low because of possible shadowing effects on the cosine receptors oron the white panel. Therefore, ZA greater than 80° can be strongly affected by measurement artefacts and the corresponding *pe* values can be misleading. Overall, the *pe* variation (as maximum around 10%) is similar in the red and in the NIR region for the white panel and FSF IS (in Figure 4.4 grey and green line respectively). The Unimib IS (orange line, Figure 4.4) up to 80° never exceed a *pe* value of 20% and the decrease of the *pe* value between 25° and 60° is in agreements with the AR depicted in Figure 4.3. The CC3 is overestimating the reflectance both in the red and in the NIR region of the spectrum. In the NIR region the overestimation is higher compared to the red region and generally CC3 (blue line in Figure 4.4) appears the RS more affecting the broad reflectance regions considered (25% at 60°). On the contrary UNI435 (red line in Figure 4.4) shows *pe* values lower than 20% up to ZA of 80° in the red region, and in the NIR region this effect is even more reduced.

The true reflectances have been then used to determine the impact of the RSs on the VIs calculation. The comparison between VIs calculated on the true and modeled spectra has been reported in terms of *pe*. Examples of the worsts *pe* obtained on the four indices considered of all the possible combinations are reported in Figure 4.5. In all the case analysed UNI435 showed the higher variation for all the indices. The results refer to Erectophile canopies with all the LAI values and Chl content of 50 µg /cm^2.

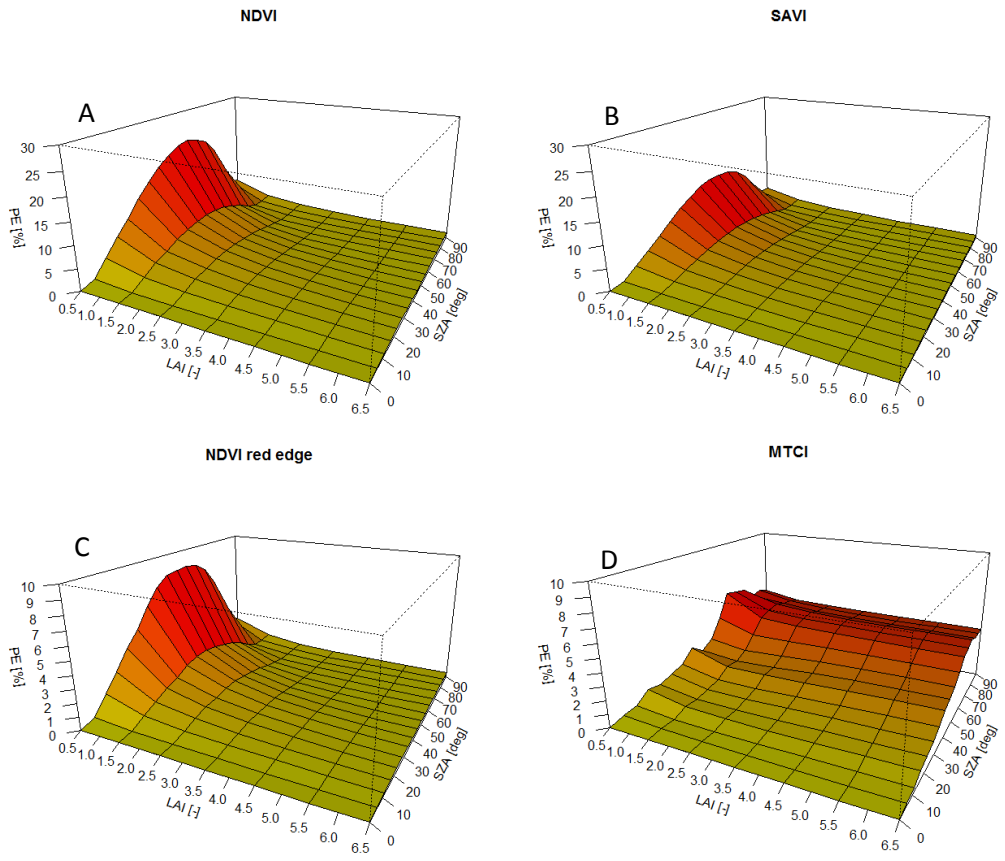

Figure 4.5 Percentage error variation of: A) NDVI, B) SAVI, C) $NDVI_{rededge}$, D) MTCI. The PE refer toUNI435 at different LAI and ZA. In general a higher pe value is noticeable for low LAI value at ZA varying in the range of 30-60 degree.

Figure 4.5 shows the dependency of *pe* on LAI and ZA for the four indices analysed. The *pe* values are higher for low LAI values in the case of NDVI, SAVI and $NDVI_{rededge}$ and they increase for intermediate ZA. In general, NDVI show the higher *pe* value (27%) while *pe* on MTCI (low values obtained, 6%) increase accordingly to the ZA independently to LAI values. In order to give an overall view of the results the worst *pe* obtained between all the combinations consideredis reported in Table 4.3. The worst results always achieved refer to indices calculated on the UNI435 mode-ref for Erectophile canopies. On the other hand better results (data not shown) are generally obtained with mode-ref calculated using the white panel AR. Between the VIs considered, the highest *pe* was recorded for SAVI where the error exceeds the 20%.

Index	Worst result
NDVI	27%
$NDVI_{rededge}$	9%
SAVI	13%
MTCI	6%

Table 4.3 Highest percentage variation observed for each VI. The worst results obtained refer to UNI435.

4.3.3 Angular response effect on Chl and LAI estimates

The empirical models between VIs and Chl content or LAI values have been formulated considering different ZA using both the true and modelled data. An example of the relationship between MTCI and Chl content is reported in Figure 4.6. The Figure depicts the different MTCI values calculated on the true-ref (black dots in Figure 4.6) and the mod-ref. In particular the true-ref used for the MTCI calculation refers to an Erectophile canopy with 10 different values of Chl content calculated at ZA equal to 70°.

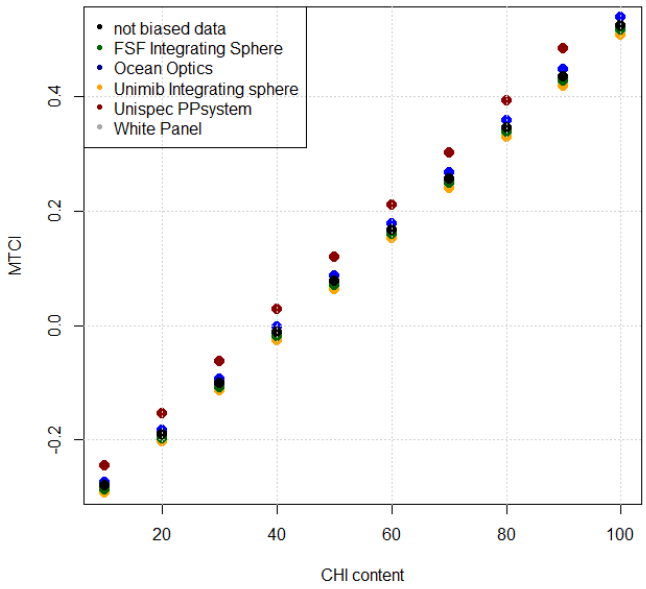

Figure 4.6. The linear relationship between MTCI and Chl content is here reported. The different colours refer to the MTCI calculated using the RS mod-ref.

Figure 4.6 shows that the relationship obtained with the indices computed from UNI435 and CC3 mod-ref (red and blue dots respectively) are those differing the most from the relationship based on true-ref values. In particular, the index values computed from UNI345 and CC3 data are always overestimated.

The linear or logarithmic models applied to all the combinations of the considered variables (VIs and Chl or LAI values) have been inverted to retrieve the Chl content or LAI values derived from the mod-ref. The percentage error has been then reported according to LAI or Chl value and ZA variability (Figure 4.7) for the worsts cases obtained (CC3 and UNI435).

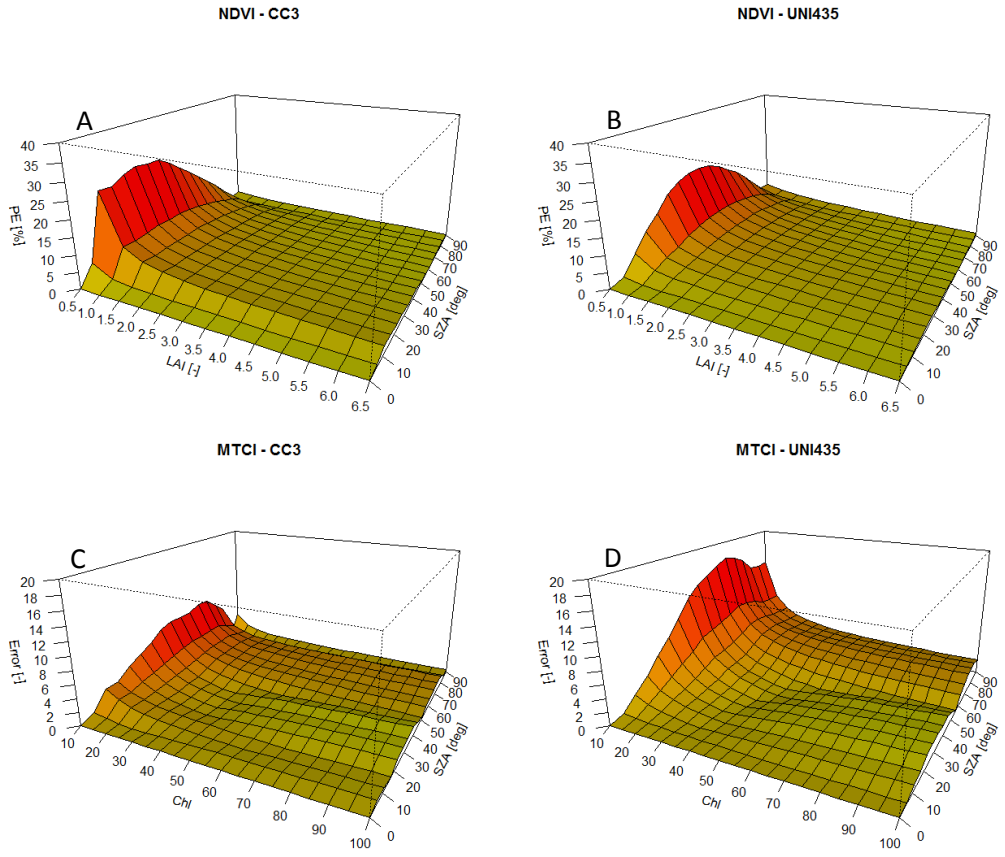

Figure 4.7*Pe* on the LAI values estimation due to the angular response of the five RSs considered. The reported results refer to the worst cases detected in the LAI and Chl content estimation. They refer to Erectophile canopy. A) *Pe* obtained considering the CC3 effect on the NDVI vs LAI empirical modelling (logarithmic relationship); B) *Pe* obtained considering the UNI435 effect on the NDVI vs LAI empirical modelling (logarithmic relationship); C) *Pe* obtained considering the CC3 effect on the MTCI vs Chl content empirical modelling (linear relationship); D) *Pe* obtained considering the UNI435 effect on the MTCI vs LAI empirical modelling (linear relationship).

The *pe* is reported separately for the two RSs and for LAI or Chl content variation. The example refers to the *pe* of the worst case obtained considering the relation NDVI vs. LAI in an erectophile canopy (Figure 4.7 A and B) for CC3 and UNI435 using logarithmic model applied. On the other hand the linear model applied between MTCI andChl content are depicted in Figure 4.7C and D for CC3 and UNI435 respectively. Generally it can be observed that the *pe* values derived from NDVI - LAI relationship follow the *pe* distribution of the index analysed (Figure 4.5). Therefore, the *pe* increases at low LAI values and for intermediate ZA. The values (reported in Table 4.4 as the worst cases detected) reach the 27% for low LAI values, but it immediately decreases considering greater values of LAI. On the contrary the *pe* variation of the Chl content estimation is lower (maximum 17 % for UNI435) and it increases according to the ZA variation. It's important to notice that also in this case the percentage error is higher for low Chl values and it tend to quickly decline increasing the Chl content values.

Table 4.4shows the results of the worst cases of error distribution in the relation VIs vs. Chl content and LAI values. The results show that an effect of the angular response of the RSs in the biophysical/biochemical parametersempirical estimationexists. At the same time the results

show a maximum variation due to the cosine receptor equal to 27% in LAI estimation (UNI435). The worst cases have been detected in correspondence to the intermediate ZA and considering LAI value of 0.5 with cosine receptors that have the worst cosine response (with a significant deviation from the cosine response in the NIR region).

Index	Parameter	Cosine receptor	Worst case
NDVI	LAI	Ocean Optics	27%
SAVI	LAI	Unispec	14%
$NDVI_{(red\ edge)}$	Chl content	Ocean Optics	11%
MTCI	Chl content	Unispec	17%

Table 4.4 Results of the percentage error distribution on the biophysical/biochemical parameter estimation due to the cosine receptor effect. The index considered and the parameters estimated by the index are reported in the two first columns. The third column refers to the cosine receptor that causes the greater error in the estimation, the worst case is reported in the last column

In summary, the laboratory characterization of the angular response of the five RSs analysed allowed the determination of differences between the RS for different ZA. Generally the differences tend to increase for high ZA, apart from the Unimib IS and UNI435 where the higher differences are detected between 25° and 65°. In particular the higher differencescan be observed for CC3 and UNI435 in the reflectance regions.

Nevertheless, the AR laboratory characterization allowed the determination of the RSs impact on reflectance in different spectral regions, VI values and Chl and LAI empirical estimations. The two broad reflectance regions considered, as expected from the RSs angular responses, are more affected for high ZAs. The worst case presented in Figure4.4 showed an average error of 10% starting from ZA equal to 50° both in the red and NIR regions. The highest errors are detected when reflectances are recalculated using the CC3 AR. This can be explained looking at the AR reported in Figure4.3D, where a significant decrease of the response starts in the NIR region after 950 nm.

The errors due to the AR on the VI values were higher considering the UNI435 cosine receptor. In general lower *pe* values have been achieved compared to reflectance. In the VI analysis the AR effect is smoothed due to the fact that such indices are calculated as normalized difference of bands. Therefore spectrally stable ARs are affecting in the same way the regions of the spectrum used to calculate the indices. Moreover, this effect decreases when the spectral distance between the bands selected for the determination of the index is lower. In fact the best results are achieved with MTCI computed using bands within a range of ~70 nm (Table 4.2). On the contrary, the NDVI is calculated on a wider spectral range (210 nm, Table 4.2). This can explain whyNDVI is the index more affected by the AR, especially when computed using UNI435 data, characterized by the worst spectral AR.

Finally, the effect of the AR on the estimation of Chl content and LAI values has been evaluated. Simple empirical models have been applied because generally used in field works. The reduced effect of the AR on VIs is maintained if considering the biochemical or biophysical parameter

estimation. In fact when the *pe* is reported according to ZA and LAI variation the results show the maximum impact (i.e. 27%) for CC3, a cosine receptor with a known bad angular response. Nevertheless, this high impact is immediately reduced for LAI value higher than 1.5 (lower than 10%). This range of error distribution is in line with uncertainties of the LAI measured in the field (5%-20%, Richardson et al., 2011) while for chlorophyll estimation the 17% can be considered low especially considering that this value refers only to low Chl content value for erectophile canopies and it immediately decreases to 10% considering Chl content of 20 µg /cm^2. This value is in line with the expected uncertainty due to chlorophyll content determination (Gitelson, 2005; Palta, 1990).

4.4 Conclusions

The determination of the angular response in laboratory condition allowed the evaluation of the impact of the five reference standard angular response on the: i) vegetation spectral reflectance factor; ii) Vegetation Indices, iii) biochemical and biophysical parameter retrieval. The five reference standards characterized in laboratory showed a different angular response. The AR impact has been evaluated for different Zenith Angles and different canopy types. In particular, regarding the RSangular responses a significant variation across the spectrum has been highlighted in CC3and in UNI435 (more accentuated in the NIR spectral region).

The effects of the angular response on the simulated vegetation reflectances depend on the reference standard used, on the ZA and on the canopy type. The effect is generally increasing with ZA. In the worst case a variation of 40%has been detected for ZA greater than 70°, both in the red and NIR region for CC3 and UNI435, while variations of at most 20% for the other RSs.

AR effect on the VI calculation depends on the considered VI, therefore on its calculation. The effect seems directly proportional to the spectral distance between the bands used for the calculation of the index. Generally, the effect is lower in VIs than in reflectance. In the worst case (NDVI) a variation of 27% has been found.

The AR effect on biochemical or biophysical parameter empirical estimation is even lower with regard reflectance and VIs. The error, which increases accordingly to the variation of the index used to parameterise the relationship, was 27% for LAI and 19% for Chl content estimation in the worst cases (UNI435 and CC3). These worst cases refer to extremely low parameter values (LAI 0.5 and Chl 10 µg/cm^2) while for higher values lower error can be found. A part from the lower parameter values the overall errors obtained are comparable to the errors achievable in the field for the biophysical variable measurements. Therefore we conclude that the use of RSs tested in laboratory could affect in a different way the spectral reflectance measurements in the field, in case of UNI435 and CC3 considerably. For this reason is suggested to avoid using CC3 and UNI435 for reflectance measurements for ZA higher than 60°, unless the data acquired are used for VIs calculation or biochemical/biophysical parameter estimation, where the effect is almost negligible for most of the cases.On the contrary, the other RSs (the best AR achieved is referred to the white spectralon panel) showedlower effect on reflectances, VIS and

biochemical/biophysical parameter estimation, therefore are preferable compared to the others.

Acknowledgement

This work was funded by COSTAction, ES0903 (EUROSPEC) in the context of a Short Term Scientific Mission at the NERC Field Spectroscopy Facility, University of Edinburgh. The main researchers involved in the project: *Fava, F., Mac Arthur, A., Pacheco-Labrador, J. and Rossini, M*

.

References

Bruegge, C.J., Stiegman, A.E., Coulter, D.R., Hale, R.R., Diner, D.J., Springsteen, A.W., 1991. Reflectance stability analysis of Spectralon diffuse calibration panels, in: Guenther, B.W. (Ed.), Orlando '91, Orlando, FL. International Society for Optics and Photonics, pp. 132–142.

Card, D.H., Peterson, D.L., Matson, P.A., Aber, J.D., 1988. Prediction of leaf chemistry by the use of visible and near infrared reflectance spectroscopy. Remote Sens. Environ. 26, 123–147.

Carmagnola, C.M., Domine, F., Dumont, M., Wright, P., Strellis, B., Bergin, M., Dibb, J., Picard, G., Libois, Q., Arnaud, L., Morin, S., 2013. Snow spectral albedo at Summit, Greenland: measurements and numerical simulations based on physical and chemical properties of the snowpack. Cryosph. 7, 1139–1160.

Dash, J., Curran, P.J., 2004. The MERIS terrestrial chlorophyll index. Int. J. Remote Sens. 25, 5403–5413.

Filella, I., Serrano, L., Serra, J., Peñuelas, J., 1995. Evaluating Wheat Nitrogen Status with Canopy Reflectance Indices and Discriminant Analysis. Crop Sci. 35, 1400.

Gitelson, A., Merzlyak, M.N., 1994. Spectral Reflectance Changes Associated with Autumn Senescence of Aesculus hippocastanum L. and Acer platanoides L. Leaves. Spectral Features and Relation to Chlorophyll Estimation. J. Plant Physiol. 143, 286–292.

Gitelson, A.A., 2005. Remote estimation of canopy chlorophyll content in crops. Geophys. Res. Lett. 32, L08403.

Gitelson, A.A., Gritz, Y., Merzlyak, M.N., 2003. Relationships between leaf chlorophyll content and spectral reflectance and algorithms for non-destructive chlorophyll assessment in higher plant leaves. J. Plant Physiol. 160, 271–82.

Gitelson, A.A., Merzlyak, M.N., 1997. Remote estimation of chlorophyll content in higher plant leaves. Int. J. Remote Sens. 18, 2691–2697.

Haboudane, D., 2004. Hyperspectral vegetation indices and novel algorithms for predicting green LAI of crop canopies: Modeling and validation in the context of precision agriculture. Remote Sens. Environ. 90, 337–352.

Haboudane, D., Miller, J.R., Tremblay, N., Zarco-Tejada, P.J., Dextraze, L., 2002. Integrated narrow-band vegetation indices for prediction of crop chlorophyll content for application to precision agriculture. Remote Sens. Environ. 81, 416–426.

Huete, A.., 1988. A soil-adjusted vegetation index (SAVI). Remote Sens. Environ. 25, 295–309.

Hyer, E.J., Goetz, S.J., 2004. Comparison and sensitivity analysis of instruments and radiometric methods for LAI estimation: assessments from a boreal forest site. Agric. For. Meteorol. 122, 157–174.

Jacquemoud, S., Verhoef, W., Baret, F., Bacour, C., Zarco-Tejada, P.J., Asner, G.P., François, C., Ustin, S.L., 2009. PROSPECT+SAIL models: A review of use for vegetation characterization. Remote Sens. Environ. 113, S56–S66.

Jonckheere, I., Fleck, S., Nackaerts, K., Muys, B., Coppin, P., Weiss, M., Baret, F., 2004. Review of methods for in situ leaf area index determination. Agric. For. Meteorol. 121, 19–35.

Li, X., Zhang, Y., Bao, Y., Luo, J., Jin, X., Xu, X., Song, X., Yang, G., 2014. Exploring the Best Hyperspectral Features for LAI Estimation Using Partial Least Squares Regression. Remote Sens. 6, 6221–6241.

Lichtenthaler, H.K., Buschmann, C., Rinderle, U., Schmuck, G., 1986. Application of chlorophyll fluorescence in ecophysiology. Radiat. Environ. Biophys. 25, 297–308.

Lubin, D., Vogelmann, A.M., 2011. The influence of mixed-phase clouds on surface shortwave irradiance during the Arctic spring. J. Geophys. Res. 116, D00T05.

Meywerk, J., Ramanathan, V., 1999. Observations of the spectral clear-sky aerosol forcing over the tropical Indian Ocean. J. Geophys. Res. 104, 24359.

Milton, E.J., Schaepman, M.E., Anderson, K., Kneubühler, M., Fox, N., 2009. Progress in field spectroscopy. Remote Sens. Environ. 113, S92–S109.

Moran, J.A., Mitchell, A.K., Goodmanson, G., Stockburger, K.A., n.d. Differentiation among effects of nitrogen fertilization treatments on conifer seedlings by foliar reflectance: a comparison of methods. Tree Physiol. 20, 1113–1120.

Palta, J.P., 1990. Leaf chlorophyll content. Remote Sens. Rev. 5, 207–213.

Richardson, A.D., Dail, D.B., Hollinger, D.Y., 2011. Leaf area index uncertainty estimates for model–data fusion applications. Agric. For. Meteorol. 151, 1287–1292.

Rouse, J.W., Haas, R.H., Schell, J.A., Deering, D.W., 1973. Monitoring vegetation systems in the Great Plains with ERTS, in: Third ERTS Symposium, NASA SP-351. pp. 309–317.

Sims, D.A., Gamon, J.A., 2002. Relationships between leaf pigment content and spectral reflectance across a wide range of species, leaf structures and developmental stages. Remote Sens. Environ. 81, 337–354.

Zhu, Z., Bi, J., Pan, Y., Ganguly, S., Anav, A., Xu, L., Samanta, A., Piao, S., Nemani, R., Myneni, R., 2013. Global Data Sets of Vegetation Leaf Area Index (LAI)3g and Fraction of Photosynthetically Active Radiation (FPAR)3g Derived from Global Inventory Modeling and Mapping Studies (GIMMS) Normalized Difference Vegetation Index (NDVI3g) for the Period 1981 to 2. Remote Sens. 5, 927–948.

Chapter 5

Comparison of sun-induced chlorophyll fluorescence estimates obtained from four portable field spectroradiometers

This research was conducted in the framework of the FLEX-US Project, ESA/NASA Joint Campaign for the Deployment of the Airborne HyPlant Imaging Spectrometer.

Remote Sensing of Sun-Induced Chlorophyll Fluorescence (SIF) is a research field of growing interest because it offers the potential to accurately quantify terrestrial gross primary productivity/photosynthesis and to monitor plant status. New satellite missions from the European Space Agency, such as the FLuorescence EXplorer (FLEX) --currently an Earth Explorer 8 candidate, and from the National Aeronautics and Space Administration (NASA) such as the Orbiting Carbon Observatory-2 (OCO-2) launched in July 2014, provide the possibility to estimate SIF from space, sampling globally. The SIF signal is small relative to reflected radiation, so that its detection from airborne and satellite platforms is difficult, and an extremely accurate atmospheric correction is needed. At ground level the atmospheric influence in the reflected radiance is negligible. In this context field spectroscopy is considered a valuable tool for evaluating technical requirements for SIF retrieval. Furthermore, ground level estimates of SIF are useful to improve our understanding of the relationships between SIF and additional biophysical properties of vegetation and to aid in the calibration/validation activities of airborne- and satellite-derived SIF data products. Several commercially available spectroradiometers with different spectral and radiometric characteristics have been used to retrieve SIF. This chapter presents an approach and comparison exercise for evaluating the capability of four spectroradiometers to retrieve SIF. The results show that an accurate Far-red SIF estimation can be achieved using spectroradiometers with an ultrafine resolution, where the Full Width at Half Maximum (FWHM) is less than 1 nm, while the Red SIF estimation requires even higher spectral resolution (FWHM < 0.5 nm). Moreover, it is shown that the Signal to Noise Ratio (SNR) plays a significant role in the precision of the Far-red SIF measurements, since the SNR was inversely related to the magnitude of the standard deviations of the Far-red SIF retrievals.

5.1. Introduction and objectives

Sun-Induced Chlorophyll Fluorescence (SIF) is an electromagnetic signal emitted throughout the red and near-infrared (NIR) spectrum by the chlorophyll-a, the primary photosynthetic pigment in green vegetation, in response to the absorption of photosynthetically active radiation from the sun. This low signal, typically 1–5% of the reflected radiation in the NIR, is directly emitted by the photosynthetic apparatus. In the recent two decades, research studies have demonstrated the potential use of SIF to monitor photosynthesis and the functional status of vegetation(Campbell et al., 2008, 2007; Corp et al., 2003; Damm et al., 2010; Maier et al., 2003; Meroni and Colombo, 2006; Panigada et al., 2014; Zarco-Tejada et al., 2013, 2012). In recent years, the growing interest of the scientific community in remote sensing of SIF (Meroni et al., 2009, Frankenberg et al., 2014, Hand, 2014) is attested by the increasing number of scientific studies based on SIF estimation at different scales of investigation. The estimation of SIF from space globally is particularly relevant due to its potential in improving our ability to accurately quantify terrestrial vegetation photosynthesis and to monitor plant functional status. This is the idea behind the development of the FLuorescence EXplorer (FLEX), a candidate Earth Explorer 8 mission currently under evaluation by the European Space Agency (ESA). FLEX would obtain the Red, Far-red and full spectrum SIF emissions, as well as biophysical properties using traditional visible-NIR reflectance indices. At the same time, the newly launched NASA Orbiting Carbon Observatory-2 (OCO-2) has been considered a suitable sensor for retrieving the Far-red SIF signal (only) at orbital altitudes. The challenge for SIF retrievals lies in the difficulty to decouple the weak emitted SIF signal from the dominating reflected radiance. The estimation of SIF from radiances recorded both at top of canopy (TOC) (Rossini et al. 2010; Guanter et al. 2013; Daumard et al. 2010) or top of atmosphere (Guanter et al. 2014; Guanter et al. 2007; Joiner et al. 2011; Joiner et al. 2012; Joiner et al. 2013; Lee et al. 2013)exploits regions of the atmospheric spectrum where the incident irradiance is strongly reduced due to absorption in the Earth's atmosphere or in the solar atmosphere. Two telluric oxygen absorption features are frequently exploited for SIF retrievals namely, O_2-B and O_2-A bands centered at 687.0 nm and 760.4 nm, respectively. The chlorophyll fluorescence emission spectrum is characterized by two peaks in the red and in the far-red regions, approximately centered at 690 nm and 740 nm, respectively (Buschmann 2007). The O_2-B band is used to retrieve Red SIF (at 687 nm); the O_2-A band can be used for the Far-red SIF estimates (at 760 nm). To detect these narrow atmospheric absorption bands, instruments having fine (2-5 nm) or ultrafine (<2 nm) spectral resolution is required (Meroni et al., 2009), and different methods have been proposed for SIF retrieval. The ability to apply one method or another often relies on the spectral and radiometric resolution of the device used. The Spectral Fitting Methods (SFM) proposed by Meroni et al. (2010) and the statistical approaches (Guanter et al. 2013) require spectra collected with ultrafine resolution, while the Fraunhofer Line Discriminator (FLD) method (Plascyk, 1975) or its several different formulations (single FLD, sFLD), three FLD (3FLD) or improved FLD (iFLD), (see Meroni et al., 2009) can be

applied on fine resolution spectra (Damm et al. 2011). Despite the fact that several research groups are now proposing field prototypes based on different spectroradiometer models to monitor TOC SIF (Meroni et al. 2011; Drolet et al. 2014; Fournier et al. 2012; Louis et al. 2005; Rossini et al. 2010), no studies have been performed comparing SIF retrievals from different systems. To the best of our knowledge, only one study (Damm et al., 2011) quantified the expected impacts of sensor characteristics, such as spectral resolution (SR), spectral sampling interval (SSI) stability, and signal to noise ratio (SNR) on the accuracy of SIF retrieval. However, Damm et al., (2011) only examined the potential retrieval of SIF in the far-red (O_2- A band) region and was exclusively based on modeled data. This studyprovides a first quantitative assessment of the reproducibility of SIF retrieval using actual radiance spectra measured in the field by four individual spectroradiometers: three miniaturized systems from Ocean Optics (OO): two HR4000 and one QE Pro (http://www.oceanoptics.com/) and one ASD Fieldspec Pro (http://www.asdi.com/). The impact of the different device characteristics (e.g. SNR and SR) on the SIF estimates has been analyzed and discussed.

5.2. Methods

Four spectroradiometers with different characteristics in terms of SR, SSI, and SNR have been considered. The devices were used to collect measurements simultaneously above the same vegetated target. The same measurement protocol, data analysis procedure and algorithm for SIF estimation were used for all evaluations. Leaf level fluorescence emissions were also measured and used for comparison with the SIF values estimated at canopy level.

The spectroradiometers used in this study were: OO HR4000 narrow range, OO QE Pro, OO HR4000 full range and ASD FieldSpec Pro, hereafter called HRNR, QE, HRFR and ASD respectively. The instrument characteristics are summarized in Table 5.1, and the description of the methods used to characterize the devices is reported below in Section 2.1. Two HR4000s (HRNR and HRFR) were hosted in the S-FLUO box, a prototype system owned by the Jülich Research Center (Germany), and designed for high temporal frequency acquisition of continuous radiometric measurements. The S-FLUO box is based on a commercial optical multiplexer (MPM-2000, Ocean Optics, USA), able to switch between a channel measuring the incident irradiance (cosine response optic), a down-looking bare fiber (25° of Field Of View, FOV) for the measurement of the upwelling radiance and a blind channel for the spectral dark current measurement (Cogliati et al., submitted). A thermo-regulated system holds the temperature constant at 25°C while QE and ASD devices are automatically thermo-regulated.

5.2.1 Instrument characterizations

All the instruments have been characterized in terms of radiometric response, spectral noise and resolution. An additional element considered during the analysis has been the oxygen

absorption band depth. The analysis was conducted in the laboratory and outdoors, before the intercomparison experiment.

5.2.1.1 Signal to Noise Ratio & Full Width at Half Maximum characterization

The SNR characterization was accomplished following the protocol of the Schaepman and Dangel (2000) study. The SNR reported in Table 5.1 refers to the spectral average in the spectral range covered by each instrument: 400 – 1000 nm for ASD and HRFR, or 670-805 nm for HRNR and QE.

The spectral resolution, expressed as full width at half maximum (FWHM), of each device was determined by exploiting the SpecCal tool (Busetto et al. 2011; Meroni et al. 2010), which is based on the comparison between measured and modeled solar irradiance spectra. According to the spectral range of each device the number of atmospheric absorption features used for the FWHM determination varies between 4 (for the HRNR) and 11 (for the ASD). The mean FWHM values are reported in Table 5.1.

5.2.1.2 Oxygen absorption band depth

The ability of the spectrometers to resolve an O_2 absorption bands is related to their spectral, and to a lesser extent, their radiometric resolutions, with the ability to discern increasing feature depth aided by higher spectral resolution. For this reason, the O_2 absorption band depth can be considered an indicator of the capability of each device to detect the Fraunhofer features within the O_2-B (687.0 nm) and O_2-A (760.4 nm) features, respectively, even if the depths vary somewhat due to the sun's position and/or the direct/diffuse shortwave radiation ratio.

The absorption band depths have been calculated as follows:

$$\text{Band depth} = \frac{E\lambda out - E\lambda in}{E\lambda out}\ x\ 100 \qquad [5.1]$$

where E is the incident solar irradiance. The λin refers to the wavelength at the bottom of the O_2 feature: around 689 nm for the O_2-B band; or 760 nm for the O_2-A band. The λout refers to the wavelength at the shoulder that provides the maximum value in the range of 680-688 nm for the O_2-B band, or 750-755 nm for the O_2-A band. Measurements at these wavelengths were used to determine the feature depth values associated with each spectrometer, and are reported in Table 5.1.

Spectroradiometer	Spectral range [nm]	FWHM [nm]	SSI [nm]	SNR [-]	O_2-B Depth [%]	O_2-A Depth [%]
HRNR	670-857	0.2	0.05	250	42	81
QE	645-810	0.5	0.17	1080	35	80
HRFR	197- 1115	1	0.3	580	27	77
ASD	350-2500	5.5	1	2200	12	49

Table 5.1. The characteristics of each spectrometer are reported in terms of spectral range, spectral resolution (FWHM), spectral sampling interval (SSI), signal to noise ratio (SNR) and percentage depth of the two telluric oxygen absorption bands.

5.2.2 Experiment setup and canopy fluorescence measurements

The experiment was conducted at the NASA Goddard Space Flight Center in Greenbelt, Maryland (38° 59' 32.15'' N, 76° 50' 22.22'' W). The measurements were acquired between 11:00 and 13:00 solar time (Solar Zenith Angles, 27-29 degrees) on April 24, 2014 under clear sky conditions. The target selected for the intercomparison was a 50 cm x 40 cm square area of grass (*Festuca arundinacea*). Each measurement cycle consisted of four spectra: first, a measurement of the dark current followed by 3 spectra whereby a measurement of the target's reflected radiance was sandwiched between two solar irradiance measurements (e.g., dark current, irradiance, target, irradiance). The solar irradiance at the time of the target measurement was estimated by linear interpolation over the cycle's 1 minute duration (Meroni and Colombo 2009).

For the HR4000s (HRNR, HRFR), the two sensors hosted in the S-FLUO box were used to measure the up-welling target radiance (field of view, FOV of 25degrees) with the downward channels and the solar irradiance with the upward channels (Ocean Optics cosine receptors were used). The S-FLUO box's downward channels were kept fixed above the same grass area using a second tripod, while the upward channels were secured to a third levelled tripod looking at the sky. The QE and the ASD Fieldspec spectrometers were operated with bare fibre optics where the FOV was 25 and 18 degrees respectively. A rotating tripod arm with a fiber optic holder was used to ensure that the fibers of the QE, HRNR, HRFR and ASD were as close together as possible, in order to measure as similar a spatial area on the target as could be physically achieved (Figure. 5.1). The fiber optics of QE and ASDacquired alternating measurements of a calibrated white spectralon panel (99 % reflecting Labsphere Inc.) and the reflected radiance of the grass.

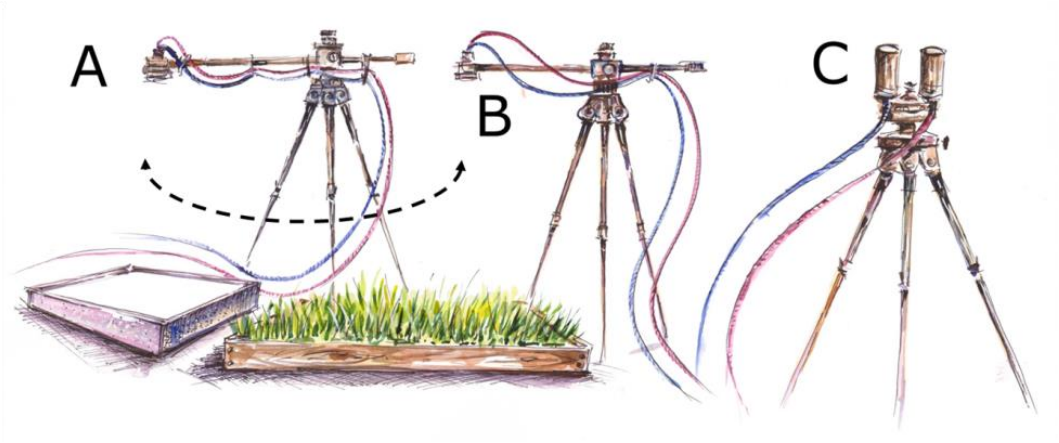

Figure 5.1.Experimental field setup. A) The fiber optics connected to ASD and QE spectrometers are secured to a rotating arm allowing the movement from the white reference panel and the vegetation target. B) The S-FLUO box downward channels (both HRNR and HRFR) are attached to a fixed tripod looking at the vegetation. C) S-FLUO box upward channels are horizontally mounted on the third tripod to collect reference measurements.

The grass target was observed from nadir at an average distance of 30 cm corresponding to a viewed area of approximately 10 or 15 cm diameter for all spectroradiometers. The integration time of the sensors was set to optimize the signal at around 80% of the dynamic range of each device. Spectrum averages varied according to the setup commonly used in the field measurements. In particular, the number of spectra averaged was set to: 3 for HRNR narrow, 5 for HRFR, 5 for QE and 25 for ASD. The instruments were warmed up for 1.5 hr before beginning the data acquisition. A total of 30 cycles of measurements were collected at the same time by each of these different instruments.

5.2.3 SIF retrieval

The different spectral resolution of the spectrometers did not allow us to perform any kind of algorithm comparison. Therefore, the SIF retrievals were conducted with FLD-like approaches which were applicable to all of the spectroradiometers used in this study. The 3FLD method was used to estimate Far-red SIF for the O_2-A band, considered to be the best option following Damm et al. (2011). The assumption of the 3FLD method cannot be considered valid for the Red SIF retrieval at the O_2-B-band. Therefore the sFLD method has been used to retrieve SIF at the O_2-B-band, using the following formula:

$$F = \frac{E\lambda out \times L\lambda in - L\lambda out \times E\lambda in}{E\lambda out - E\lambda in} \quad [-] \qquad [5.2]$$

where E is the incident solar irradiance and L is the target radiance. λin and λout refer to the wavelengths at the bottoms and at the shoulders of the absorption features, respectively. To minimize possible mismatches due to the wavelength calibrations, an automatic selection of local maxima (outside of the absorption band) and minima (inside the absorption band) was used. In particular, the radiances associated with the deepest absorption band positions at 689 nm and 760 nm were selected to determine Eλin and Lλin for the O_2-B and O_2-A bands

respectively. Lλout and Eλout in the spectral regions outside the absorption feature were parameterized as the 1 nm mean value centered on the maximum radiance values, these were measured between 750–755 nm and between772–777 nm in the O_2-A band, and between 680-688 nm for the O_2-B band. When the 3FLD is applied, the measurement made at the single reference wavelength (λout) used in the sFLD is replaced by the average value measured at the two wavelengths outside of the absorption line (Lλout and Eλout).

The Kruskall-Wallis test was performed to statistically test differences in the SIF retrieval using different spectroradiometers. When this test indicated significant results ($p \leq 0.05$), the Wilcoxon-Mann-Whitney test was employed to determine which spectroradiometer had a significantly different SIF retrieval ($p \leq 0.05$), as compared to the others.

5.2.4 Leaf level fluorescence emission measurements

Leaf fluorescence emissions were measured on ten grass leaves collected from the target and immediately analysed in laboratory. Leaf fluorescence emission spectra were measured over the wavelength range from 600 to 810 nm with a spectrofluorometer (Fluorolog-3, Model FL3-22, Spex Industries, Edison NJ). A monochromatic excitation wavelength set to 530 nm was used to simulate solar radiation, activating fluorescence. Fluorescence emissions were then measured between 640 nm and 810 nm at a sampling resolution of 1 nm. The spectrofluorometer was calibrated with NIST traceable silicon trap detectors and provides simulated SIF intensities reported in mW m^{-2} nm^{-1} sr^{-1}.

5.3. Results and discussion

The solar irradiance spectra collected by the different spectroradiometers are shown in Figure 5.2. The graph reports the mean values of the 60 solar irradiance spectra measured with the different spectroradiometers in the spectral range (670-800 nm) covered by all of the spectrometers.

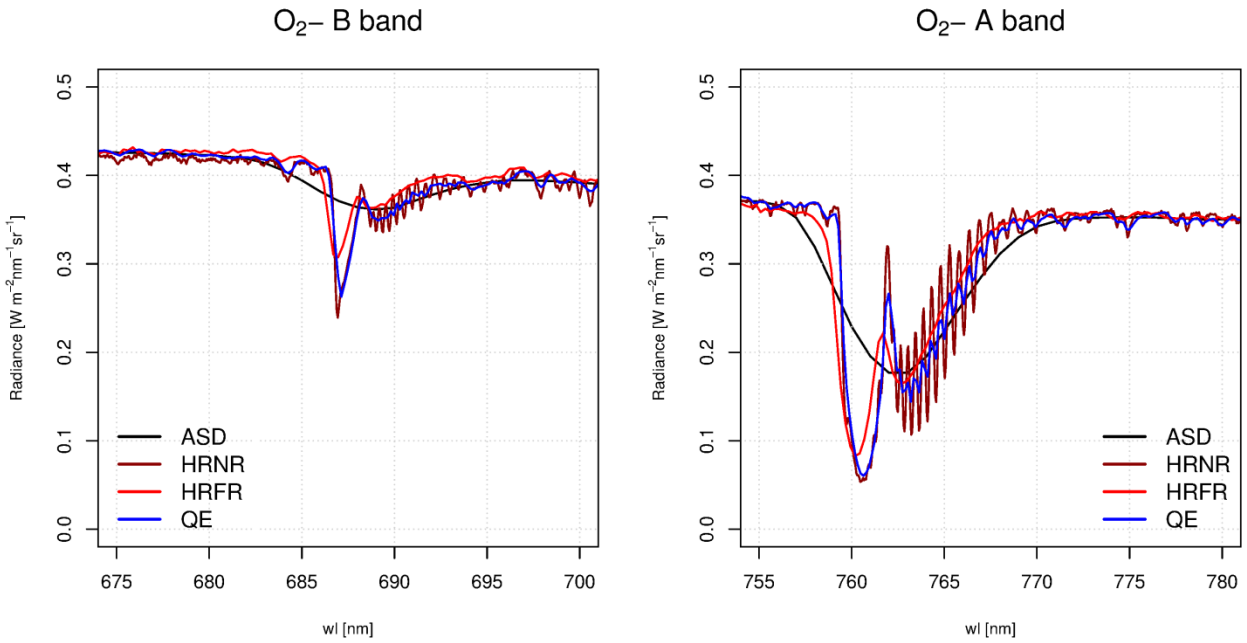

Figure 5.2. Incoming radiance measured with the 4 spectroradiometers in the O_2-B band (left panel) and in the O_2-A band (right panel). Each color represents a different instrument. The ability to detect the presence of narrow absorption features is directly related to the Spectral Resolution (i.e., FWHM) of each device.

The spectra depicted in Figure 5.2 show comparable radiance values in the plateau spectral regions. However, due to finer FWHM a higher channel-to-channel variability occurred in the Ocean Optics spectroradiometers, as compared with the ASD spectroradiometer. Differences in FWHM among the instruments are also responsible for differences in describing the shape and depth of the two absorption bands. The percent O_2-B band depth estimates were lowest when made with the ASD (12%), and highest (42%) when made with the HRNR. Comparable but higher values were obtained for the O_2-A band with the ASD (49%) and the HRNR (81%).

Note that the shape of the irradiance spectrum acquired with the HRNR (Fig. 2, dark red line) is characterized by narrow absorption features, which are possible to discern with this instrument's higher spectral resolution, FWHM 0.2 nm. These narrow features progressively disappear and the spectra appear to be progressively more smoothed as the spectral resolution of the spectroradiometers decreases for the QE, HRFR and ASD.

From Table 5.1, an inverse relationship between the FWHM and the estimated depths of the telluric oxygen bands is apparent, decreasing from the HRNR (with the smallest FWHM, 0.2 nm) up to the ASD (with the widest FWHM at 5.5 nm). The percentage value of theO_2 absorption band depths is known to vary according to environmental factors, such as the sun's zenith position the direct/diffuse shortwave radiation ratio, and surface pressure. Therefore, the results presented in this manuscript are valid for the specific conditions of the study and cannot be directly extrapolated to different geographic areas and atmospheric conditions.

Figure 5.3 shows the fluorescence values retrieved from the spectrometers considered in the study: red (left panel) and far-red (right panel). The average retrievals per band and instrument

are included in Table 5.2. Estimates of the Red SIF varied considerably among the different sensors, with values increasing in concert with the FWHM per sensor, with the lowest values obtained with the HRNR. At the far-red band, the QE and the two HR4000 (HRNR) spectroradiometers retrieved the same SIF values (from Wilcoxon-Mann-Whitney test, p-value ≤0.05). On the contrary, the ASD always overestimated the SIF values in either band by 6 or 12 times compared to the mean value estimated using HRNR, QE and HRFR.

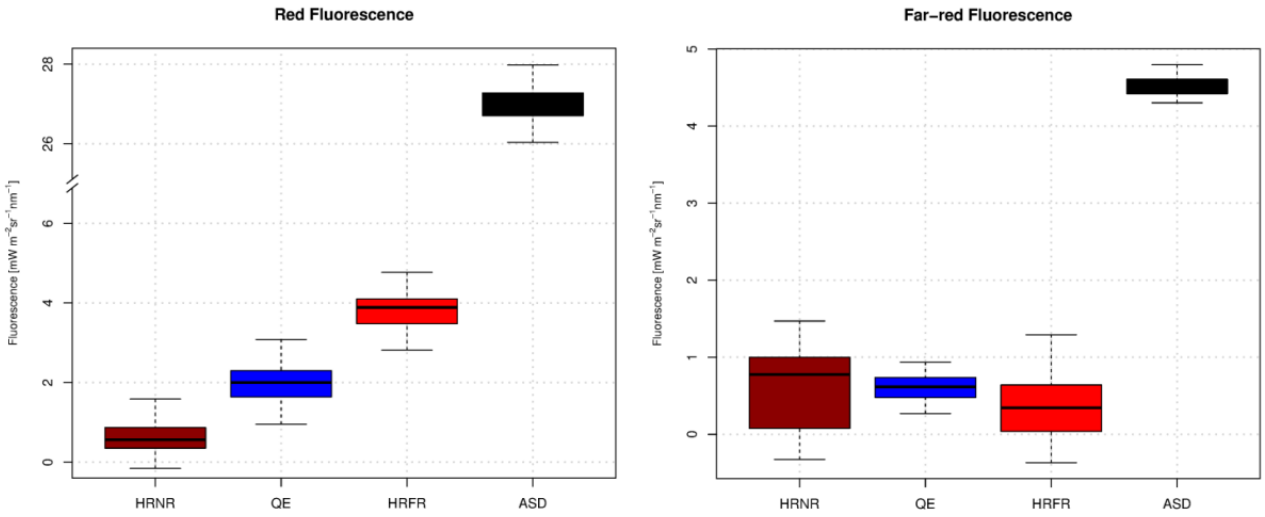

Figure 5.3. Boxplots of red (left) and far-red (right) SIF retrieval means and associated standard deviations of the 30 cycles of measurements. The instruments are reported in the order according to the increasing FWHM. The red SIF estimations differ, indicating a possible dependency on the SR of the sensor. The HRNR, QE and HRFR show comparable far-red SIF retrieval estimates. SIF estimated from the ASD is extremely high in both the red and far-red cases. The difference in the standard deviations for the far-red SIF estimates (right panel) can be explained by the differences in the SNR of these instruments.

Figure 5.3 suggests that the estimated value of Red SIF generally increases with the FWHM of the spectroradiometer used for the retrieval. Red SIF values obtained with different spectroradiometers have a similar standard deviation (SD) while the SD varied among spectroradiometers for the Far-red SIF estimation. The lowest mean and SD combination in the far-red band was obtained with the QE instrument. We hypothesize that the differences in the SD of the Far-red SIF is related to the SNR of the spectroradiometers (Damm et al. 2011), since the ASD and QE sensors had similarly low SDs.

SIF estimates at the canopy level have been then compared with the leaf level fluorescence emissions at the same wavelengths (Figure 5.4). Absolute values of leaf and canopy fluorescence are expected to differ for two main reasons. First of all, the light source used to induce laboratory leaf emissions has a peak at 532 nm, which is close to the wavelength peak of solar radiance, but the shape and intensity of the monochromatic light source differs from the natural solar irradiance.

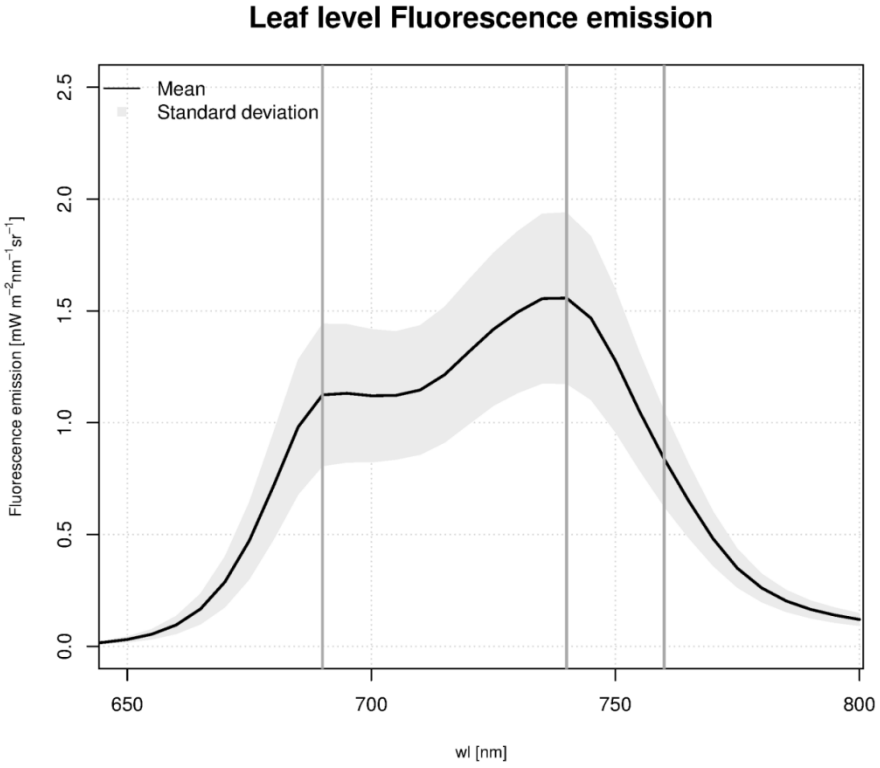

Figure 5.4. Grass leaf level fluorescence emissions acquired in the laboratory with the SPEX Fluorolog III spectrofluorometer using a 532 nm excitation wavelength. The red peak is expected to be partially reabsorbed at the canopy level. The ratio between fluorescence obtained at 690 nm and 760 (Red/far-red Ratio = 1.3) is used to qualitatively assess the SIF retrievals made at canopy level with the different instruments (see Table 5.2). Traditionally, the Red/NIR Ratio is computed with the values at the peaks (690, 740 nm), which would provide a Ratio = 0.72. Three vertical lines denote the red and NIR wavelengths used for these two Ratios.

The measured leaf level Red/Far-red ratio value using the SIF wavelengths (689, 760 nm) was 1.3, whereas the traditional Red/Far-red Ratio value using the peak wavelengths (690, 740 nm) yields a value of 0.72. According to Buschmann (2007) the red fluorescence is generally reabsorbed by photosynthetic pigments, which is expected to influence the Red/Far-red ratio determined with SIF retrievals at the canopy level more than at the individual leaf level. This means that the canopy Red/Far-red SIF ratio should be lower than the laboratory value computed at leaf level. We computed the Red/Far-red SIF ratios (Table5.2) and compared each with the leaf level value, to determine which spectrometer provided a ratio closest to, but less than, the single leaf value. This assessment was based on the quotient between the SIF and leaf ratios, yielding: 0.5 (HRNR), 2.4 (QE), 8.3 (HRFR) and 4.5 (ASD). Only the HRNR successfully obtained a 689/760 SIF ratio value lower than the leaf level value, as expected by theory.

Spectroradiometer	Red fluorescence mean value [mW m^{-2} nm^{-1} sr^{-1}]	Standard deviation	Far-red fluorescence mean value [mW m^{-2} nm^{-1} sr^{-1}]	Standard deviation	Red/far-red ratio [-]
HRNR	0.56	0.4	0.77	0.5	0.72
QE	2	0.48	0.62	0.24	3.2
HRFR	3.8	0.42	0.35	0.36	10.9
ASD	26.74	1.27	4.52	0.14	5.9

Table 5.2.The mean values and standard deviations of the red and far-red fluorescence retrieval are reported according to each spectrometer used. The last column refers to the red/far-red ratio.

Overall, a reliable estimation of the absolute value of Far-red SIF can be achieved using any of the higher resolution spectrometers examined (the HRNR, QE and HRFR), but not with the ASD. The OO devices have an ultrafine resolution (FWHM ≤ 1 nm) and a corresponding percentage depth of the O_2-A band greater than 75%, a value that we should consider as a reasonable threshold to obtain reliable Far-red SIF data. For the Far-red SIF, the smaller SDs for the QE and ASD sensors is clearly related to their very high SNR (>1000). For the ASD, the small SD for the Far-red SIF is related as well to the high number of scans averaged (25). However, the ASD's large SIF overestimates in both the red and far-red is due to its relatively low spectral resolution. The repeatability of the measurements recorded by devices with a low SNR was noted. This implies a larger number of replicates may be needed to obtain less variable (i.e., more reliable) mean values with the HRNR and HRFR OO sensors. For example, it would be a simple revision in the data collection protocol for the HRNR to increase the number of scans utilized. Further investigations are necessary to understand the capabilities of these sensors to capture the relative variability of Far-red SIF on targets emitting fluorescence with known intensities.

In comparison to the Far-red SIF, there was no agreement among the four sensors examined for the Red SIF. The Red SIF retrieval exhibits a strong dependency of the absolute mean SIF values on the SR of the devices. This SR effect is apparently more important than the SNR for retrievals within this narrow O_2-B feature (<5 nm), in contrast to the retrieval for the wider (~8 nm) and deeper O_2-A NIR band, since the variation around the mean values (the SDs) were similar across sensors.

A limitation to this empirical experiment is that a "true" value of fluorescence does not exist for use as a reference to evaluate the SIF retrievals made with different spectroradiometers. However the leaf level fluorescence spectrum can provide reasonable information about the expected ratio between Red and Far-red SIF. According to the leaf level fluorescence emission, the TOC SIF results indicate that the HRNR has the highest potential for accurate field SIF measurements in both SIF bands, a result obtained with the smallest number of scan collections. We note that two of the ultrafine sensors (QE and HRFR) overestimated the Red SIF using the sFLD retrieval method. Therefore, further study is necessary to determine the optimal measurement

configurations and retrieval methods to boost the measurement success of all three of the OO sensors. Further analyses are needed to identify the SR limit in capturing relative changes of Red SIF on vegetation targets with different fluorescence emissions.

5.4 Conclusions

The results presented only refer to the particular instruments used, to the specific grass target considered, and to the methodologies used both in acquiring the measurements and in retrieving the SIF values. Nevertheless, credible results have been achieved to demonstrate the relative suitability for SIF retrieval of the instruments examined. Within this study an empirical inter-comparison between spectroradiometers with different performance characteristics and their impacts on SIF retrievals was conducted.The results of the experiment suggest that spectroradiometers with a high spectral resolution (FWHM ≤ 1 nm) are able to estimate the absolute value of Far-red SIF, based on the 3FLD retrieval method. Moreover, in order to improve the precision on the Far-red SIF estimation a high SNR value (>1000) is preferred. The O_2-B absorption band is itself less wide and deep compared to the O_2-A band, introducing a physical constraint in the Red SIF absolute value retrieval. Only the HRNR device, which has the highest ultrafine spectral resolution (FWHM of 0.2 nm) among the instruments tested in this study, gave the most reliable Red SIF estimates (and using the sFLD method). Nevertheless, its reliability might be enhanced by adjusting the measurement protocol, using either more repeated scans or longer integration times. Further study should also be designed to investigate different approaches in SIF retrieval (e.g. Spectral Fitting Method, statistical approaches) since the performance of the fluorescence algorithms may significantly change when applied to different instruments. In addition new studies must be developed to determine the optimum devices for detecting SIF variability, both time series and for different canopies in validation activities.

This study should be considered a first step in evaluating the best instruments and measurement protocols for their use in field research and for measurements to validate space-based remote sensing retrievals.

Acknowledgement

The main researchers involved in the project are:Lawrence A. Corp, Micol Rossini, Andreas Burkart, Sergio Cogliati, Neville Davies, Milton Hom, Alasdair Mac Arthur, Elizabeth M. Middleton, Uwe Rascher, AnkeSchickling and Roberto Colombo

References

Buschmann, Claus. 2007. "Variability and Application of the Chlorophyll Fluorescence Emission Ratio Red/far-Red of Leaves." *Photosynthesis Research* 92: 261–71.

Busetto, L., M. Meroni, G.F. Crosta, L. Guanter, and R. Colombo. 2011. "SpecCal: Novel Software for in-Field Spectral Characterization of High-Resolution Spectrometers." *Computers & Geosciences* 37 : 1685–91.

Campbell, P. K. E, E M. Middleton, J. E. McMurtrey, L. A. Corp, and E. W. Chappelle. 2007. "Assessment of Vegetation Stress Using Reflectance or Fluorescence Measurements." *Journal of Environmental Quality* 36. American Society of Agronomy, Crop Science Society of America, Soil Science Society: 832–45.

Campbell, P. K. E., E. M. Middleton, L. A. Corp, and M S Kim. 2008. "Contribution of Chlorophyll Fluorescence to the Apparent Vegetation Reflectance." *The Science of the Total Environment* 404: 433–39.

Corp, Lawrence A., James E. McMurtrey, Elizabeth M. Middleton, Charles L. Mulchi, Emmett W. Chappelle, and Craig S.T Daughtry. 2003. "Fluorescence Sensing Systems: In Vivo Detection of Biophysical Variations in Field Corn due to Nitrogen Supply." *Remote Sensing of Environment* 86: 470–79.

Damm, A., Elbers, J., Erler, A., Gioli, B., Hamdi, K., Hutjes, R., Kosvancova, M., Meroni, M., Miglietta, F., Moersch, A., Moreno, J., Schinckling, A., Sonnenschein, R., Udelhoven, T., Vand Der Linden, S., Hostert, P. and Rascher, U.. 2010. "Remote Sensing of Sun-Induced Fluorescence to Improve Modeling of Diurnal Courses of Gross Primary Production (GPP)." *Global Change Biology* 16: 171–86.

Damm, A., Erler, A., Hillen, W., Meroni, M., Schaepman, M. E., Verhoef, W. and Rascher U.. 2011. "Modeling the Impact of Spectral Sensor Configurations on the FLD Retrieval Accuracy of Sun-Induced Chlorophyll Fluorescence." *Remote Sensing of Environment* 115: 1882–92.

Daumard, F., Champagne, S., Fournier, A., Goulas, Y., Ounis, A., Hanocq, J. F. and Moya I.. 2010. "A Field Platform for Continuous Measurement of Canopy Fluorescence." *IEEE Transactions on Geoscience and Remote Sensing* 48: 3358–68.

Drolet, G., Wade T., Nichol, C. J., MacLellan, C., Levula, J., Porcar-Castell, A., Nikinmaa, E. and Vesala T.. 2014. "A Temperature-Controlled Spectrometer System for Continuous and Unattended Measurements of Canopy Spectral Radiance and Reflectance." *International Journal of Remote Sensing* 35. Taylor & Francis: 1769–85.

Fournier, A., F. Daumard, S. Champagne, A. Ounis, Y. Goulas, and I. Moya. 2012. "Effect of Canopy Structure on Sun-Induced Chlorophyll Fluorescence." *ISPRS Journal of Photogrammetry and Remote Sensing* 68: 112–20.

Frankenberg, C., O'Dell, C., Berry, J., Guanter, L., Joiner, J., Köhler, P., Pollock, R. and Taylor T. E.. 2014. "Prospects for Chlorophyll Fluorescence Remote Sensing from the Orbiting Carbon Observatory-2." *Remote Sensing of Environment* 147: 1–12. doi:10.1016/j.rse.2014.02.007.

Guanter, L., Alonso, L., Gòmez-Chova, L., Amoròs-Lòpez, J., Vila, J. and Moreno J.. 2007. "Estimation of Solar-Induced Vegetation Fluorescence from Space Measurements." *Geophysical Research Letters* 34.

Guanter, L., Rossini, M., Colombo, R., Meroni M., Frankenberg, C., Lee, J. E. and Joiner J.. 2013. "Using Field Spectroscopy to Assess the Potential of Statistical Approaches for the Retrieval of Sun-Induced Chlorophyll Fluorescence from Ground and Space." *Remote Sensing of Environment* 133: 52–61.

Guanter, L., Zhang, Y., Jung M.,, Joiner, J., Voigt, M., Berry, J. A., Frankenberg, C. et al. 2014. "Global and Time-Resolved Monitoring of Crop Photosynthesis with Chlorophyll Fluorescence." *Proceedings of the National Academy of Sciences of the United States of America* 111: E1327–33.

Hand, Eric. 2014. "Carbon-Mapping Satellite Will Monitor Plants' Faint Glow." *Science (New York, N.Y.)* 344 (6189): 1211–12.

Joiner, J., L. Guanter, R. Lindstrot, M. Voigt, A. P. Vasilkov, E. M. Middleton, K. F. Huemmrich, Y. Yoshida, and C. Frankenberg. 2013. "Global Monitoring of Terrestrial Chlorophyll Fluorescence from Moderate-Spectral-Resolution near-Infrared Satellite Measurements: Methodology, Simulations, and Application to GOME-2." *Atmospheric Measurement Techniques* 6. Copernicus GmbH: 2803–23.

Joiner, J., Y. Yoshida, A. P. Vasilkov, L. A. Corp, and E. M. Middleton. 2011. "First Observations of Global and Seasonal Terrestrial Chlorophyll Fluorescence from Space." *Biogeosciences* 8. Copernicus GmbH: 637–51.

Joiner, J., Y. Yoshida, A. P. Vasilkov, E. M. Middleton, P. K. E. Campbell, A. Kuze, and L. A. Corp. 2012. "Filling-in of near-Infrared Solar Lines by Terrestrial Fluorescence and Other Geophysical Effects: Simulations and Space-Based Observations from SCIAMACHY and GOSAT." *Atmospheric Measurement Techniques* 5. Copernicus GmbH: 809–29.

Lee, J. E., C., Frankenberg, C., van der Tol, J. A., Berry, L. Guanter, C. K. Boyce, J. B. Fisher, et al. 2013. "Forest Productivity and Water Stress in Amazonia: Observations from GOSAT Chlorophyll Fluorescence." *Proceedings. Biological Sciences / The Royal Society* 280 (1761): 20130171.

Louis, J., A. Ounis, J. M. Ducruet, S. Evain, T. Laurila, T. Thum, M.Aurela, et al. 2005. "Remote Sensing of Sunlight-Induced Chlorophyll Fluorescence and Reflectance of Scots Pine in the Boreal Forest during Spring Recovery." *Remote Sensing of Environment* 96: 37–48.

Maier, S. W., K. P. Günther, and M. Stellmes. 2003. "Sun-Induced Fluorescence: A New Tool for Precision Farming." In *Digital Imaging and Spectral Techniques: Applications to Precision Agriculture and Crop Physiology*, 209–22.

Meroni, M, A Barducci, S Cogliati, F Castagnoli, M Rossini, L Busetto, M Migliavacca, et al. 2011. "The Hyperspectral Irradiometer, a New Instrument for Long-Term and Unattended Field Spectroscopy Measurements." *The Review of Scientific Instruments* 82: 043106.

Meroni, M., L. Busetto, R. Colombo, L. Guanter, J. Moreno, and W. Verhoef. 2010. "Performance of Spectral Fitting Methods for Vegetation Fluorescence Quantification." *Remote Sensing of Environment* 114: 363–74.

Meroni, M., and R. Colombo. 2006. "Leaf Level Detection of Solar Induced Chlorophyll Fluorescence by Means of a Subnanometer Resolution Spectroradiometer." *Remote Sensing of Environment* 103: 438–48.

Meroni, M., M. Rossini, L. Guanter, L. Alonso, U. Rascher, R. Colombo, and J. Moreno. 2009. "Remote Sensing of Solar-Induced Chlorophyll Fluorescence: Review of Methods and Applications." *Remote Sensing of Environment* 113: 2037–51.

Meroni, Michele, and Roberto Colombo. 2009. "3S: A Novel Program for Field Spectroscopy." *Computers & Geosciences* 35: 1491–96.

Panigada, C., M. Rossini, M. Meroni, C. Cilia, L. Busetto, S. Amaducci, M. Boschetti, et al. 2014. "Fluorescence, PRI and Canopy Temperature for Water Stress Detection in Cereal Crops." *International Journal of Applied Earth Observation and Geoinformation* 30: 167–78.

Plascyk, J.A. 1975. "The MK II Fraunhofer Line Discriminator /FLD-II/ for Airborne and Orbital Remote Sensing of Solar-Stimulated Luminescence." *Optical Engineering* 14: 339–46.

Rossini, M., M. Meroni, M. Migliavacca, G. Manca, S. Cogliati, L. Busetto, V. Picchi, A. Cescatti, G. Seufert, and R. Colombo. 2010. "High Resolution Field Spectroscopy Measurements for Estimating Gross Ecosystem Production in a Rice Field." *Agricultural and Forest Meteorology* 150: 1283–96.

Schaepman, Michael E., and Stefan Dangel. 2000. "Solid Laboratory Calibration of a Nonimaging Spectroradiometer." *Applied Optics* 39. OSA: 3754.

Zarco-Tejada, P.J., V. González-Dugo, and J.A.J. Berni. 2012. "Fluorescence, Temperature and Narrow-Band Indices Acquired from a UAV Platform for Water Stress Detection Using a

Micro-Hyperspectral Imager and a Thermal Camera." *Remote Sensing of Environment* 117: 322–37.

Zarco-Tejada, P.J., A. Morales, L. Testi, and F.J. Villalobos. 2013. "Spatio-Temporal Patterns of Chlorophyll Fluorescence and Physiological and Structural Indices Acquired from Hyperspectral Imagery as Compared with Carbon Fluxes Measured with Eddy Covariance." *Remote Sensing of Environment* 133: 102–15.

Part 2 - Monitoring of terrestrial vegetation using proximal sensing sensors

Using digital camera images to analyse snowmelt and phenology of a subalpine grassland

This research was conducted in the framework of the PhenoALP Project. The study has been published inAgricultural and Forest Meteorology, Volumes 198–199, November–December 2014, Pages 116–125.

Plant phenology is a commonly used and suitable indicator of the impact of climate change on vegetation. In mountainous areas phenology is governed by environmental drivers such as air temperature, photoperiod and the presence of snow. In this study, digital images collected over 3 years (2009, 2010 and 2011) in a subalpine grassland site were used to investigate the relationship between the timing of snowmelt and the beginning of the growing season in both the spatial and the temporal dimension. The image analysis was conducted for a wide area corresponding to approximately 150 m^2 to characterize the spatial heterogeneity of grassland phenology. The investigated area was divided into 855 10x10 pixel cells, and for each cell annual time series of green chromatic coordinates (*gcc*) were computed from hourly images. To analyse the spatial pattern of phenology, the beginning of the season for each cell was extracted from the *gcc* time series. Based on the same grid dimension, three maps of yearly snowmelt date corresponding to the day of the year in which the snow in each cell disappeared from the ground were obtained.

Although complete snowmelt in the area occurred rapidly, within a maximum of six days, several distinct spatial patterns were identified with snowmelt occurring earlier in convex compared to concave areas. Differences in snowmelt dates were quite unexpectedly negatively related to the beginning of the growing season. The negative correlation was explained considering that areas characterized by different microtopography have also a different species composition: the growing season began earlier in concave areas preferred by opportunistic species with a fast development after snowmelt while phenological development of grass typical of convex areas can take longer.

6.1 Introduction

Climate change is expected to strongly influence high altitude ecosystems in Europe by increasing temperature and inducing modifications in precipitation seasonal distribution and snow-pack duration (Alcamo et al., 2007; Auer et al., 2007; Beniston, 2005; Gobiet et al., 2013).

Plant phenology is highly sensitive to climate variability (Menzel et al., 2006) and, particularly in ecosystems with strong seasonality, a noteworthy correspondence between climate and phenological patterns have been observed (Richardson et al., 2013). Together with other environmental parameters, snow is among the most important environmental factors controlling high-altitude plant phenology (Cornelius et al., 2013a; Cornelius et al., 2013b; Wipf et al., 2009), providing frost protection for covered plants in winter (Inouye and Wielgolaski, 2013), and water supply and nutrient mobilisation at snowmelt (Keller and Körner, 2003). Any changes in the date of snowmelt or snow cover establishment can induce strong ecosystem responses such as changes *i)* in seasonal patterns of ecosystem carbon and water fluxes related to plant photosynthesis and growth (i.e. snow-free season, Galvagno et al., 2013; Rossini et al., 2014)*ii)* in interactions between species (Wipf et al., 2006), e.g. between plants and their pollinators, pests or pathogens (Roy et al., 2004), and *iii)* in the timing of soil nutrient availability and thus ecosystem functioning(Saccone et al., 2013; Schimel et al., 2004). According to recent literature, the expected warming of the Alpine region will lead to more frequent early snowmelt events (Foppa and Seiz, 2012) which will in turn cause changes in phenological patterns in alpine vegetation. Therefore, efforts have been made to investigate the effect of changing snow cover on alpine plant phenology by means of direct snow manipulation experiments (Cornelius et al., 2013b; Wipf and Rixen, 2010). These studies highlight a highly variable response related to several factors such as plant species, growth forms and habitat (e.g. snowbed, fellfield). Some authors (Keller and Körner, 2003; Wipf and Rixen, 2010; Wipf et al., 2006) have proposed that species adapted to habitats characterised by different snow cover duration (such as snowbed or fellfield) can show distinct responses to snowmelt advancement or delay.

Since many vegetation-climate feedbacks (albedo, evapotranspiration and CO_2 fluxes) are mediated by phenology (Richardson et al., 2013), the monitoring and modelling of vegetation phenological cycles have become a major issue in global change research (Cleland et al., 2007). Traditional methods used to monitor plant phenology mainly consist of field observations and remote sensing data (e.g. Busetto et al., 2010; Linderholm, 2006). However, both strategies present some limits in terms of spatial and temporal resolution. Direct phenological surveys can hardly provide continuous and quantitative information on plant phenology and do not allow the covering of wide areas (Schwartz et al., 2002). Moreover, those observations do not often refer to the phenology of a whole community but to single species, and they might be affected by observer subjectivity. While satellite products can provide invaluable synoptic phenological information, they do not allow a detailed evaluation of the variability in species responses (Ide

and Oguma, 2013). Furthermore, the use of medium to coarse resolution satellite data in mountainous areas is often challenging due to complex topography and habitat fragmentation. Several studies have demonstrated the capability of Red-Green-Blue (RGB) digital imagery to provide accurate phenological information (Ahrends et al., 2009; Ahrends et al., 2008; Alberton et al., 2014; Bater et al., 2011; Migliavacca et al., 2011; Mizunuma et al., 2013; Richardson et al., 2007; Richardson et al., 2009). The digital cameras are usually fixed above a vegetated target (e.g. forests, croplands, grasslands and peatlands) and the images are continuously acquired during the season. The colour information contained in the images (chromatics coordinates) is then used as an index of canopy development and the time series of indices extracted from the digital cameras can be used to identify the timing of key phenological events.

Traditionally, digital images collected to track vegetation phenology are processed by analysing a single Region of Interest (ROI) within the image, considered as a reference of the mean behaviour of the entire ecosystem (Migliavacca et al., 2011; Richardson et al., 2006; Sonnentag et al., 2012). Few published studies use more than one ROI to evaluate phenological differences between plants included in the same image (Ahrends et al., 2008; Alberton et al., 2014; Henneken et al., 2013; Mizunuma et al., 2013) and only the study by Ide and Oguma(2013) performs a pixel per pixel analysis. An interesting and poorly investigated improvement of this technique is to analyse the spatial information in the considered frame to identify spatial differences in phenology within the image (Ide and Oguma, 2013).

RGB images can also be used to retrieve important information on snowmelt processes, as reported in literature (Hinkler et al., 2002; Parajka et al., 2012). Therefore, the combination of spatial phenological information and spatial characterization of the snowmelt process may improve knowledge of the response of plant development to snowmelt timing.

This study tests the hypothesis that separate phenological behaviours related to site microtopography and snow patches can be distinguished in the same ecosystem. Since mountain ecosystems are generally characterised by complex topography, the presence of microhabitats and related differences in snow dynamics induce patches with uneven distribution of the species representing vegetation types with different developmental strategies, even within the same alpine plant community. The observed phenological patterns may reflect distinct adaptations to resource use efficiency, reproductive competition, site microtopography and life cycle completion strategies (Keller and Körner, 2003). Monitoring of diverse phenological patterns in a plant community is useful in interpreting the whole ecosystem response to environmental and climate variability. In heterogeneous plant communities, such as mountain grassland, disentangling the contribution of single species to community phenology is time-consuming and data are often more qualitative than quantitative. To our knowledge no method has been proposed for long-term monitoring of community-level phenological responses to snowmelt variability in snow patches due to complex topography.

In this study temporal and spatial patterns of phenology and their relationship to snowmelt using digital images collected in a grassland site located in an Alpine environment were investigated. Specifically, the following questions have been addressed*: i)* can digital camera images be a tool for identifying spatial patterns of phenology within the image and their relation with snowmelt? *ii)*how does the spatial pattern of phenology change in response to an exceptionally early snowmelt year?

To reach these objectives, snowmelt and spring phenology maps were computed from digital images of the subalpine grassland for three years (2009, 2010 and 2011) and their spatial patterns were evaluated and discussed.

6.2 Materials and methods

6.2.1 Site description

The study area is located in the north-western Italian Alps (Aosta Valley, IT) at 2160 m a.s.l. (45° 50'40''N, 7° 34'41''E) and is exhaustively presented by Migliavacca et al. (2011), Rossini et al. (2012) and Galvagno et al. (2013). The area is a subalpine unmanaged pasture classified as intra-alpine with semi-continental climate. The site is generally covered by snow from the end of October to late May. The vegetation is characterized by the dominant oligotrophic grass *Nardus stricta* and the forbs *Geummontanum*, *Crocus albiflorus,Arnica montana, Potentillacrantzii, Trifoliumalpinum*, *Ranunculuspyrenaeus*, *Leontodonhispidus*, *Hieraciumpilosella*, *Polygonumbistorta*and *Ranunculusacris*. The plant community, as a whole, has been classified to the *Sieversio-Nardetum* phytosociological association. Two vegetation types characterise the site: the first is mainly grasses (grass only, GO) dominated by *Nardus stricta* and the second, in which *Nardus stricta* has an average cover of ~50%, is characterized by the co-occurrence of forbs (grass and forbs, GF), the most abundant species being *Geummontanum,Crocus albiflorus* and *Arnica montana*. The two vegetation types compose a heterogeneous pattern related to different micro-topographical conditions: the first one occurs on the convex areas while the second on areas with a concave topography. The experimental site belongs to the Phenocam network (http://phenocam.sr.unh.edu/webcam/) and is equipped with a webcam system and an eddy covariance flux tower for continuous measurements of net ecosystem carbon dioxide exchange (Figure 6.1).

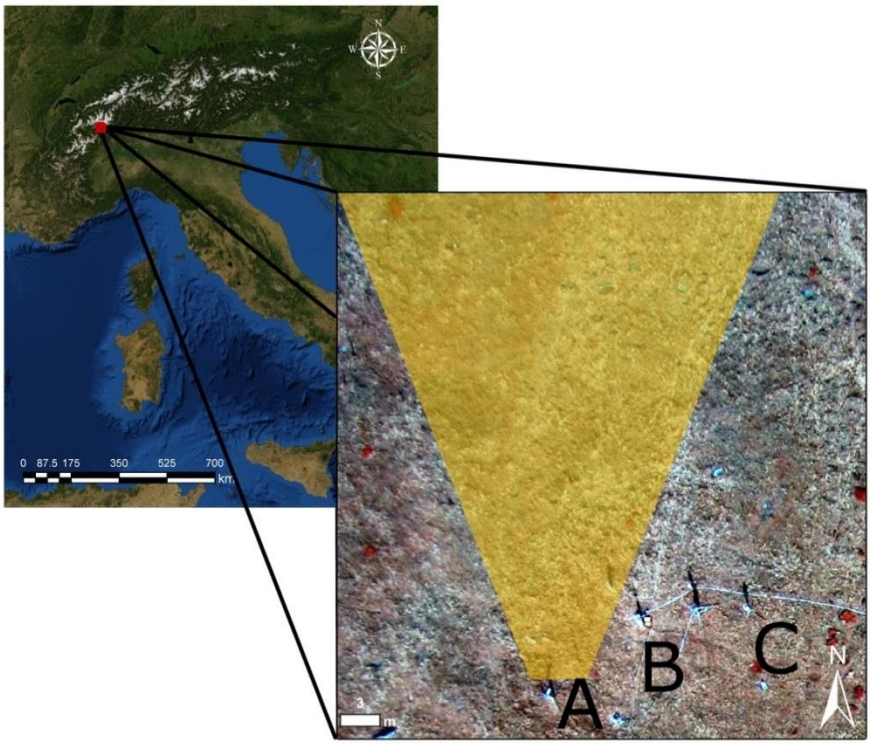

Figure 6.1.Location of the experimental site (red point) in the Italian Alps. False colour representation of a Near Infra-Red (NIR) aerial photograph of the Torgnon (AO, Italy) study site (recorded in October 2012 by an unmanned aerial vehicle, UAV). The yellow mask approximately refers to the view area of the Campbell digital camera used in the study located at A. B and C refer to the eddy covariance tower and the micrometeorological station respectively. The image shows the heterogeneity of the grassland analysed.

6.2.2 Data collection

Two sources of data were collected for this study: digital time-lapse images and a field survey of species composition.

Digital images were collected using a Campbell digital camera (model CC640 Campbell Scientific, Logan, UT, USA) installed at the experimental site in 2009. Following Richardson et al. (2007), the camera was pointed north and set at an angle of about 20° below horizontal. Camera focal length was 3.5 mm and the field of view was approximately 79.8°. The camera was fixed at 2.5 m above ground and the same view scene was captured (Figure 6.2). The images were collected in Joint Photographic Experts Group format (JPEG) and present a resolution of 0.3 megapixels, with three colour channels, namely red, green and blue, at 8 bits of radiometric resolution. The images were collected hourly from 10 am to 5 pm and exposure mode and white balance were set to automatic. Overall, 5644 images were collected between 21st May 2009 and the 22nd November 2011 and were available for this study.

The plant survey was conducted in May 2012 when the vegetation clearly showed two different patterns: the early greening vegetation type, corresponding to the concave slope areas, and the late greening vegetation type, corresponding to the convex areas. Sixteen plots, visible within the digital camera images, were selected and sampled using a visual estimation survey

method for the evaluation of the species composition and percentage cover. The whole site was completely covered by vegetation and no bare ground was visible. Finally, species composition was expressed in terms of percentage cover of each species.

Air temperature and snow height were measured respectively by a HMP45 (Vaisala Inc.) and a sonic snow depth sensor (SR50A, Campbell Scientific, Inc.). Air temperature data were then used to compute the Thawing Degree-Day from snowmelt (TDDsm) (Hollister et al., 2005), representing progressive heat accumulation in the season TDDsm were calculated as the area under the curve of daily temperature range above 0 °C as reported below:

$$TDDsm = \sum_{i=1}^{n} Tair_i \quad [6.1]$$

Where n is the number of daily air temperature measurements (above 0 °C) collected after the snowmelt date. The daily TDDsm time series has been filtered using a moving average with window size equal to 9 days.

6.2.3 Image analysis

In this study digital images were used for monitoring phenology and the snowmelt process occurring in the subalpine grassland. A ROI was firstly identified and selected in the image to analyse snowmelt and vegetation phenology (Figure 6.2).

Figure 6.2. The region of interest (ROI) in red was chosen in the foreground to avoid problems related to distance, weather and excessive pixel size differences. The ROI was then divided using a grid with a grid cell size of 10x10 pixels. Nineteen rows and forty-nine columns result from the division.

The ROI was restricted to the foreground part of the grassland in the image, which was less affected by clouds occasionally observed in the background (Migliavacca et al., 2011). Pixel size within the ROI corresponded to 1 to 4 cm in field and the analysed area of the ROI to approximately 150 m^2 in nature. In order to investigate the spatial variability of greening and

snowmelt, the analysis was conducted by resampling the original ROI on a 10x10 pixel grid (Figure 6.2) providing 855 grid cells (19 rows and 45 columns). The grid cell size changes according to the distance from the camera and it ranges approximately between 10 and 40 cm^2. This dimension has the same order of magnitude of areas with homogeneous or heterogeneous species composition and can be considered large enough to distinguish the vegetation types present at the study site.

6.2.3.1 Snowmelt maps

Snowmelt maps were computed at pixel level by performing a k-means unsupervised classification (Hartigan and Wong, 1979) on each image in the three years examined (2009, 2010, 2011). The pixel values were clustered by the k-means method, partitioning the values into 2 groups such that the sum of squares from points to the assigned cluster centres was minimized. Two classes were identified corresponding to "snow" and "no snow" covered pixels. In a second step, the date of snowmelt for each cell of the grid was defined as the Day of Year (DOY) when more than 50% of pixels of the cell were classified as ''no snow''. Finally, spatial anomalies of snowmelt dates were computed for each year as the difference between cell values and mean annual snowmelt date of the entire ROI.

The accuracy of the k-means unsupervised classification was evaluated on three images, one per year, characterized by a snow cover of about 50% of the image. On each classified image 100 pixels have been randomly selected (45% ± 5 and 55% ± 5 belonging to "snow" and "no snow" classes respectively). Each pixel has been analysed on the original images, attributing to each of them a flag of "snow" or "not snow" based on a visual inspection. The overall accuracy of the unsupervised classification was then computed as the ratio between the number of the pixels correctly classified and the total number of pixels considered. The obtained accuracy was greater than 90% for the three years analysed.

6.2.3.2 Spring phenological maps

The chromatic information contained in the collected images was extracted using indices that synthesize the primary colour content of the images. To minimise the effects of illumination conditions and the camera acquisition setup the original RGB images were transformed into RGB chromatic coordinates (i.e. the green and blue chromatic coordinates, *gcc* and *bcc*, respectively) (e.g. Gillespie et al., 1987; Woebbecke et al., 1995) as follow:

$$gcc = G/(R + G + B) \quad [6.2]$$

$$bcc = B/(R + G + B) \quad [6.3]$$

where R, G, B are the red, green and blue digital number (DN) values of each colour channel, respectively. The green chromatic coordinates were computed for each pixel and then averaged for each cell for all the images recorded during the three years, resulting in cell-based *gcc* time series.

After computation of the chromatic coordinates, the time series were filtered to reduce data noise. This step was necessary since illumination change within the field of view, especially due to cloudy sky conditions, affected the diurnal variation and the seasonal trend of the indices, thus producing undesired spikes. The filtering strategy was based on two steps:

I) using a threshold on the blue channel to discard cloudy images. The diffuse light conditions affect the blue channel, (Ide and Oguma, 2010) and when the weather conditions were not stable, the blue channel values showed larger daily variability compared to clear sky days. Therefore a threshold on the *bcc* was selected and the images were discarded accordingly:

$$bcc_{dm} - (bcc_{sd})\ 5^{th} < bcc < bcc_{dm} + (bcc_{sd})\ 5^{th} \quad [6.4]$$

where bcc is the blue chromatic coordinate defined in formula 6.3, bcc_{dm} is the daily mean value of bcc and (bcc_{sd}) and 5^{th} is the fifth percentile of the seasonal standard deviation of *bcc*.

From a visual inspection, the filter based on bcc time series removed all the cloudy images and also some of the clear sky ones. Thus, a high temporal resolution time series (i.e. 5-8 images each day) is required when applying this filter;

II) using a further filtering technique to obtain *gcc* time series with constant time steps from daily to three daily composites. For this purpose, the approach suggested by Sonnentag et al. (2012) was used which consists of a 3-day moving-window assigning the 90th percentile to the centre day (calculated using all the *gcc* values referred to the images acquired in 3 days of measurements).

Finally, the *gcc* time series was fitted with a cubic smoothing spline according to Migliavacca et al. (2011). The beginning of the season (BOS) was defined as the time when the greenness curve reaches the half maximum of spring growth (Bradley et al., 2007; Fisher et al., 2006; White et al., 1997). The methodology was automatically applied first to the average ROI values and subsequently to all grid cells leading to a BOS map. A no-data flag was assigned to grid cells having BOS values outside the period from snowmelt dates to end of July (13%, 16%,24% in 2009, 2010 and 2011 respectively). Annual BOS anomaly maps were obtained by subtracting the mean BOS value of the ROI from the corresponding mean BOS of each cell.

6.2.4 Comparison of the beginning of the season and the snowmelt dates

To evaluate the relationship between snowmelt and spring phenology, BOS and snowmelt maps of the three years were initially compared using the non-parametric Kendall correlation test. To reduce data noise this analysis was conducted on aggregated data: grid cells were grouped into 15 classes according to snowmelt date quantiles and their BOS median dates were computed. Lastly, generalized linear models (McCullagh and Nelder, 1989) were used to analyse the sensitivity of BOS to snowmelt, considering the entire community (i.e. the ROI) and the vegetation types (GF and GO) separately.

The Kruskall-Wallis test was performed to statistically test significant differences of spatially distributed BOS within the three years analysed. If the test resulted significant ($p<0.05$), the Wilcoxon-Mann-Whitney test was used to asses which group pairs significantly differ ($p<0.05$).

6.3 Results

6.3.1 Snowmelt and spring phenology of the subalpine grassland

During the three years analysed the air temperature time series were generally comparable except for a warm spring spell of about 10 days in April 2011 which was responsible for the extremely early snowmelt in that year (Figure6.3a and 6.3b, Galvagno et al., 2013).

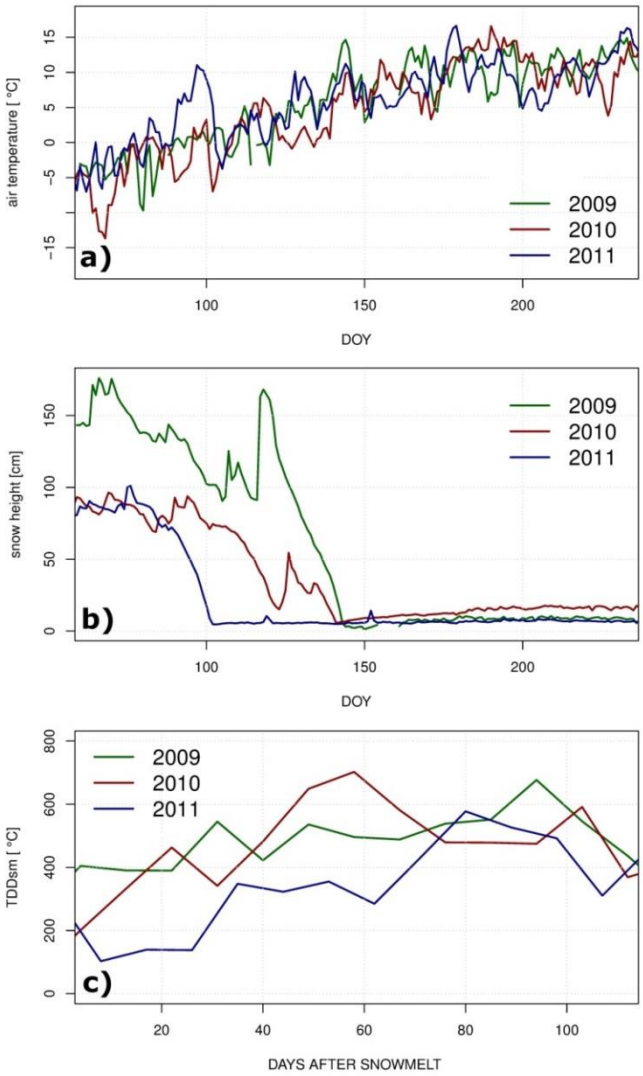

Figure 6.3. Annual time series of meteorological variables collected at the experimental site. a) air temperature [°C]; b) snow depth [cm] ; c) Thawing Degree Day after snowmelt (TDDsm) [°C]. Air temperature and snow height are presented as the daily median value. The TDDsm is depicted as 9 days averaged value after the annual snowmelt date. The different colours refer to the three years analysed (2009, 2010 and 2011).

Snowmelt occurred on DOY 145 and 143 in 2009 and 2010, respectively, while it was observed 40 days earlier in 2011 on DOY 103. The 2011 snowmelt was followed by air temperature values lower than those recorded after the snowmelt in 2009 and 2010 causing a flatter daily increase of TDDsm compared to the two previous years. As reported in Figure 6.3c, the 2011 TDDsm (blue line) shows a delay of approximately a month in reaching values close to 400 thawing degree days compared to the two previous years.

Although only three years were evaluated and the size of the area investigated was quite small, significant dynamics in greening phenology and snowmelt could be observed within this ecosystem.

Digital images clearly showed similar spatial patterns of snowmelt in the three years (Figure 6.4, left panel). The complete snowmelt process occurred in 3 days in 2009 and 2010 while it was slower in 2011, lasting 6 days (Figure 6.5, bottom panel).

The BOS anomaly maps showed consistent interannual spatial patterns (Figure 6.4, right panel). Mean BOS occurred on DOY 172, 173, 162 in 2009, 2010, 2011, respectively, and a large spatial variability of BOS dates was found in each year with strong negative and positive anomalies (66, 70, 93 days in 2009, 2010, 2011, respectively, Figure 6.4).

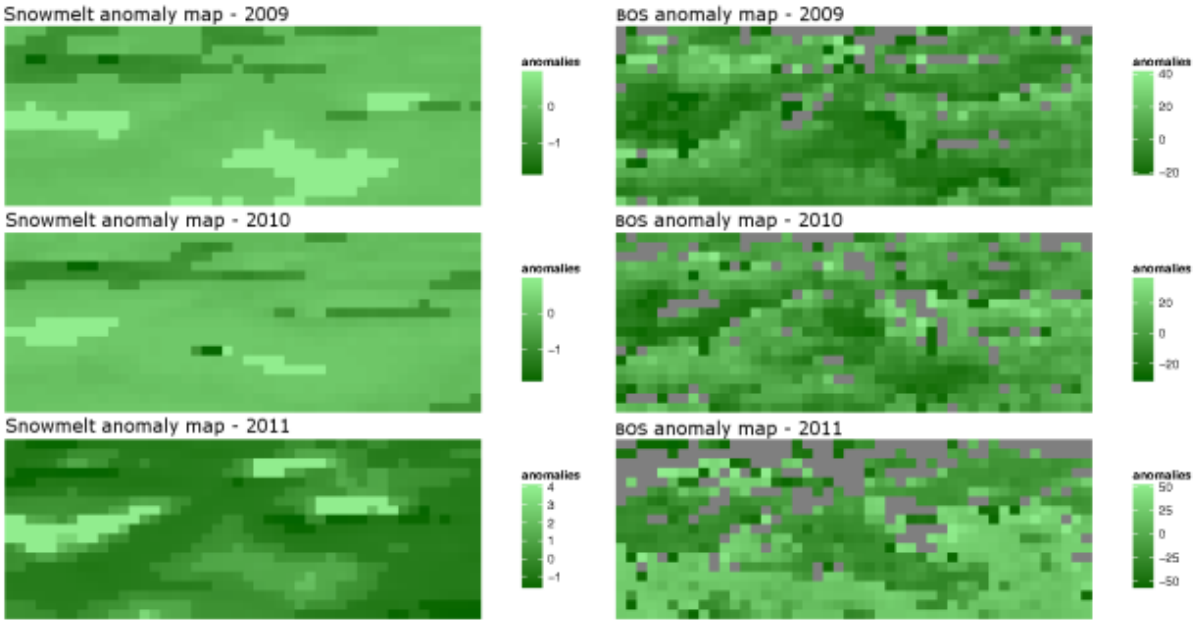

Figure6.4. Left panel: Snowmelt anomaly maps computed against the annual mean value of the entire ROI; right panel: maps of the anomaly of BOS (beginning of season) computed against the annual mean BOS of the entire ROI. The colour scales represent the range of variation of the snowmelt / greening dates in the images. Dark green highlights areas with early dates, while the light green refers to areas where snowmelt or BOS were delayed. Grey colour represents the no data, excluded during the filtering phase.

The years 2009 and 2010 were characterised by a unimodal distribution of BOS dates and, quite surprisingly, two clear modes were evident in the 2011 BOS frequency distribution (Figure 6.5).

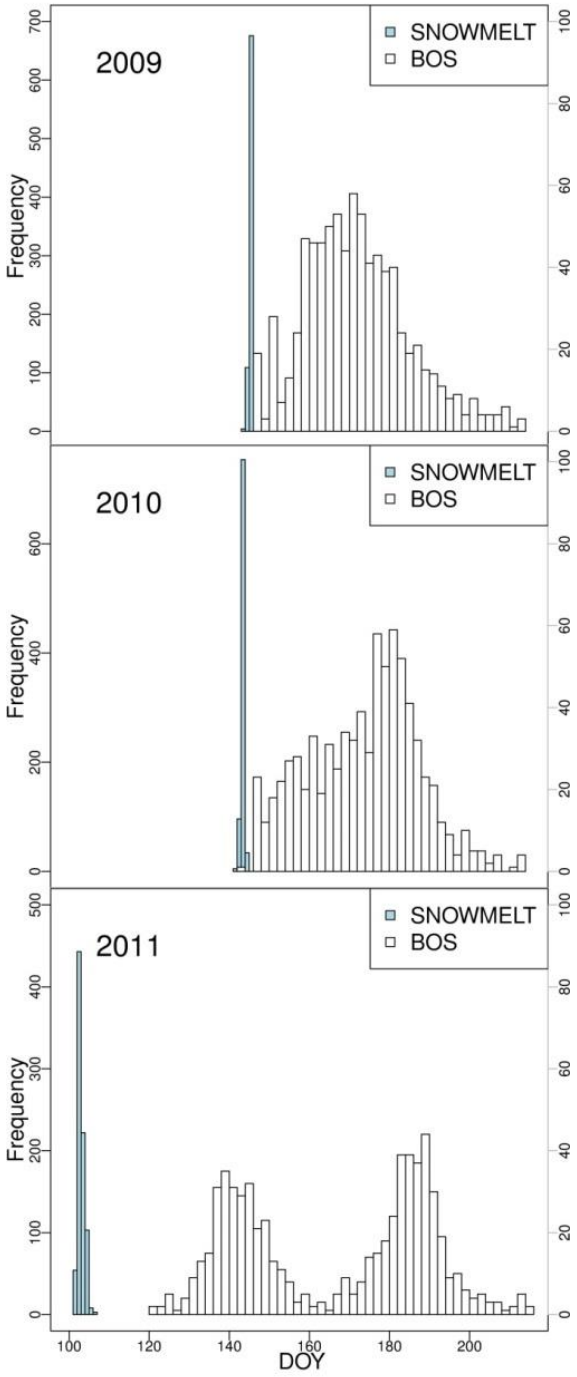

Figure 6.5. Frequency distribution in terms of number of cells of snowmelt (light blue) and BOS (white) in the three study year with unimodal BOS distribution in the first two years and a bimodal one in 2011. In2011 the date of snowmelt date was 40 days earlier than in 2009 and 2010.

6.3.2 Phenology of vegetation types: the effect of early snowmelt

The bimodal BOS frequency distribution of 2011 allowed analysing the BOS spatial distribution during the spring which followed an exceptionally early snowmelt. According to the field surveys, the areas characterized by an earlier BOS (first mode in Figure 6.5, bottom panel) corresponded to the vegetation type with higher abundance of forbs (GF) while the vegetation

type with late BOS was dominated by grass, mainly *Nardus stricta* (GO) (Table 6.1). However it should be noted that the areas dominated by one of the two main vegetation types can have a different degree of homogeneity. Forbs represent from 50 to 90% cover of the early greening vegetation areas and grasses from 78 to 95% cover of the late greening vegetation areas assessed in the field.

	Early greening vegetation areas (GF)			**Late greening vegetation areas (GO)**		
	A	**B**	**C**	**A**	**B**	**C**
BOS (DOY)	132±2	141±5	149±5	192±4	181±5	169±6
Total Grasses (% cover)	10	20	50	95	85	78
Total Forbs (% cover)	90	80	50	5	15	22
Snowmelt date (DOY)	105.58±0.2	103.54±0.4	102.66±0.3	101.58±0.3	102.58±0.2	102.66±0.3

Table 6.1 Summary of the images analysis data results and field phenological survey. The table contains the average beginning of the season date in 2011, species composition (percentage of cover) and the 2011 average snowmelt date (expressed as Day of the Year) of the areas analysed in the field. The plots were chosen in the field according to the digital camera images, distinguishing areas characterized by an early beginning of the season (early greening vegetation) and areas where the beginning of the season took place later (later greening vegetation). The subcategories A, B and C refer to areas with a different degree of homogeneity from A to C.

Using the bimodal distribution in 2011, a threshold (DOY 165), corresponding to the date where the two modes are clearly separated (Figure 6.5), was used to discriminate early and late BOS areas within the ROI and to classify the cells accordingly. The areas dominated by the GF vegetation type are those represented in dark green in Figure 6.4 (right panel). On the contrary the areas mainly dominated by the grasses (GO) are depicted in light green. A significant advance in BOS date was only observed for GF in 2011 (Figure 6.6, p-value < 0.05 performing the Mann-Whitney test). In particular the averaged GF BOS date in 2011, occurred 26 days earlier compared to the two previous years. In contrast, the total ROI and GO BOS dates did not show any significant variation (according to the Mann-Whitney test).

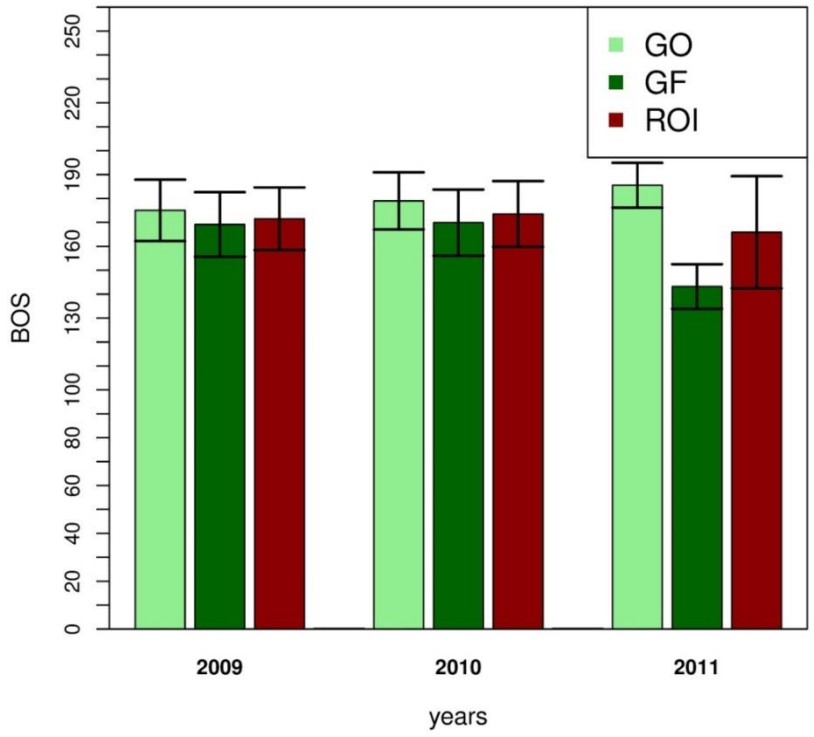

Figure 6.6. The graph shows the 3-year averaged beginning of the season and related standard deviation obtained by distinguishing between the two main vegetation types (grass only, GO and mixed grass and forb, GF) and the overall region of interest value. The beginning of the season related to the mixed grass and forbs vegetation type is strongly anticipated in 2011 (26 days before the two previous years) while the variation of beginning of the season related to the grass only is stable in the three years considered.

6.3.4 Spatial relationship between phenology and snowmelt

The correlation analyses between snowmelt and the spring phenology maps showed significant inverse correlations (p value <0.05; Kendall correlation coefficient (τ) values of -0.89, -0.63, -0.73 for 2009, 2010 and 2011, respectively), meaning that later snowmelt areas corresponded to early BOS areas.

Results of the sensitivity analysis conducted using the generalised linear model are shown in Figure 6.7 and Table 6.2 and refer to the model applied separately on the entire ROI and on the two vegetation types (GF and GO) separately.

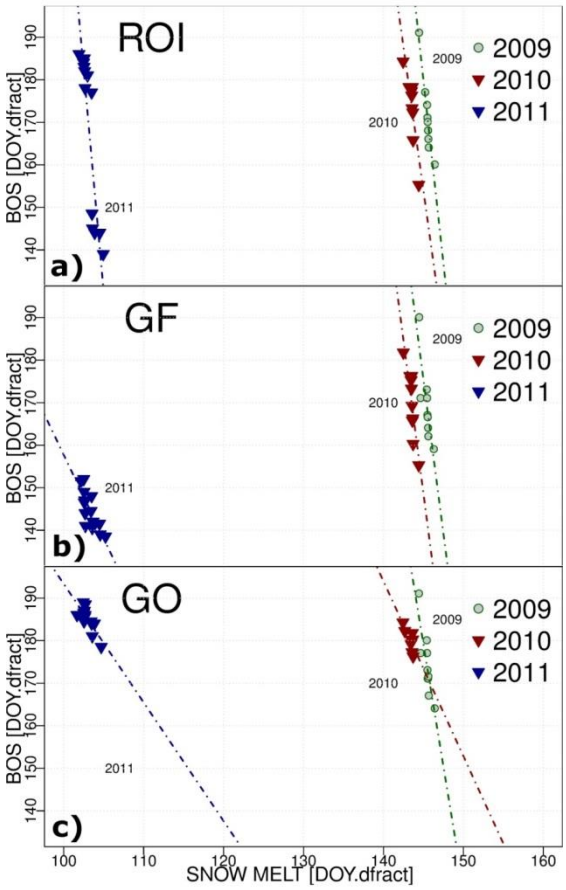

Figure 6.7. Relationship between snowmelt date and BOS analysed using the generalized linear model (glm). The models were applied considering the whole region of interest (ROI) (A), and distinguishing the vegetation types existing at the grassland site (B, C). In particular, the B graph represents the analysis carried out considering only mixed grass and forbs (GF), while the C graph refers to the grass only vegetation type (GO). Day of the year (DOY) and decimal fraction of the day (dfract) have been used to represent the different time of the day when the snowmelt and the beginning of the season occurred.

A strong negative correlation was found between BOS and snowmelt dates. This indicates that, in the spatial domain, areas characterised by early snowmelt corresponded to the area where BOS took place later (and vice versa). In particular, the results show a significant negative relationship in the 3 years considered (Figure 6.7, top panel). Similar results were obtained also separately considering the two vegetation types: middle and bottom panels in Figure 6.7 show the relationship between snowmelt dates and BOS having a negative slope for both vegetation types (GF and GO) in the three years.

	All					Early greening vegetation (GF)					Late greening vegetation (GO)				
	Nr of cell .	**r^2**	**M**	**SE**	**P**	**Nr of cell**	**r^2**	**m**	**SE**	**P**	**Nr of cell**	**r^2**	**M**	**SE**	**P**
2009	809	0.90	-17.21	1.93	< 0.01	494	0.70	-14.48	3.5	< 0.01	479	0.74	-11.48	2.46	< 0.01
2010	785	0.75	-13.50	3.12	< 0.01	470	0.75	-14.40	3.2	< 0.01	467	0.56	-4.11	1.29	0.02
2011	655	0.80	-20.84	3.29	< 0.01	380	0.60	-3.93	0.8	< 0.01	373	0.63	-2.79	0.68	< 0.01

Table 6.2 Results of the analysis conducted using the Generalized Linear Model (*glm*). The relationship between the beginning of the season and snowmelt dates is reported here in terms of number of cell investigated, r^2, slope (m), standard error (SE) and p value. The table distinguishes between analysis conducted on the whole scene, or divided into the two main vegetation types, the first one dominated by forbs and the second dominated by grasses.

6.4 Discussion

The results of this study underline the potential of using repeat digital photography as a proximal remote sensing system for monitoring patterns of phenology in relation to snowmelt variability. The combination of temporal and spatial information gave important insights on the heterogeneity of vegetation among sites and also on the different responses of vegetation types, showing different ecological requirements of grasses and forbs. In turn, the spatial analysis of the snowmelt can provide useful information for interpreting the complex relationships between snowmelt, the heterogeneous microtopography and the phenological behaviour of the different vegetation types in the ecosystem.

The results show the importance of using a pixel per pixel analysis instead of considering an overall ROI. One out of three years (2011) was characterised by an extremely anticipated snowmelt in 2011. As observed in Figure 6.6 and better displayed in Figure6.8, without disentangling the contribution of forbs and grasses, the temporal pattern of the phenological development of the ROI is similar in the three years. In fact if the BOS mean value of the entire ROI is considered (Fig 6.6, red bars) no significant advance can be found in 2011. On the contrary, when the two vegetation types are separately considered, significant differences appear in the mean BOS value of the vegetation type characterized by abundance of forbs (GF) in 2011. This finding suggests that the two vegetation types react in a different way to an extremely early snowmelt and underlines that snowmelt is the key environmental factor at the studied site for species with known opportunistic behaviour (Keller and Körner, 2003), like *Geummontanum*, *Crocus albiflorus,Arnica montana, Potentillacrantzii*. However for the vegetation type dominated by grasses other environmental factors, such as air temperature (Figure 6.3), can have a role in driving BOS date. Irrespective of the timing of snowmelt, grass phenological development starts when TDDsm reaches values close to 400 °C. This occurred 40 and 80 days after snowmelt in 2009-10 and in 2011 respectively. Furthermore the BOS GO date didn't differ between the three years considered, thus an effect of the photoperiod length on the grass phenological response cannot be excluded (Keller and Körner, 2003). This difference in GF and GO response to early snowmelt is in agreement with Inouye (2013) where a species specific relationship between flowering and the time of snowmelt is shown.

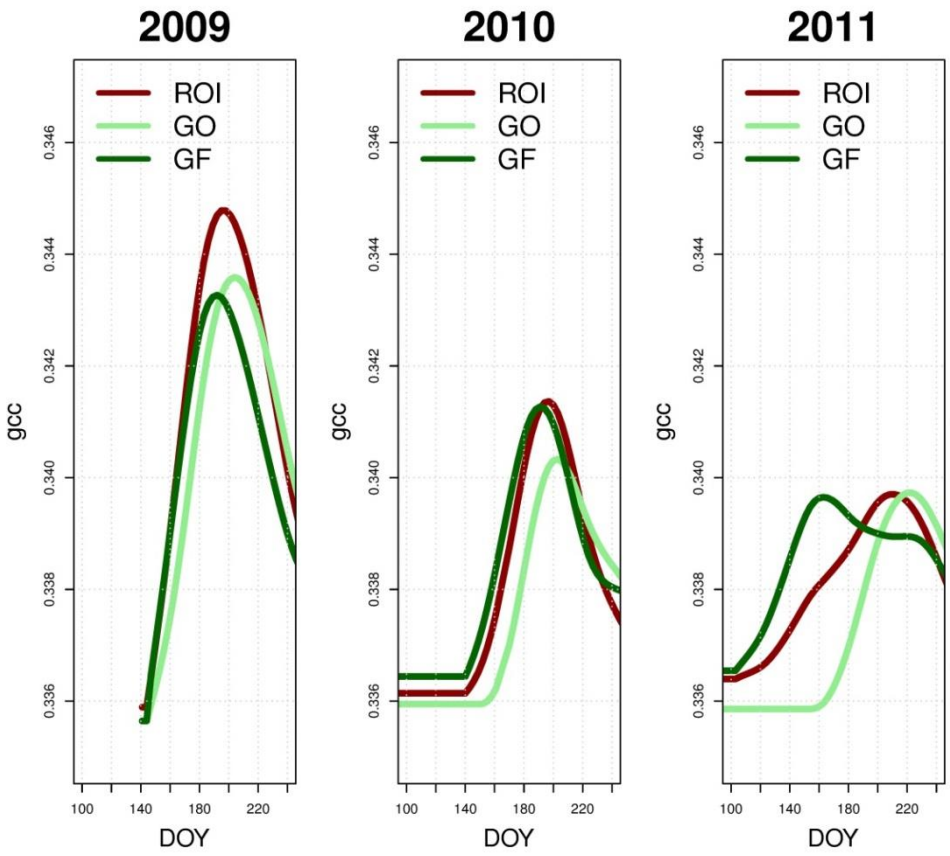

Figure 6.8. The 3-year green chromatic coordinates (*gcc*) time series are separately plotted considering the average value of the overall ROI value (red line), and the two vegetation types characterized by dominance of the two vegetation types (GF, grass and forb, dark green line and GO, grass only, light green line). The year 2011 was characterized by a strong advance in the growth of GF while in 2009 and 2010 the difference between the two vegetation types was not so sharp.

Considering the spatial relation between snowmelt and phenology (Table 6.2, Figure6.7), the impact of site microtopography on species compositions and thus on phenology emerged. Each year, the complete snowmelt occurs within a few days (at most 6 days in 2011) and the different patches of snowmelt reflect micro-topographical differences of the site. In the convex areas the snow melts earlier, while in the concave areas the snow lasts longer. Therefore the snowmelt can be considered as a proxy of microtopography, and indirectly of different site ecological conditions affecting the species distribution. The dominance of different species found in concave (i.e. GF vegetation type) or convex (GO) areas can be determined by several factors, such as the influence of snow, the higher nutrient availability during and after the snowmelt period, differences in soil chemical and physical properties (Schuerings et al., 2013) and, finally, differences in water availability depending on the microtopography (Michalet et al., 2002). The counter intuitive negative correlation between snowmelt and BOS on the whole scene (Table 6.2) can be explained considering that snow melts later in areas dominated by species with opportunistic behaviour (GF), able to quickly develop after snowmelt, and snow melts earlier in areas preferred by GO known to have a slower development affected by factors other than snow cover. Thus the negative relationship is driven by the presence of areas with

different species composition. This is especially evident in 2011 (Figure 6.7a, blue triangles) where the two clusters of points clearly represent areas dominated by one of the two vegetation types (GF and GO). The separation of GF and GO is more difficult in 2009 and 2010 because the development of the two vegetation types occurred in a narrow time period. When GF and GO are separately considered the negative relationship is maintained (Table 6.2). GF and GO represent areas with abundance of grass or forbs, but in such a complex ecosystem a gradient of species distribution is still present. The spatial analysis of BOS date is able to capture the different species distribution within the same vegetation type (Table 6.1). In fact concave areas, at the bottom of the pit, show higher percentage of forbs if compared to the sides. The contrary occurs in the convex areas, where the percentage of forbs increases moving away from the mound.

In summary, these results appear to indicate that forbs, whose opportunistic behaviour is well known in the literature (Keller and Körner, 2003), are capable of quickly tuning their growth even in years with anticipated snowmelt. Indeed, in 2011, the year characterized by an extremely early snowmelt, a strong advance of BOS was observed in areas of the grassland dominated by forbs (on average 26 days in advance compared to 2009 and 2010). Conversely, the grasses (mainly *Nardus stricta*) showed a "safer" behaviour and started to develop in relatively constant periods of the years and showed no advancement in BOS even in the extreme year 2011 (mean BOS date of grasses occurred around DOY 180 in all the three years). These results are consistent with the studies carried out by Wipf and Rixen(2010) where grasses showed no significant response to snow manipulations. On the contrary, forbs are sensitive precursors of snowmelt (Keller and Körner, 2003). Forbs plasticity may represent the response of species adapted to growth in areas with a long persistence of snow. While in habitats with early snowmelt (e.g. convex areas), any advancement of snowmelt may lead to frost-damage, hence later BOS may be a safer strategy for this species. Differences in phenological development may also have an important role in all ecosystem processes, especially during years characterised by extreme early snowmelt. For example, a reduction in net CO_2 ecosystem uptake was observed in spring/summer 2011 (Galvagno et al., 2013) and this may in part be due to the later development of grasses compared to forbs (less abundant at the ecosystem level).In this context, the use of digital images for inferring the phenological cycle of different vegetation types represents a great opportunity to gain new insights for interpretation of eddy covariance measurements.

6.5 Conclusions

In this study, the possibility of exploiting digital time-lapse camera images for monitoring the phenology and snowmelt process in subalpine grassland environment was investigated. Within such a heterogeneous ecosystem, we emphasize the importance of analysing the image at pixel per pixel level instead of considering single ROI areas, thus providing a more detailed description in order to improve the knowledge of phenological and snowmelt processes and the

ecological requirements ofspecies. In particular, in 2011 an exceptionally early snowmelt occurred, and it was possible to distinguish the phenological development of the two main vegetation types at the ecosystem level. Finally, this study highlights for the first time a significant inverse empirical relationship between spatial phenology and snowmelt as indirect indicator of microtopography, which may have important implications for ecological studies in alpine areas. Further investigations are however needed to better evaluate the role of microtopography and snowmelt through the influence they exert on species distribution.

In summary, this research demonstrates that digital time-lapse images can provide reliable spatial and temporal information on snowmelt and plant phenology in a heterogeneous ecosystem. Digital photography is therefore a promising and low-cost tool for long-term monitoring of the environment and may help to describe different ecosystem processes in scientific studies.

Acknowledgement

The researchers involved in the study are: Cremonese E., Migliavaccac,M., Colombo,R., Galvagno,M., Siniscalco, C., Rossini, M., Fava,F., Cogliati, S, Morra di Cella, U, Menzel, A.

Reference

Ahrends, H. et al., 2009. Tree phenology and carbon dioxide fluxes: use of digital photography for process-based interpretation at the ecosystem scale. Climate Research, 39: 261-274.

Ahrends, H.E. et al., 2008. Quantitative phenological observations of a mixed beech forest in northern Switzerland with digital photography. Journal of Geophysical Research: Biogeosciences, 113(G4): G04004.

Alberton, B. et al., 2014. Using phenological cameras to track the green up in a cerrado savanna and its on-the-ground validation. Ecological Informatics(0).

Alcamo, J., FlÖRke, M. and MÄRker, M., 2007. Future long-term changes in global water resources driven by socio-economic and climatic changes. Hydrological Sciences Journal, 52(2): 247-275.

Auer, I. et al., 2007. HISTALP—historical instrumental climatological surface time series of the Greater Alpine Region. International Journal of Climatology, 27(1): 17-46.

Bater, C. et al., 2011. Using digital time-lapse cameras to monitor species-specific understorey and overstorey phenology in support of wildlife habitat assessment. Environmental Monitoring and Assessment, 180(1-4): 1-13.

Beniston, M., 2005. Mountain Climates and Climatic Change: An Overview of Processes Focusing on the European Alps. pure and applied geophysics, 162(8-9): 1587-1606.

Bradley, B.A., Jacob, R.W., Hermance, J.F. and Mustard, J.F., 2007. A curve fitting procedure to derive inter-annual phenologies from time series of noisy satellite NDVI data. Remote Sensing of Environment, 106(2): 137-145.

Busetto, L. et al., 2010. Remote sensing of larch phenological cycle and analysis of relationships with climate in the Alpine region. Global Change Biology, 16(9): 2504-2517.

Cleland, E.E., Chuine, I., Menzel, A., Mooney, H.A. and Schwartz, M.D., 2007. Shifting plant phenology in response to global change. Trends in Ecology & Evolution, 22(7): 357-365.

Cornelius, C., Estrella, N., Franz, H. and Menzel, A., 2013a. Linking altitudinal gradients and temperature responses of plant phenology in the Bavarian Alps. Plant Biology, 15: 57-69.

Cornelius, C. et al., 2013b. Phenological response of grassland species to manipulative snowmelt and drought along an altitudinal gradient. Journal of Experimental Botany, 64(1): 241-251.

Corripio, J.G., 2004. Snow surface albedo estimation using terrestrial photography. International Journal of Remote Sensing, 25(24): 5705-5729.

Fisher, J.I., Mustard, J.F. and Vadeboncoeur, M.A., 2006. Green leaf phenology at Landsat resolution: Scaling from the field to the satellite. Remote Sensing of Environment, 100(2): 265-279.

Foppa, N. and Seiz, G., 2012. Inter-annual variations of snow days over Switzerland from 2000-2010 derived from MODIS satellite data. The Cryosphere, 6(2): 331-342.

Galvagno, M. et al., 2013. Phenology and carbon dioxide source/sink strength of a subalpine grassland in response to an exceptionally short snow season. Environmental Research Letters, 8(2): 025008.

Gillespie, A.R., Kahle, A.B. and Walker, R.E., 1987. Color enhancement of highly correlated images. II. Channel ratio and "chromaticity" transformation techniques. Remote Sensing of Environment, 22(3): 343-365.

Gobiet, A. et al., 2013. 21st century climate change in the European Alps—A review. Science of The Total Environment(0).

Hartigan, J.A. and Wong, M.A., 1979. Algorithm AS 136: A K-Means Clustering Algorithm. Journal of the Royal Statistical Society. Series C (Applied Statistics), 28(1): 100-108.

Henneken, R., Dose, V., Schleip, C. and Menzel, A., 2013. Detecting plant seasonality from webcams using Bayesian multiple change point analysis. Agricultural and Forest Meteorology, 168(0): 177-185.

Hinkler, J., Pedersen, S.B., Rasch, M. and Hansen, B.U., 2002. Automatic snow cover monitoring at high temporal and spatial resolution, using images taken by a standard digital camera. International Journal of Remote Sensing, 23(21): 4669-4682.

Hollister, R.D., Webber, P.J. and Bay, C., 2005. Plant response to temperature in northern Alaska: implications for predicting vegetation change. Ecology, 86(6): 1562-1570.

Ide, R. and Oguma, H., 2010. Use of digital cameras for phenological observations. Ecological Informatics, 5(5): 339-347.

Ide, R. and Oguma, H., 2013. A cost-effective monitoring method using digital time-lapse cameras for detecting temporal and spatial variations of snowmelt and vegetation phenology in alpine ecosystems. Ecological Informatics, 16(0): 25-34.

Inouye, D. and Wielgolaski, F., 2013. Phenology at High Altitudes. In: M. Schwartz (Editor), Phenology: An Integrative Environmental Science. Springer Science+Business Media B.V., pp. 249-272.

Jacobs, N. et al., 2009. The global network of outdoor webcams: properties and applications, Proceedings of the 17th ACM SIGSPATIAL International Conference on Advances in Geographic Information Systems. ACM, Seattle, Washington, pp. 111-120.

Keller, F. and Körner, C., 2003. The Role of Photoperiodism in Alpine Plant Development. Arctic, Antarctic, and Alpine Research, 35(3): 361-368.

Lieth, H., 1974. Purposes of a Phenology Book. In: H. Lieth (Editor), Phenology and Seasonality Modeling. Ecological Studies. Springer Berlin Heidelberg, pp. 3-19.

Linderholm, H.W., 2006. Growing season changes in the last century. Agricultural and Forest Meteorology, 137(1–2): 1-14.

McCullagh, P. and Nelder, J.A., 1989. Generalized linear models (Monographs on statistics and applied probability 37). Chapman Hall, London.

Menzel, A. et al., 2006. European phenological response to climate change matches the warming pattern. Global Change Biology, 12(10): 1969-1976.

Michalet, R., Gandoy, C., Joud, D., Pages, J.-P. and Choler, P., 2002. Plant community composition and biomass on calcareous and siliceous substrates in the northern French Alps: comparative effects of soil chemistry and water status. Arctic, Antarctic, and Alpine Research: 102-113.

Migliavacca, M. et al., 2011. Using digital repeat photography and eddy covariance data to model grassland phenology and photosynthetic CO2 uptake. Agricultural and Forest Meteorology, 151(10): 1325-1337.

Mizunuma, T. et al., 2013. The relationship between carbon dioxide uptake and canopy colour from two camera systems in a deciduous forest in southern England. Functional Ecology, 27(1): 196-207.

Parajka, J., Haas, P., Kirnbauer, R., Jansa, J. and Blöschl, G., 2012. Potential of time-lapse photography of snow for hydrological purposes at the small catchment scale. Hydrological Processes, 26(22): 3327-3337.

Richardson, A. et al., 2007. Use of digital webcam images to track spring green-up in a deciduous broadleaf forest. Oecologia, 152(2): 323-334.

Richardson, A.D., Bailey, A.S., Denny, E.G., Martin, C.W. and O'Keefe, J., 2006. Phenology of a northern hardwood forest canopy. Global Change Biology, 12(7): 1174-1188.

Richardson, A.D., Braswell, B.H., Hollinger, D.Y., Jenkins, J.P. and Ollinger, S.V., 2009. Near-surface remote sensing of spatial and temporal variation in canopy phenology. Ecological Applications, 19(6): 1417-1428.

Richardson, A.D. et al., 2013. Climate change, phenology, and phenological control of vegetation feedbacks to the climate system. Agricultural and Forest Meteorology, 169(0): 156-173.

Rossini, M. et al., 2012. Remote sensing-based estimation of gross primary production in a subalpine grassland. Biogeosciences, 9(7): 2565-2584.

Rossini, M. et al., 2014. Remote estimation of grassland gross primary production during extreme meteorological seasons. International Journal of Applied Earth Observation and Geoinformation, 29(0): 1-10.

Roy, B.A., Güsewell, S. and Harte, J., 2004. Response of plant pathogens and herbivores to a warming experiment. Ecology, 85(9): 2570-2581.

Saccone, P. et al., 2013. The effects of snowpack properties and plant strategies on litter decomposition during winter in subalpine meadows. Plant and Soil, 363(1-2): 215-229.

Schimel, J.P., Bilbrough, C. and Welker, J.M., 2004. Increased snow depth affects microbial activity and nitrogen mineralization in two Arctic tundra communities. Soil Biology and Biochemistry, 36(2): 217-227.

Schuerings, J. et al., 2013. Absence of soil frost affects plant-soil interactions in temperate grasslands. Plant and Soil, 371(1-2): 559-572.

Schwartz, M.D., Reed, B.C. and White, M.A., 2002. Assessing satellite-derived start-of-season measures in the conterminous USA. International Journal of Climatology, 22(14): 1793-1805.

Sonnentag, O. et al., 2012. Digital repeat photography for phenological research in forest ecosystems. Agricultural and Forest Meteorology, 152(0): 159-177.

White, M.A., Thornton, P.E. and Running, S.W., 1997. A continental phenology model for monitoring vegetation responses to interannual climatic variability. Global Biogeochemical Cycles, 11(2): 217-234.

Wipf, S. and Rixen, C., 2010. A review of snow manipulation experiments in Arctic and alpine tundra ecosystems. Polar Research, 29(1): 95-109.

Wipf, S., Rixen, C. and Mulder, C.P.H., 2006. Advanced snowmelt causes shift towards positive neighbour interactions in a subarctic tundra community. Global Change Biology, 12(8): 1496-1506.

Wipf, S., Stoeckli, V. and Bebi, P., 2009. Winter climate change in alpine tundra: plant responses to changes in snow depth and snowmelt timing. Climatic Change, 94(1-2): 105-121.

Woebbecke, D.M., Meyer, G.E., Von Bargen, K. and Mortensen, D.A., 1995. Color indices for weed identification under various soil, residue, and lighting conditions. Transactions of the American Society of Agricultural Engineers, 38(1): 259-269.

Chapter 7

Early stress detection using optical remotely sensed indicators application

Data presented in this chapter were acquired in the frame of the HyFLEX campaign funded by the European Space Agency (ESA) (ESA ESTEC RFQ-3-13566/12/NL/LF).

Early plant stress can be tracked using indicators derived from hyperspectral optical remotely sensed data. Photochemical Reflectance Index and Sun-Induced chlorophyll Fluorescence (SIF) have been identified as potential indicators of plant physiological status, thus immediately responding to plant stress. The study presented in this chapter is dedicated to evaluate the suitability of these indicators for monitoring plant stress in an early phase. In the context of the European Space Agency (ESA) FLuorescence EXplorer (FLEX) mission, a field campaign was conducted in September 2012 in Czech Republic. The aim of the campaign was to evaluate the possibility of detecting Sun-Induced chlorophyll Fluorescence (SIF) emission from an airborne platform. To enhance differences in plant physiological status an artificial controlled experiment was set: two grass lawns were on purpose located at the experimental site and one was treated with an herbicide (DCMU) known to block photosynthetic electron flow and thus reduce photosynthetic activity, modifying energy dissipative pathways (i.e. fluorescence emission and non-photochemical quenching). During the entire campaign optical proximal sensing measurements were collected at ground level in order to validate airborne products. The analysis of field data showed that the application of DCMU on the grass lawn caused a significant increase of SIF and PRI in the treated grass whereas the traditional Normalized Difference Vegetation Index (NDVI) was not notably different from the lawn that remained untreated. The study demonstrates that both SIF and PRI are capable to detect short term plant stress. In particular SIF seems to be immediately affected even with lower herbicide concentration treatment.

7.1. Introduction and objectives

During the photosynthesis process the plants transform carbon dioxide and water into carbohydrate macromolecules and oxygen with energy of photons absorbed between 400 and 700 nm (Lange et al., 1981). Plant photosynthesis is an actively regulated process with a highly variable efficiency to adjust for dynamic environmental conditions (Schulze and Caldwell, 1994). These adjustments occur on a short-term by altering or rearranging the pigments within the leaves without determining any detectable change in reflectance regions (Red and Near Infrared regions) traditionally used for the calculation of vegetation indices (VI) such as the Normalized Difference Vegetation Index (NDVI). Photosynthesis starts with absorption of light by photosynthetic pigments, mainly by chlorophyll molecules. Under normal physiological conditions, the major part of absorbed light is used for photosynthetic quantum conversion. Under stress conditions photosynthesis declines and the absorbed light exceeding the energy demand has to be dissipated by plants to avoid oxidative damage. Two dissipative defensive strategies are used by plants: chlorophyll fluorescence and non-photochemical quenching. Fluorescence is the process by which the light energy absorbed by chlorophyll pigments at one wavelength is re-emitted at a different wavelength (Papageorgiou, 2004). NPQ involves acidification of the thylakoid lumen, the operation of the xanthophyll cycle pigments and specific components of the antenna (Papageorgiou, 2004) for the thermal dissipation of excess energy. In recent years two indicators derived from optical hyperspectral remotely sensed data and related to these two dissipative mechanisms have been proposed and investigated: Photochemical Reflectance Index (PRI) and Sun-induced Chlorophyll fluorescence (SIF). As described in chapter 2 these indicators are related to changes in the de-epoxidation state of the xanthophyll cycle pigments (PRI, Gamon et al., 1992) and to the direct emission of chlorophyll fluorescence. In recent years these indicators have been used to detect oxidative stress conditions with different degrees of success (Berni et al., 2009; Meroni et al., 2008; Panigada et al., 2014; Rossini et al., 2013; Suárez et al., 2010, 2008). In this study a dedicated experiment was designed to produce a variation in plant photosynthetic efficiency in a short time period. The experiment consisted in two grass lawns, one of them treated with DCMU (3-(3',4'-dichlorophenyl)-1,1-dimethylurea) (DCMU) and the other used as a control. DCMU selectively binds to PSII and blocks its reoxidation by the plastoquinone pool (*Van Rensen*, 1989). The DCMU treated grass cannot perform the photosynthetic electron transport and the excess energy is dissipated as elevated chlorophyll fluorescence emission. Filed spectra measurements were collected simultaneously above the two carpets and spectral indices were calculated. In this chapter the feasibility of detecting early plant stress induced by DCMU application by using hyperspectral field data is evaluated and presented. More in detail NDVI, PRI and SIF response on the grass treated with the herbicide was compared to the response of the control plot.

7.2 Materials and Methods

7.2.1 Herbicide treatment

The experimental study site was located at Bíly Kriz (Moravian-Silesian Beskydy Mts., Czech Republic, 18.54◦E, 49.49◦N, 860 m a.s.l.). Two commercially produced grass lawn carpets (12x8 m each) were used during the experiment (Figure 7.1). The dominant species of the grass were *Festuca rubra, Loliumrepenne, Poapratensis.* One of the two carpet was treated with 3-(3',4'-dichlorophenyl)-1,1-dimethylurea (DCMU) on Sept 5th, 2012 at 08:00 local time by DCMU diluted to 10^{-5} M in 1% ethanol/water. On Sept 9th at 10:00 local time the carpet was treated a second time with 10 times higher herbicide concentration (10^{-4} M DCMU). On both days the control carpet was treated at the same time with 1% ethanol/water without the herbicide.

7.2.2 Leaf chemical analyses

Fresh leaf samples (typically 100 mg) were taken for chlorophyll and carotenoid analysis and frozen in liquid nitrogen. Chlorophyll and carotenoid pigments were extracted in 100% acetone with addition of $MgCO_3$ using mortar and pestle. The homogenate was centrifuged at 6000 rpm and then diluted to 80% solution of chlorophyll in acetone. Samples were analyzed using UV/VIS spectrometer (Specord 250 Plus, Analytik Jena AG, Germany) at an absorbance of 710.0 nm, 663.2 nm, 646.8 nm and 470.0 nm. Samples were diluted into cuvette using 80% acetone so that their absorbance at 663.2 was between 0.25 and 0.75. The chlorophyll and carotenoid concentrations per unit leaf mass (µg g–1) were calculated based on the extinction coefficients derived by Wellburn (1994).

7.2.3 Top of canopy hyperspectral ground measurements

Measurements of grass lawn top of canopy radiance were performed from a distance of 4.2 m by an ASD spectroradiometer (ASD FieldSpec-3, Boulder, CO, USA) positioned alternatively over the DCMU treated and control grass lawn areas using a small hydraulic movable platform (Figure 7.1). The ASD FieldSpec-3 covers the spectral range 350–2500 nm with a spectral resolution of 3 nm at 700 nm and a sampling interval of 1.4 nm. For each grass treatment 20 acquisitions were collected moving the arm of the hydraulic platform. One measurement of a white reference calibrated panel (Spectralon, LabSphere, USA) was performed every 4 target measurements for the computation of the Hemispherical-Conical Reflectance Factor (HCRF, Schaepman-Strub et al., 2006). With a field of view of 25°, the diameter of each acquisition was about 1.8 m.

Simultaneously, the grass radiances were measured with an automatic system named S-FLUO box (Cogliati et al., submitted). The S-FLUO box system hosts two portable spectrometers

(HR4000, Ocean Optics, USA) characterized by different spectral resolutions. The first one covers the visible and near-infrared range (400-1000 nm) with a full width at half maximum (FWHM) of 1 nm and allows the computation of different vegetation indexes. The second one covers with a finer resolution (FWHM = 0.1 nm) a restricted spectral range (700-800 nm) and it is specifically intended for far-red sun-induced fluorescence measurements (at O_2-A band positioned at 760 nm). This system used a commercial optical multiplexer (MPM-2000, OceanOptics, USA) to switch between a channel measuring the incident irradiance using a cosine-response optic (cc3, OceanOptics, USA), a 25° down-looking bare fiber for the measurement of the upwelling radiance and a "blind" channel for the dark current measurement. Spectrometers were housed in thermally regulated boxes controlling the internal temperature in order to reduce dark current drift. Spectrometers were spectrally calibrated with known standards (CAL-2000 mercury argon lamp, OceanOptics, USA) before the campaign while the radiometric calibration has been inferred from cross-calibration measurements performed with a calibrated FieldSpec Pro spectrometer (ASD, USA). The Ocean Optics spectrometer fibers were mounted on a tripod placed between the two grass carpets. The average canopy plane was observed from nadir at a distance of about 1.6 m corresponding to an area on the ground of 0.7 m diameter. The manual rotation of a mast mounted horizontally on the tripod allowed the alternative observation of the DCMU-treated and control grass lawn areas (Figure 7.1). The field spectroscopy technique referred to as "single beam" (Milton and Rollin, 2006) was employed to evaluate the incident and upwelling fluxes. Target measurements were sandwiched between two incident irradiance measurements made by a single device a few seconds apart. The incident irradiance at the time of the target measurement was estimated by linear interpolation. Additionally, the instrument dark current was collected for every set of measurements. Spectral data were acquired with a dedicated software (Meroni and Colombo, 2009) and processed with an IDL (ITTvis IDL 7.1.1®) application specifically developed. Visible and near-infrared reflectance derived from both the ASD and Ocean Optics spectrometers were used to compute the normalized difference vegetation index (NDVI, Rouse et al., 1973)and the Photochemical Reflectance Index (PRI, Gamon et al., 1992)according to the following equations:

$$PRI = (R_{531} - R_{570})/(R_{531} + R_{570}) \quad [7.1]$$

$$NDVI = (R_{800} - R_{680})/(R_{800} + R_{680}) \quad [7.2]$$

where R represent the reflectance at the specified wavelength in nm.

Far-Red SIF was estimated from the high resolution Ocean Optics spectrometer using the spectral fitting method described in Meroni et al., (2010), assuming a linear variation of reflectance and fluorescence in the O_2-A absorption band region. The spectral interval used for Far-Red SIF estimation was set to 759.00 - 767.76 nm for a total of 439 spectral channels used. An apparent fluorescence yield (Fyield) was also computed as the ratio between Far-Red SIF and

the radiation incident in a nearby restricted spectral range not including the oxygen absorption band.

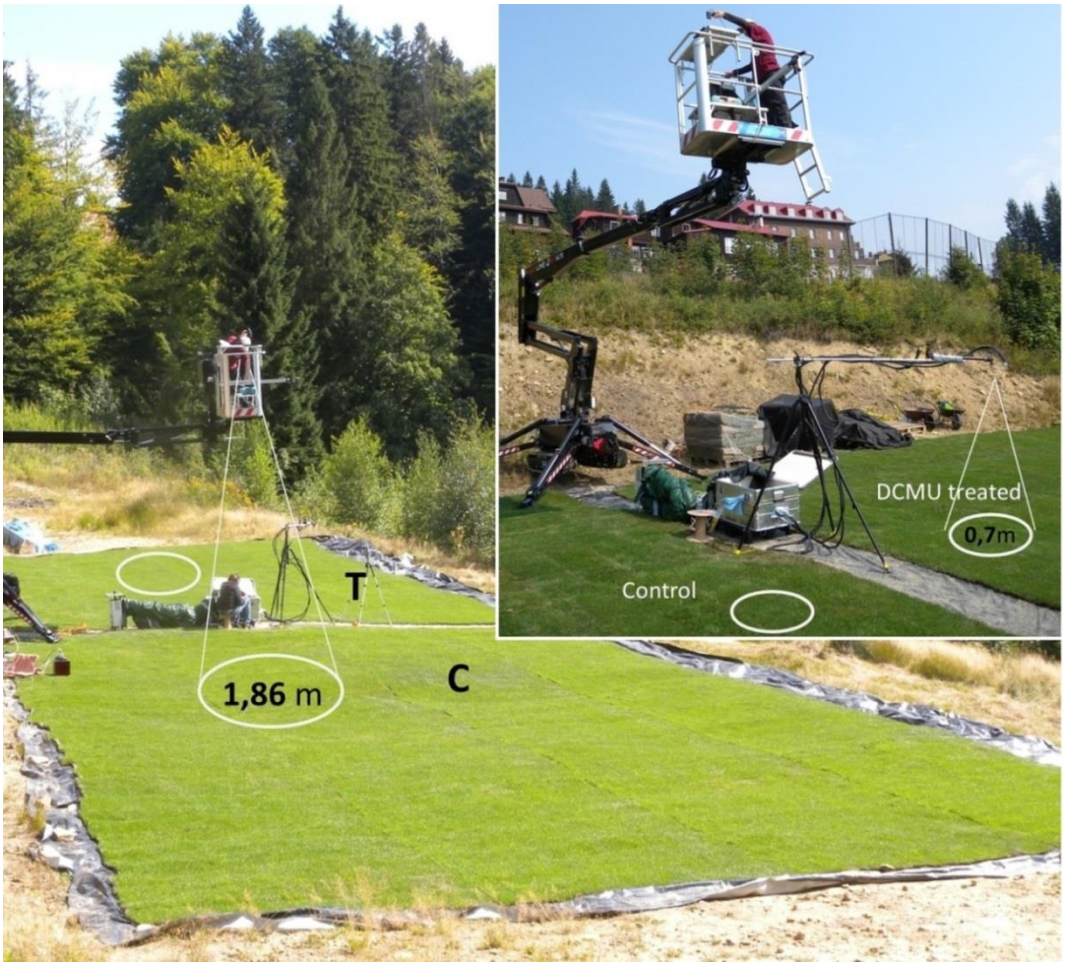

Figure 7.1. Experimental setup at Bíly Kriz site. The two lawn carpets are depicted in Figure. C is for control and T is for herbicide treated carpet. The position of the portable spectrometric system hosting two Ocean Optics spectrometers and the ASD spectroradiometer is shown together with the dimension of the field of view of each instrument.

7.2.4 Statistical analysis

Comparisons between control and treated leaf biochemical variables were performed according to Student's t-test. The level of statistical significance was set at P = 0. Leaf measurements are expressed as the mean ± standard deviation of seven measurements per thesis for the two days of sampling.

The variation induced by the herbicide application in the two dates on the four indices considered has been assessed computing the percentage temporal variation (PVD) and the percentage treatment variation (PVT) according to the following formulas:

$$\mathrm{PVT(d)} = \frac{\mathrm{VIt - VIc}}{\mathrm{VIc}}\ x\ 100 \qquad [7.4]$$

$$\mathrm{PVD(p)} = \frac{\mathrm{VId1 - VId2}}{\mathrm{VId1}}\ x\ 100 \qquad [7.5]$$

where d is the day (September 5th or 9th), p is the plot (control or DCMU treated), VI is midday mean value of the vegetation index referred to DCMU treated (t) or control (c) lawn carpet in September 5th (d1) or 9th (d2). Values of VIs measured between 11.00 and 12.00 solar time have been used to minimize undesired effects due to low sun zenith angles.
Moreover normalized difference of the VI values has been calculated between control and treated grass on the two dates. The ratio between the difference of control and treated at different days indicates the capability of the VI to detect physiological status changes due to the two herbicide treatments. The normalized difference has been calculated as follow:

$$\mathrm{ND} = \frac{\mathrm{VIt9} - \mathrm{VIc9}}{\mathrm{VIt5} - \mathrm{VIc5}} \qquad [7.6]$$

where ND is the normalized difference, VI is the vegetation index referred to DCMU treated (t) or control (c) lawn carpet and 5 and 9 are the date (September 5th or 9th).

7.3 Results and discussion

7.3.1 Leaf chemical analyses

The average chlorophyll and carotenoid concentrations in control and DCMU-treated samples are reported in Table 7.1. The t-test indicated that pigment concentration was similar in control and treated samples on both September 5th and September 9th indicating that the application of DCMU didn't cause any significant change in leaf pigment composition at the temporal scale of the experiment.

	5 Sept		9 Sept	
	Control	**DCMU**	**Control**	**DCMU**
Chl ab (mg g^{-1})	2.30 ± 0.44	2.48 ± 0.54	2.71 ± 0.49	2.61 ± 0.59
Car (mg g^{-1})	0.41 ± 0.11	0.46 ± 0.10	0.48 ± 0.08	0.46 ± 0.12

Table 7.1 Average and standard deviation of chlorophyll and carotenoid concentration in control and DCMU-treated samples on September 5th and 9th.

7.3.1 Field top of canopy spectral measurements

The normalized difference vegetation index (NDVI) and the photochemical reflectance index (PRI) computed from the measurements collected with the ASD spectrometer are reported in Figure 7.2a and 7.2b. VIs calculated from ASD measurements are reported because they are representative of a wider area. Results obtained with the Ocean Optics spectrometer covering the visible-near infrared region were similar (data not shown). The percentage variation (PV) and the normalized difference (ND) between VIs on treated and control grass are reported in Table 7.2.

	Percentage temporal variation PVD [%]		Percentage treatment variation PVT [%]		Normalized difference ND [-]
	Control	DCMU	5th	9th	
NDVI	1.6	4	-3	-1	0.39
PRI	-106	87	-85	85	2.26
Far-Red	22	91	48	134	3.37
Fyield	20	80	55	134	2.88

Table 7.2. Percentage temporal and treatment variation between the two dates and the two plots is reported. Last column refers to the normalized difference.

The NDVI course was quite stable during the day (Figure 7.2a) with a slight increase of NDVI value from September the 5th and the 9th. This increase was slightly higher (PVD = 4%, Table 7.2) for the DCMU treated grass compared to control one (1.6%, Table 7.2). In addition it can be noticed that NDVI values of the treated plot were always lower than the control plot PVT (negative values of PVT, Table 7.2) and the difference of the NDVI value measured on the treated and the control plot decreased from September 5th to 9th (ND = 0.39). The midday PRI mean absolute value of the control lawn carpet was more than the double of the treated one on September the 5th (PVT = -85%, Table 7.2). In the second day (September 9th) a 106% decrease of the control grass value was noticed while an almost 90% increase of PRI value on the treated sample has been detected (Table 7.2). The ND equal to 2.26 (meaning an increase of the difference between treated and control in the two days) depends both on the decrease of PRI in the control grass and on the PRI increase on the DCMU treated one. PRI is supposed to track changes in the de-epoxidation state of the xanthophyll cycle pigments (related to heat dissipation) and is also known to change according to the chlorophyll/carotenoid ratio. This latter did not change during the two dates (Table 7.1), therefore the PRI variation is expected to be dependent on physiological changes of the grass. Under excess light the conversion of violaxanthin to zeaxanthin (i.e. de-epoxidation), via the xanthophyll cycle pigments, is responsible for the majority of dissipation of the excess excitation energy as heat, a process also known as non-photochemical quenching (NPQ). This reaction is reversed under low light levels (i.e. epoxidation). PRI is expected to decrease with increasing NPQ (Filella et al., 2009; Penuelas et al., 1997). Therefore the extreme decrease of PRI on November 9th can be explained considering the ~10% rise of PPFD between the two dates (Figure 7.2, blue dots). On the contrary regarding the treated plot PRI values are higher than in the control suggesting that DCMU induced a decrease of the NPQ value. This effect has been already observed in samples treated with atrazine (Frankart et al., 2003), a herbicide known to have a mode of action similar to DCMU and in laboratory experiment where leaves were exposed to DCMU (Saura and Quiles, 2009). Both herbicides affect photosynthesis by binding to the second electron acceptor (Q_B) then strongly inhibiting the electron transport shortly after PSII. This will subsequently induce an over-excitation of PSII (Conrad et al., 1993) and cause an increase of the steady state fluorescence level. Instead, the energy-dependent NPQ related to a buildup of the

transthylakoid ΔpH generated by the photosynthetic electron transport (Ruban et al., 1992) is inhibited by DCMU. The ΔpH is also responsible for the activation of the xanthophyll cycle involved in photoprotection of the photosynthetic apparatus (Ruban et al., 2001). The reduced activation of the xanthophyll cycle is detected remotely as a higher PRI value in DCMU-treated compared to control grass. This behavior is even more enhanced comparing the control PRI reference value which decrease between the two dates considered.

The time courses of Far-Red SIF are reported in Figure 7.2c. As expected, during the day the intensity of Far-Red SIF is generally proportional to the incident radiance, being maximum at solar noon. On the contrary, the apparent fluorescence yield shows a more stable daily course (Figure 7.2d) with a trend generally opposite to the one of the incident radiance. The application of DCMU caused an increase of Far-Red SIF at 760 nm up to 5 mW m^{-2} sr^{-1} nm^{-1} on September 9th, while the 5th recorded values are ~50% higher on the treated grass compare to the control (PVT in Table 7.2). On average a 91% increase (midday mean, Table 7.2) is noticed comparing the treated grass values between 5th and 9th, while a smaller increase (22%) is found on the control lawn carpet. Finally the normalized difference between the two days is equal to 3.37. This is the highest difference recorded indicating the capability of Far-Red SIF in detecting the physiological change induced by the higher dose of DCMU. However the Far-Red SIF is known to be proportional to the solar irradiance, thus the high ND value can be enhanced by the 10% higher incoming radiation measured the November 9th. Nevertheless high ND (2.88, Table 7.2) value is reached also considering the Fyield, which gives more reliable comparison between the two dates.

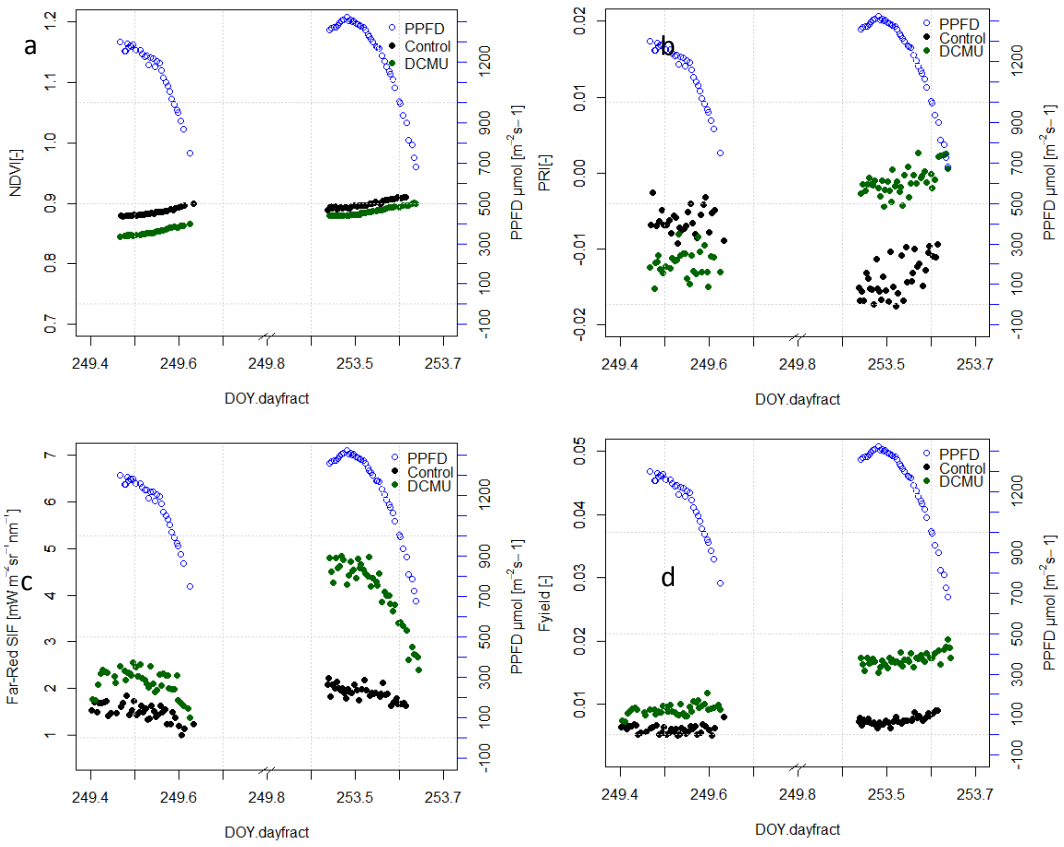

Figure 7.2.Time courses of the NDVI (a) and the photochemical reflectance index (PRI) (b) derived from the ASD spectrometer, far-red sun-induced fluorescence at 760 nm (Far-Red SIF) (c) and apparent fluorescence yield at 760 nm (Fyield) (d) derived from the high resolution Ocean Optics spectrometer, measured over the control (black) and the DCMU treated (green) grassland carpets during September the 5th (Day Of the Year 249) and September the 9th (Day Of the Year 253).

In summary the DCMU treatment has been shown to produce the higher effect in Far-Red SIF and in the related Fyield. Unfortunately the uncertain weather conditions occurred the days before the experiment setup prevented to measure the treated grass before the DCMU treatment. Therefore no reference values of the untreated condition have been acquired and the comparison between control and treated carpets before the treatment is missing. Nevertheless assuming that the differences of NDVI detected in September 5th do not refer to DCMU treatment but to the natural variability within the lawn carpets the consequent fluorescence values are expected to be higher in the control (direct relationship between NDVI and fluorescence is expected). On the contrary the opposite result suggests that the increase of the fluorescence emission is directly related to the DCMU application also in the first day of treatment, progressively enhanced after the second higher dose DCMU application. PRI differences between control and treated grass at the two dates strongly increased both due to the treatment and PPFD intensity changes, confirming also the PRI as plant stress indicator. As expected NDVI was the index with the smaller variation detected between the treated and untreated grass.

7.4 Conclusions

The first top of canopy measurements used to quantitative estimate the DCMU effect on plant physiological status have been presented in this study. DCMU treatment caused significant variation of the grass physiological status, in fact the DCMU treatment had no effects on leaf pigments in the duration of the experiment. The NDVI values, mainly driven by leaf Chlorophyll content were stable after the two treatments, confirming the inability of this index to detect early stress due to physiological changes. On the contrary both PRI and Far-Red SIF strongly increased in the treated grass lawn carpet immediately after the higher dose of DCMU was applied (September the 9th). The Far-Red SIF is directly affected by the incoming solar irradiance therefore more comparable results can be obtained using the Fyield which still confirm fluorescence as early stress indicator. Unfortunately we were not able to perform spectral measurements on the treated carpet before any treatment was applied. This prevented to quantify in an absolute way the effect of the two different DCMU doses on the fluorescence signal and on the PRI variation. Nevertheless it seems that the Far-red SIF is more responsive to the treatment even, to lower dose, compared to PRI which is also extremely dependent on light stress conditions. Further studies should be provided in order to determine DCMU doses effect on the two early stress detection indicators.

Acknowledgement

The main researchers involved in the project are listed below:
M. Rossini, C. Panigada, R. Colombo, F. Zemek, S. Cogliati J. Hanus, A. Schickling, U. Rascher

References

Berni, J., Zarco-Tejada, P.J., Suarez, L., Fereres, E., 2009. Thermal and Narrowband Multispectral Remote Sensing for Vegetation Monitoring From an Unmanned Aerial Vehicle. IEEE Trans. Geosci. Remote Sens. 47, 722–738.

Chlorophyll a Fluorescence: A Signature of Photosynthesis. Springer, Dordrecht 2004.

Conrad, R., Büchel, C., Wilhelm, C., Arsalane, W., Berkaloff, C., Duval, J.-C., 1993. Changes in yield ofin-vivo fluorescence of chlorophyll a as a tool for selective herbicide monitoring. J. Appl. Phycol. 5, 505–516.

Filella, I., Porcar-Castell, A., Munné-Bosch, S., Bäck, J., Garbulsky, M.F., Peñuelas, J., 2009. PRI assessment of long-term changes in carotenoids/chlorophyll ratio and short-term changes in de-epoxidation state of the xanthophyll cycle. Int. J. Remote Sens. 30, 4443–4455.

Frankart, C., Eullaffroy, P., Vernet, G., 2003. Comparative effects of four herbicides on non-photochemical fluorescence quenching in Lemna minor. Environ. Exp. Bot. 49, 159–168.

Gamon, J.A., Peñuelas, J., Field, C.B., 1992. A narrow-waveband spectral index that tracks diurnal changes in photosynthetic efficiency. Remote Sens. Environ. 41, 35–44.

Dodge AD, editor. Herbicides and plant metabolism. Society for Experimental Biology, Seminar Series 38.

Cambridge University Press, Cambridge, New York, Port Chester, Melbourne, Sydney, 1989Lange, O.L., Nobel, P.S., Osmond, C.B., Ziegler, H. (Eds.), 1981. Physiological Plant Ecology I. Springer Berlin Heidelberg, Berlin, Heidelberg.

Meroni, M., Busetto, L., Colombo, R., Guanter, L., Moreno, J., Verhoef, W., 2010. Performance of Spectral Fitting Methods for vegetation fluorescence quantification. Remote Sens. Environ. 114, 363–374.

Meroni, M., Colombo, R., 2009. 3S: A novel program for field spectroscopy. Comput. Geosci. 35, 1491–1496.

Meroni, M., Rossini, M., Picchi, V., Panigada, C., Cogliati, S., Nali, C., Colombo, R., 2008. Assessing Steady-state Fluorescence and PRI from Hyperspectral Proximal Sensing as Early Indicators of Plant Stress: The Case of Ozone Exposure. Sensors 8, 1740–1754.

Milton, E.J., Rollin, E.M., 2006. Estimating the irradiance spectrum from measurements in a limited number of spectral bands. Remote Sens. Environ. 100, 348–355.

Panigada, C., Rossini, M., Meroni, M., Cilia, C., Busetto, L., Amaducci, S., Boschetti, M., Cogliati, S., Picchi, V., Pinto, F., Marchesi, A., Colombo, R., 2014. Fluorescence, PRI and canopy temperature for water stress detection in cereal crops. Int. J. Appl. Earth Obs. Geoinf. 30, 167–178.

Penuelas, J., Llusia, J., Pinol, J., Filella, I., 1997. Photochemical reflectance index and leaf photosynthetic radiation-use-efficiency assessment in Mediterranean trees. Int. J. Remote Sens. 18, 2863–2868.

Rossini, M., Fava, F., Cogliati, S., Meroni, M., Marchesi, A., Panigada, C., Giardino, C., Busetto, L., Migliavacca, M., Amaducci, S., Colombo, R., 2013. Assessing canopy PRI from airborne imagery to map water stress in maize. ISPRS J. Photogramm. Remote Sens. 86, 168–177.

Rouse, J.W., Haas, R.H., Schell, J.A., Deering, D.W., 1973. Monitoring vegetation systems in the Great Plains with ERTS, in: Third ERTS Symposium, NASA SP-351. pp. 309–317.

Ruban, A.V., Rees, D., Pascal, A.A., Horton, P., 1992. Mechanism of ΔpH-dependent dissipation of absorbed excitation energy by photosynthetic membranes. II. The relationship between LHCII aggregation in vitro and qE in isolated thylakoids. Biochim. Biophys. Acta - Bioenerg. 1102, 39–44.

Ruban, A. V, Wentworth, M., Horton, P., 2001. Kinetic analysis of nonphotochemical quenching of chlorophyll fluorescence. 1. Isolated chloroplasts. Biochemistry 40, 9896–901.

Saura, P., Quiles, M.J., 2009. Assessment of Photosynthesis Tolerance to Herbicides, Heat and High Illumination by Fluorescence Imaging. Open Plant Sci. J. 3, 7–13.

Schaepman-Strub, G., Schaepman, M.E., Painter, T.H., Dangel, S., Martonchik, J. V., 2006. Reflectance quantities in optical remote sensing-definitions and case studies. Remote Sens. Environ. 103, 27–42.

Schulze, E.-D., Caldwell, M.M. (Eds.), 1994. Ecophysiology of Photosynthesis. Springer Berlin Heidelberg, Berlin, Heidelberg.

Suárez, L., Zarco-Tejada, P.J., González-Dugo, V., Berni, J.A.J., Sagardoy, R., Morales, F., Fereres, E., 2010. Detecting water stress effects on fruit quality in orchards with time-series PRI airborne imagery. Remote Sens. Environ. 114, 286–298.6

Suárez, L., Zarco-Tejada, P.J., Sepulcre-Cantó, G., Pérez-Priego, O., Miller, J.R., Jiménez-Muñoz, J.C., Sobrino, J., 2008. Assessing canopy PRI for water stress detection with diurnal airborne imagery. Remote Sens. Environ. 112, 560–575.

Wellburn, A.R., 1994. The Spectral Determination of Chlorophylls a and b, as well as Total Carotenoids, Using Various Solvents with Spectrophotometers of Different Resolution. J. Plant Physiol. 144, 307–313.

Conclusion

This research addresses on the use of optical proximal sensing technique for evaluating the role of multispectral and hyperspectral devices for monitoring vegetation parameters and processes (i.e. biophysical/biochemical parameters and plant status processes). In this context specific objectives of the study were: i) characterization and reduction of the measurement uncertainty sources; ii) application of improved optical sensing techniques based on multispectral and hyperspectral data to monitor terrestrial ecosystems.

In the proximal sensing community there is no agreement on one particular instrument to be used for vegetation monitoring. Often, different objectives or economic constraints limit the choice of the systems to be deployed in the field. Therefore, the collection of reliable and repeatable high quality data is strictly related to the definition of standard protocol used. People dealing with optical proximal sensing have to deeply know the instrumental characteristics of the device used and the site characteristics they want to measure (e.g. heterogeneity of the canopy to determine the proper acquisition scheme, shadows change during the day, hotspot and darkspot of the target, etc.). The reduction of the instrumental uncertainty sources is useless if the system is finally wrongly installed in the field (e.g. the monitored area is not representative of the surrounding area). The sensors characterization presented in Chapter 3, 4, and 5 focused on spectroradiometers which enable the collection of hyperspectral data allowing a detailed description of the investigated vegetation target. Nevertheless, the measurements collected by such systems are considerably influenced by instrumental characteristics and the reduction of such uncertainties is a fundamental practice in order to get high quality and repeatable data. In Chapter 3 the procedures needed to reduce measurement uncertainty sources related to instrumental components have been presented and applied on several spectroradiometers. Moreover, suggestions on the installation of portable spectrometers in the field have been proposed. In summary, the quality of the collected data depends on the acquisition scheme defined for sampling the target and on the data processing chain. In fact, once the measurement is properly collected a rigorous data processing chain has to be implemented to apply a series of correction (i.e. nonlinearity factors, spectral shift correction, radiometric calibration etc.) and to filter the data time series removing data collected under unfavorable condition (e.g. variable illumination conditions, extreme values of solar zenith angle). Once good quality measurements are achieved there are still instrumental characteristics that can affect vegetation biophysical parameter estimations. This is the case of the angular response of the field reference standards commonly used in the field to collect solar irradiance measurements. The angular response is barley reducible in field condition because it depends on the diffuse to global radiation which is difficult to measure spectrally, especially with automatic system installed for long term monitoring. Thus, it is important to quantify the impact that different reference standard angular responses can have on the measurements. In Chapter

4 the results of such evaluation have been reported according to spectral reflectance regions, vegetation indices and biochemical/biophysical parameter. In general, it was established that the effect of the reference standard deviation from an ideal cosine response can vary according to the field standard used and to the goal of the analysis. In fact, on reflectance regions the variation due to differences on reference standards angular response can be high (30-40%), particularly considering high solar zenith angles. This is especially true for commercially available cosine receptors which have been showed having a significant spectral dependency. This effect is strongly reduced on normalized vegetation indices and in the biochemical/biophysical parameter estimations. In the latter,it was found that the variations due to the reference standards angular response are in line with the uncertainties expected when the parameter is directly estimated in the field.

A physical constraint that cannot be modified in a spectroradiometer is the spectral resolution. In the calculation of the most traditional broad band indices used for characterizing the amount of green biomass it was found that finer spectral resolution have not influence on the index value. Nevertheless, in Chapter 5 the intercomparison experiment presented showed that spectral resolution can instead have an important effect on the retrieval of the sun induced chlorophyll fluorescence absolute values (even in devices with ultrafine spectral resolution, i.e. FWHM lower than 1 nm). From these results it can be noticed that the spectral resolution strongly affects the retrieval of the red fluorescence compared to the far-red fluorescence. This can significantly modify the red far-red fluorescence ratio which is considered a good indicator of light use efficiency and plant status.

The second section of the dissertation has been focused on the application of proximal sensing techniques in order to describe plant phenological and physiological status. Regarding phenological studies, digital photography is considered a promising and low-cost tool for long-term monitoring. So far, the phenological analyses made by using RGB digital images have been only focused on temporal analysis. The spatial information of the images is usually ignored and lost performing the analysis at region of interest level. Within this study (Chapter 6) we developed a spatial analysis to understand in relation with snowmelt of an alpine grassland. The spatial analysis highlighted different phenological behaviours of the two main vegetation types of the studied site (grass and forbs). This suggests that the two vegetation types react in a different way to an extremely early snowmelt, underlining that snowmelt is the key environmental factor at the studied site for species with opportunistic behaviour while for the vegetation type dominated by grasses other environmental factors (temperature photoperiod) can have a role in driving the start of the season.

Finally, field spectroscopy techniques (Chapter 7) have been applied to evaluate the possibility of using hyperspectral indices (i.e. the sun induced chlorophyll fluorescence and the photochemical reflectance index) as indicators of plant physiological status under artificial induced stress. A controlled experiment was set to enhance differences in plant stress by

applying an herbicide treatment known to reduce the electron transport chain between the Photosystems I and II during the photosynthetic process. Such herbicide after few days produced a degradation of the photosynthetic pigments (chlorophyll and carotenoids) while in the short term it affected the not photochemical dissipative ways. In fact, as result, the normalized difference vegetation index, mainly related to green biomass, was not capable to detect changes in the treated plot. On the contrary, the photochemical reflectance index and the sun induced chlorophyll fluorescence showed an immediate increase only related to physiological changes. In particular, the Far-Red fluorescence (also expressed as fluorescence yield) showed the greater difference after the treatment was applied. This result confirms the capability of vegetation indices of new generation to track physiological changes of vegetation. In summary, this research allowed to understand the potential of optical proximal sensing techniques for vegetation monitoring. Reccomendation and suggestions for field spectroscopy are provided in this study and new insight, regarding vegetation monitoring in terms of phenology and plant status, were delineated.